Cellular dynamics in zebrafish optic cup morphogenesis

D i s s e r t a t i o n s s c h r i f t

zur Erlangung des akademischen Grades

Doctor of Philosophy (Ph.D.)

vorgelegt

der Medizinischen Fakultät Carl Gustav Carus

der Technischen Universität Dresden

von

Jaydeep Sidhaye, M.Sc.

aus Pune, Indien

Dresden 2017

1. Gutachter**: Prof. Dr. Marino Zerial**, MPI-CBG, Dresden

2. Gutachter: **Prof. Dr. Marius Ader,** CRTD/TUD, Dresden

Tag der mündlichen Prüfung: **2017-12-07**

gez.: ----------

Vorsitzender der Promotionskommission

NORDEN
LAB

dresden international phd program

Cellular dynamics in zebrafish optic cup morphogenesis

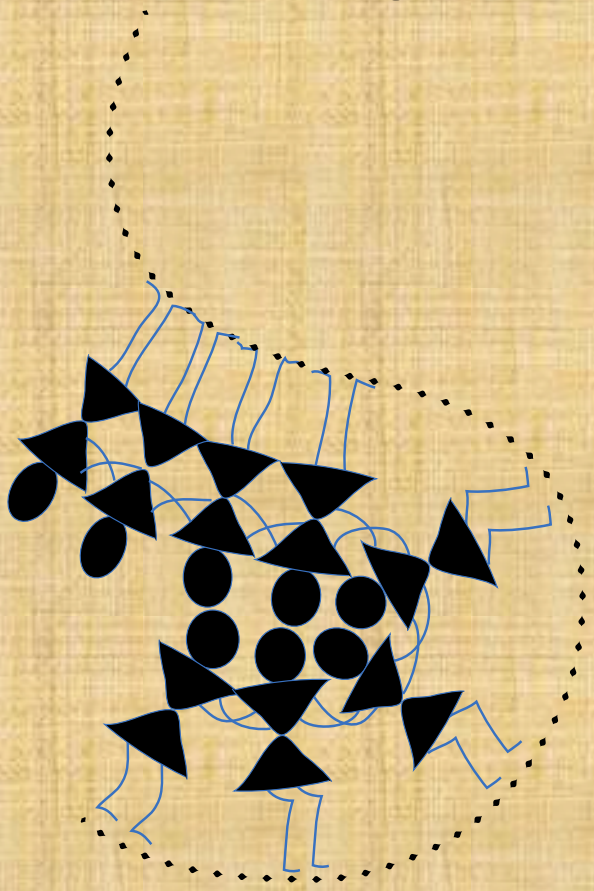

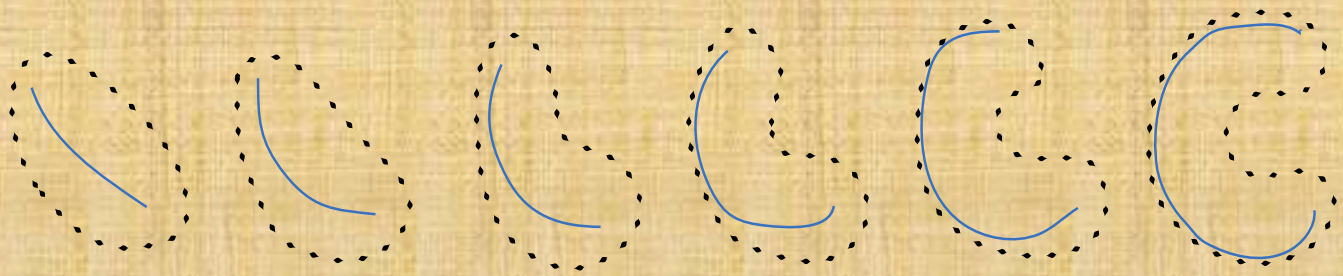

Jaydeep Sidhaye

Ph.D. Thesis
Dresden, 2017

Summary

Organ formation is an important step during development of an organism that combines different scales from the molecular to the tissue level. Many organogenesis phenomena involve epithelial morphogenesis, where sheets of cells undergo rearrangements to form complex architectures – organ precursors, which subsequently develop into mature organs. Timely development of the characteristic architectures of the organ precursors is crucial for successful organogenesis and is determined by the choice of epithelial rearrangements that organise the constituent cells in space and time. However, for many organogenesis events the cellular dynamics underlying such epithelial rearrangements remain elusive.

In the work presented here, I investigated the morphogenesis of the hemispherical retinal neuroepithelium (RNE), that serves as an organ precursor of the neural retina. Formation of RNE is an important event in vertebrates that shapes the optic cup and sets the stage for subsequent eye development. I investigated RNE morphogenesis in the developing zebrafish embryo by visualising and investigating the cellular dynamics of the process *in vivo*. My findings show that the zebrafish RNE is shaped by the combined action of two different epithelial rearrangements – basal shrinkage of the neuroepithelial cells and involution of cells at the rim of the developing optic cup. The basal shrinkage of the neuroepithelial cells bends the neuroepithelial sheet and starts the process of invagination. However, my results show that the major player in RNE morphogenesis is rim involution. Rim involution translocates prospective RNE cells to their designated location in the invaginating layer and contributes to RNE invagination. My work unravelled the so far unknown mechanism of rim involution. I show that the rim cells involute by collective epithelial migration using directed membrane protrusions and dynamic cell-matrix contacts. If rim migration is perturbed, the prospective RNE cells cannot reach the invaginating layer. As a result, these migration-defective cells attain the RNE fate at an ectopic location and disrupt the tissue architecture. Therefore, rim migration coordinates the cellular location with the timing of RNE fate determination and orchestrates RNE morphogenesis in space and time. Overall, my work highlights how morphogenetic processes shape the organ precursor architecture and ensure timely organ formation. These findings provide important insights not only for eye development but also for epithelial morphogenesis and organogenesis in many other systems.

Zusammenfassung

Für die Entwicklung eines Organismus ist die Bildung von Organen (Organogenese) von zentraler Bedeutung. Organogenese umfasst Prozesse auf allen Ebenen der Längenskala: von der molekularen Ebene, der Gewebeebene, bis hin zur Ebene des ganzen Organismus. Viele Phänomene der Organogenese beinhalten dabei Veränderungen von Epithelien, bei der sich Schichten von Zellen zu komplexen Strukturen - Organvorläufern - umwandeln. Diese entwickeln sich später zu vollständigen Organen. Die rechtzeitige Entwicklung der charakteristischen Architektur der Organvorläufer ist entscheidend für eine erfolgreiche Organogenese und wird durch die Wahl der epithelialen Umwandlungsprozessen bestimmt, welche die Zellen in Raum und Zeit koordinieren müssen. Für viele dieser Prozesse ist jedoch genau diese zugrundeliegende Zelldynamik unklar.

In der hier vorgestellten Arbeit untersuchte ich die Bildung des hemisphärischen retinalen Neuropepithels (RNE). Das RNE ist der Organvorläufer der neuralen Retina, weshalb dessen korrekte Bildung die Voraussetzung für die korrekte Entwicklung der Augen ist. Ich untersuchte die RNE-Morphogenese in sich entwickelnden Zebrafisch-Embryos durch Visualisierung und Untersuchung der zellulären Dynamik der beteiligten Prozesse *in vivo*. Meine Ergebnisse zeigen, dass das RNE in Zebrafischen durch die kombinierte Umwandlung von zwei verschiedenen Epithelien geformt wird. Zum einen findet eine Verkleinerung des basalen Prozesses der neuroepithelialen Zellen statt, zum anderen die Involution von Randzellen. Die basale Verkleinerung der neuroepithelialen Zellen verbiegt die neuroepitheliale Schicht und führt zur Einstülpung des RNE. Meine Ergebnisse zeigten allerdings, dass Involution von Randzellen noch bedeutsamer für die RNE-Morphogenese ist. Die involution von Randzellen transportiert potenzielle RNE-Zellen in das Neuroepithel und trägt zur RNE-Einstülpung bei. Die Bedeutung meiner Arbeit liegt darin, den bisher unbekannten Mechanismus der Randzell-Involution entdeckt zu haben. Ich zeigte, dass die Randzellen sich aktiv durch kollektive epitheliale Migration bewegen indem sie gerichtete Membranforsätze und dynamische Zell zu Matrix Kontakte etablieren. Wird die Migration der Randzellen inhibiert, so führt dies dazu, dass diese Zellen die eingestülpte RNE Schicht nicht erreichen. Sie landen dann an den falschen Positionen, wo sie die Gewerbearchitektur stören können. Daher koordiniert die Randzellmigration die Position der Zellen und orchestriert die RNE-Morphogenese in Raum und Zeit. Insgesamt zeigt meine Arbeit, wie morphogenetische Prozesse die Organvorläuferarchitektur prägen und eine rechtzeitige Organbildung sicherstellen. Diese Erkenntnisse sind sowohl für das Verständnis der Augenentwicklung, als auch für das der epithelialen Morphogenese und Organogenese in anderen Systemen von großer Bedeutung.

List of publications:

1. **Sidhaye, J.**, & Norden, C. (2017). Concerted action of neuroepithelial basal shrinkage and active epithelial migration ensures efficient optic cup morphogenesis. *eLife*, *6*, e22689.

2. Icha, J., Schmied, C., **Sidhaye, J**., Tomancak, P., Preibisch, S., & Norden, C. (2016). Using light sheet fluorescence microscopy to image zebrafish eye development. *Journal of visualized experiments: JoVE*, (110).

3. Strzyz, P. J., Lee, H. O., **Sidhaye, J.**, Weber, I. P., Leung, L. C., & Norden, C. (2015). Interkinetic nuclear migration is centrosome independent and ensures apical cell division to maintain tissue integrity. *Developmental cell*, *32*(2), 203-219.

Contents

1. Introduction

A milestone in the evolution of multicellular organisms has been the hierarchical organisation of cells into tissues and in turn into organs/organ systems. It has allowed division of labour for different physiological functions and has led to the emergence of a wide range of organs, varying in their function, size and shape. For example, formation of photosensitive cells allowed the early bilaterians to sense light. Later, the coevolution of an 'eye-vesicle' and a translucent layer of skin cells over this light sensing organ probably allowed the detection of shadows. Finally, the invagination of the translucent cells to form a simple lens allowed image-forming capabilities and led to the basic design of the vertebrate camera-like eye (Gregory, 2008; Lamb et al., 2007). Thus, the hierarchical organisation of cells into more complex structures has possibly improved the fitness of organisms by supporting and elaborating novel biological structures such as an eye or a wing and complex traits such as sensory perception, locomotion, immunity or cognition. Not surprisingly, a defect in the structure and function of the organs may impact the fitness and even survival of the organisms. Therefore, it is important to understand how cells form organs and what determines the final structure and possibly the function of a given organ.

To answer the above questions, one needs to inspect the development of an organism and study organogenesis, the process of organ formation. The importance of organogenesis is highlighted by various developmental disorders resulting from genetic or environmental factors that disturb the process of organogenesis and lead to organ malfunction. For example, autosomal recessive primary microcephaly, characterised by small brain size, results from the defects in neurogenesis during fetal brain development (Cox et al., 2006; Megraw et al., 2011). In another example, the drug Thalidomide shows teratogenic effects when prescribed to pregnant women and severely affects the fetal limb development (D'Amato et al., 1994). Therefore, understanding how different organs form is a fundamental question in biology, relevant for wide topics including developmental biology, evolutionary biology, synthetic biology (for tissue and organoid engineering) as well as biomedical research.

In this chapter, I will discuss the general principles of organogenesis and its spatiotemporal organisation (1.1). Next, I will introduce epithelial organogenesis (1.2) and I will describe the molecular and cellular features of epithelial cells (1.2.1). Then, I will summarise different cellular rearrangements involved in diverse contexts of morphogenesis of epithelial tissues (1.2.2) and focus on two major epithelial rearrangements, namely invagination (1.2.3) and

collective epithelial migration (1.2.4). Finally, I will introduce the organogenesis process that is focus of my work: morphogenesis of the retinal neuroepithelium during vertebrate optic cup formation (1.3). I will discuss the current literature with open questions, the model system of choice and finish with the specific aims of my work.

1.1 Organogenesis: From organ precursor to mature organs, a cellular choreography in space and time

Organogenesis is a complex multi-scale process that involves changes at the molecular, cellular and tissue level that collectively build a biological structure to perform a certain bodily function. It is an emergent feature of collective action of genetic *(patterning, signalling and gene regulation)*, cellular *(intracellular machineries of cytoskeleton, adhesion, polarity etc.)* and mechanical factors (forces generated and/or experienced by a cell) that feedback onto each other to shape the organ (Gilmour et al., 2017) (Summarised in Figure 1.1). Organogenesis starts after gastrulation, when the embryonic cells are organised into different germ layers, and continues throughout the development of the organism and even after the birth in case of some organs. Initially, the cells in the germ layers are organised into distinct 'tissue anlage' either as sheets of connected cells, the so-called 'epithelia' or lumps of loose cells, the so-called 'mesenchyme'. At specific locations guided by patterning cues, such sheets or lumps of cells (sometimes alternating in their form) organise into distinct architectures to build 'organ precursors'. Subsequently, these organ precursors grow and mature to give rise to the adult organs. For instance, during embryonic development of *Drosophila*, at specific locations epithelial cells of the ectoderm invaginate to form the imaginal discs. These imaginal discs serve as organ precursors and subsequently develop into different organs in the adult fly such as the eyes and the appendages (Morata, 2001). In another example, the vertebrate presomitic mesoderm, which is mesenchymal in nature, organises into somites that later give rise to structures such as vertebrae and muscles (Maroto et al., 2012). Thus, organogenesis is a hierarchical process and understanding it requires studying two important aspects: A. Processes that regulate 'spatial organisation' of cells and govern the organ architecture and B. 'Temporal regulation' of events that couple different processes to coordinate the timely organ formation. These two aspects are discussed below.

1.1.1 Spatial organisation during organogenesis

Organogenesis is regulated at the global level by external signals *(developmental signaling, extracellular matrix (ECM) and mechanics)* and locally orchestrated by the intracellular machinery *(cytoskeleton, adhesion, polarity, trafficking etc.)*. Both global and local factors

ultimately influence the morphology, number and location of cells to guide their spatial organisation and 3D architecture (Lecuit and Le Goff, 2007). Often, the 3D architecture of a mature organ is crucially linked with its function and hence it is important to specify the correct architecture of the organ precursor early on during organ development. If the formation of the organ precursor architecture is impaired, the structure and function of the mature organ can be compromised. For instance, early defects in the formation of the wing imaginal disc can later result in blistered wings (Dominguez-Gimenez et al., 2007). Similarly, problems in closure of the neural tube, the organ precursor of the brain and the spinal cord, can generate severe birth defects in mammals such as spina bifida (incomplete closure of bones around the spinal cord raising the risk of nerve damage) or anencephaly (missing part of forebrain) (Greene and Copp, 2014). Therefore, the formation of organ precursors lays the foundation for subsequent organogenesis steps. Thus, understanding how cells are organised spatially into distinct tissue architectures is an important aspect in organogenesis. It requires investigating the role of the external signals as well as the cellular machinery.

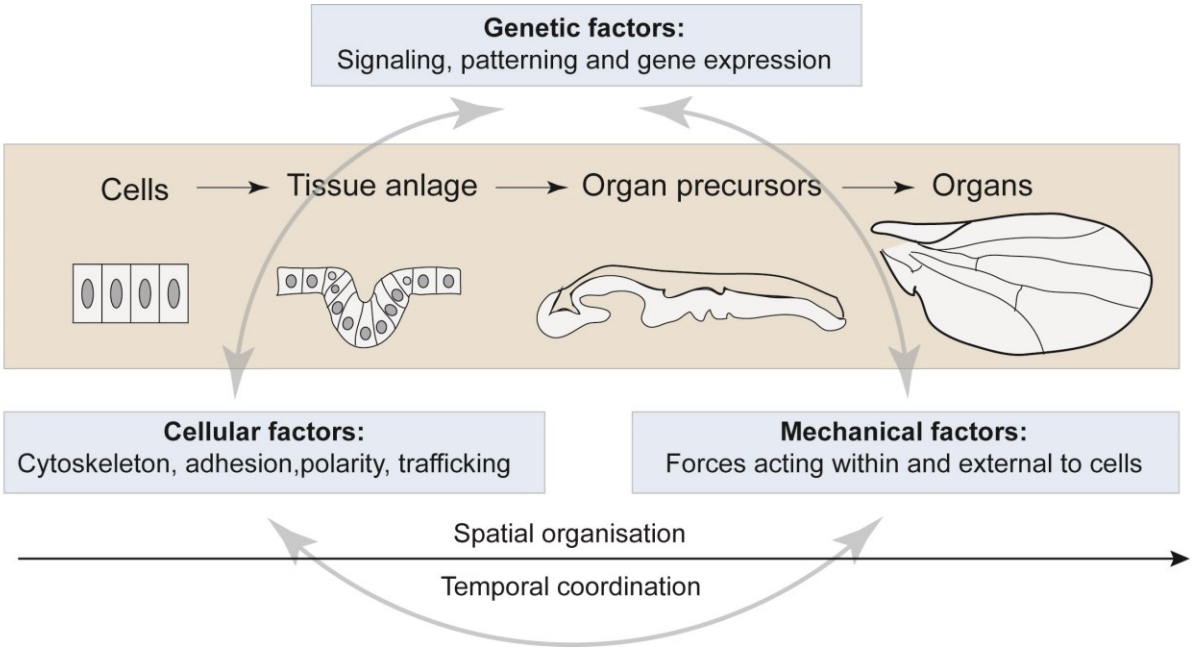

Figure 1.1: A schematic cartoon of hierarchical organisation of organogenesis and its regulators.
Under the influence of the genetic, cellular and mechanical factors, cells organise into tissues and organ precursors which later mature and grow to form organs. The process is well-coordinated in space and time. The schematic shows an example of the hierarchical organisation of development of an insect wing.

1.1.2 Temporal regulation of organogenesis

An additional crucial component of organogenesis is 'time'. Timely development of the organs is important to start their function at the appropriate developmental stage, which can be crucial for the survival of the organism. This 'time management' occurs at multiple levels. At the cellular level, timely gene expression regulates the cell cycle, the cell differentiation program and the cellular behaviours. This is best exemplified by the segmentation clock that regulates somitogenesis. The periodic expression of genes in the presomitic mesoderm is coupled with the differentiation program to form a new somite boundary and sets the pace of somitogenesis (Maroto et al., 2012). The timely coordination of development also occurs at the tissue level. Development of different tissues and organs is often interdependent (e.g. through signaling mechanisms or mechanical coupling) and thus, requires the respective tissues to develop on time. For example, the development and growth of the brain and the skull are coordinated in time. Premature fusion of one or more cranial sutures (craniosynostosis) has severe impact on brain development and results in distortion of skull shape and associated cognitive defects (Johnson and Wilkie, 2011). Finally, the timing of organogenesis is also regulated at the organismal level. Every species has a very stereotypic developmental time course. For instance, the teleost fish, medaka and zebrafish differ significantly in their developmental timeline (Furutani-Seiki and Wittbrodt, 2004). Even in such species from the same class, the development of the same organs can differ in time, indicating possible differences in the mechanisms utilised during organogenesis. Deciphering the reasons underlying such differences is also crucial to understand the aspect of timing in organogenesis.

Taken together, organogenesis is an important step in the life history of an organism. An early defect in organ formation can impact the functioning of the mature organ and possibly the fitness of the organism, depending on the organ and the severity of the phenotype. Yet, in majority of the cases the development is robust. Many of the genetic and environmental perturbations are tolerated by the organisms and cause very low phenotypic variation (Felix and Barkoulas, 2015). Such robustness is partly achieved by the use of multiple redundant strategies for a biological process (Felix and Barkoulas, 2015) and allows formation of stereotypic organ structures in a reproducible and timely manner. Therefore, to understand organogenesis in a holistic manner it is also crucial to understand how the mechanisms regulating spatial and temporal organisation of the process contribute to the robustness of organ formation.

1.2 Epithelial organogenesis: Transforming epithelial sheets into diverse 3-dimensional architectures

Many organs in the metazoan body including the central nervous system, the epidermis, and the organs of the gut develop from epithelia. Epithelia are a type of tissue composed of sheet of cells adhering to each other via cell-cell junctions. They have remarkable ability to remodel their cellular organisation and shape. Furthermore, the mechanical coupling of the epithelial cells allows tissue-wide coordination of cellular behaviours. These properties possibly make epithelia a good choice of tissue to build various organs. In this section, I introduce the hierarchical organisation of epithelial organogenesis. I first discuss the typical features of an epithelial cell and its molecular toolkit. Next, I discuss how the epithelial cells use the molecular toolkit to create cellular changes. Finally, I describe how the cellular changes drive tissue rearrangements to shape the 3-D architecture of epithelial organs and organ precursors.

1.2.1 The molecular toolkit and cellular attributes of epithelial cells

Cellular adhesion and polarity are the defining features of epithelia that guide epithelial properties, morphogenesis as well as function (Fristrom, 1988). Epithelial cells are polarised with distinct apical and basolateral plasma membrane domains with different lipid and protein composition. The apicobasal polarity also translates into polarised distribution of various cellular organelles and components and allows the two membrane domains to have distinct features. The prominent cellular features showing polarised localisation are the components of the adhesion and cytoskeletal machinery. Apically, epithelial cells are attached to each other by adherens junctions. The adherens junctions closely interact with apical actin cytoskeleton and stabilise the cell shape by maintaining the cell-cell contacts (Harris and Tepass, 2010). More mature epithelia are further connected apically via tight/septate junctions that segregate the apical and basolateral plasma membrane domains. In the majority of epithelia, the centrosome is also located apically, where it anchors the primary cilium and organises apico-basal microtubule arrays (Tang and Marshall, 2012). At the basal side, epithelia are lined by a layer of ECM, the basal lamina, rich in proteins such as laminin, nidogen, perlecan and type IV collagen (Jayadev and Sherwood, 2017; Yurchenco, 2011). The basal lamina is crucial for the survival of the epithelial cells and serves as the initial cue to establish apicobasal polarity in many systems (Morrissey and Sherwood, 2015). Epithelial cells attach to the basal lamina using integrin based focal adhesions, which closely interact with the actin cytoskeleton and stabilise the cellular location on the lamina. Together these features define the archetypical epithelial characteristics (summarised in Figure 1.2) that build stable sheets of cells.

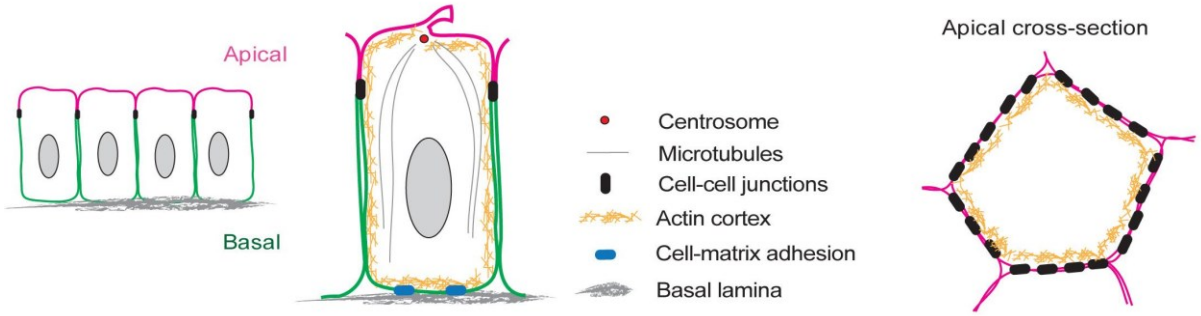

Figure 1.2: Cellular attributes of an epithelial cell
Schematic cartoon of an epithelial sheet and a typical epithelial cell showing the hallmark features of apicobasal polarity and adhesion.

In addition, epithelial cells also share the basic molecular toolkit common to many other cells in the body. It includes the cytoskeleton, cytoskeletal regulators and trafficking machinery. 1) The actin and microtubule cytoskeleton play an important role in defining the cell shape. An important player in this process is the cell cortex, a thin crosslinked actin network located beneath the plasma membrane (Salbreux et al., 2012). The myosin motor activity makes the cell cortex contractile and other components of the cortex such as the ERM family proteins connect this contractile actomyosin network to the plasma membrane. Therefore, the contractile properties of the cortex directly feedback onto the plasma membrane and thereby regulate the cellular stiffness and the cell shape (Salbreux et al., 2012). For example, an increase in the cortical contractility shrinks the surface area of the cell. A local detachment of the cortex from the plasma membrane releases the local cortical tension and can result in formation of a membrane protrusion called ‘bleb’ (Charras and Paluch, 2008). 2) All the cytoskeletal assemblies are controlled by ‘cytoskeletal regulators’ that regulate nucleation, elongation, cross-linking and depolymerisation of the cytoskeletal filaments. For example, Rho GTPases play an important role in forming growing-actin-networks by facilitating actin polymerization or in forming contractile actin-networks by activating myosin contractility (Heasman and Ridley, 2008). 3) The cytoskeleton also plays an important role in trafficking of cellular components. The trafficking machinery includes machineries of endocytosis and exocytosis that deliver membrane and proteins to different cellular locations. All these components together form the basic molecular toolkit of cells. However, this raises the question: how do epithelial cells use this generic molecular toolkit to bring about specific cellular changes that can guide epithelial tissue rearrangements?

The unique property of epithelial cells to remodel their cellular organisation and shape is attributed to polarity and adhesion that help in localised activation of the cytoskeletal

regulators and polarised trafficking machinery. Ultimately, the action of these factors modulates the plasma membrane/cortical domains, the adherens junctions or the focal adhesions to bring about the cellular changes. This way the molecular toolkit of epithelial cells produces cellular changes that can drive tissue-level changes (summarised in Figure 1.3).

1) ***Modulating plasma membrane domains****:* Uniform change in the plasma membrane area allows the cells to change in size. On the other hand, change in the area of specific plasma membrane domains allows the cells to change their shape. For example, a change in the lateral domains can modulate the cell height (Figure 1.3A) and a change in the apical or basal membrane area can transform the cell morphology to cone-like (Figure 1.3B). Such plasma membrane modulations often involve polarised trafficking (endocytosis/exocytosis) and change in cortical actomyosin contractility. Alternatively, the plasma membrane can be modulated by extending membrane protrusions. The force for the protrusion formation is often supported by local actin polymerisation and generates different types of cellular protrusions. Activation of Rho GTPase Rac promotes branched actin networks and broad, flat protrusions called lamellipodia (Heasman and Ridley, 2008). On the other hand, activation of Rho GTPase Cdc42 promotes bundled actin networks and thinner and longer protrusions called filopodia (Heasman and Ridley, 2008). Such protrusions are usually transient and allow the cell to explore its environment. If they persist long enough, these protrusions can support formation of new integrin-mediated adhesions to the basal lamina and thus cell migration (Figure 1.3E) (Krause and Gautreau, 2014).

2) *Modulating adherens junctions**:*** Adherens junctions and the associated actin cytoskeleton resist the cortical tension and stabilise the cell shape by maintaining the cell-cell contacts. Therefore, activation of actomyosin contractility at specific cell-cell contacts can modulate the epithelial cell shape (Harris and Tepass, 2010). Constricting all cell-cell contacts can drive apical constriction (Figure 1.3B). In contrast, constricting specific cell-cell contacts can help the cells in intercalation (Figure 1.3C). Adherens junctions are also essential for epithelial integrity and loss of adherens junction can result in delamination of the cell, a mechanism utilised in epithelial-to-mesenchymal transition (Figure 1.3D) (Harris and Tepass, 2010).

3) *Modulating cell-ECM attachment:* Turnover of cell-matrix attachment supports migration. The lamellipodia-like plasma membrane protrusions provide the cell an opportunity to form new integrin mediated adhesions to the basal lamina at this new ‘leading edge’. The detachment from the other ‘rear edge’ allows the cell to contract its rear side and propel forward using the traction force generated by the new focal contacts. Repeated cycles of directed leading edge protrusions, focal contact turnover and lagging-edge contraction brings effective cell migration (Ridley et al., 2003) (Figure 1.3D,E).

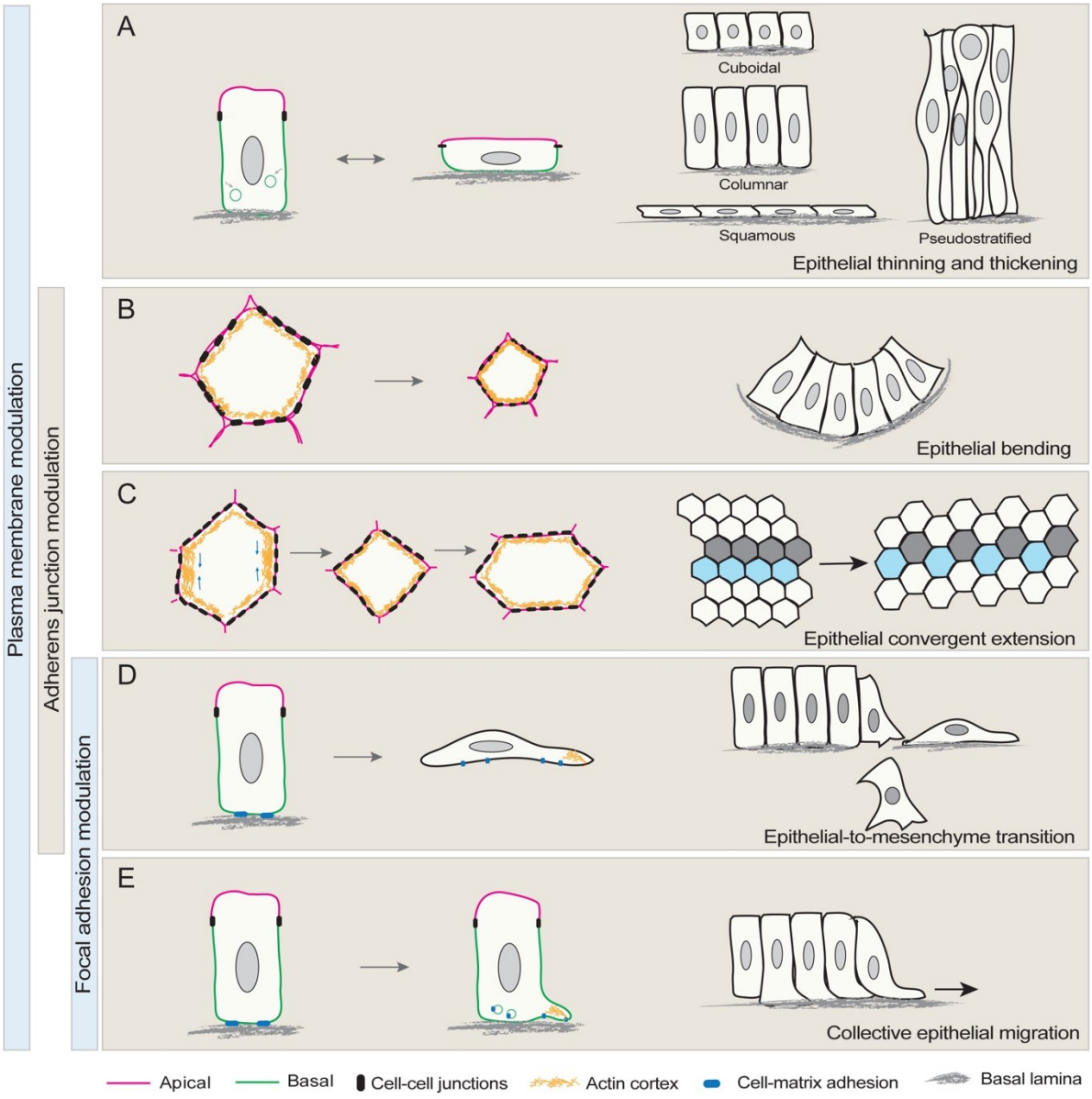

Figure 1.3: Epithelial morphogenesis: molecular toolkit, cellular changes and tissue rearrangements.
Schematic drawing showing the molecular modulations and the effective cellular changes, which shape the epithelial tissues.
A) Epithelial thinning and thickening creates different forms of epithelia.
B) Epithelial bending or invagination
C) Epithelial convergent extension changes the aspect ratio of the tissue.
D) Epithelial-to-mesenchyme transition (EMT): Cells lose epithelial integrity and become migratory.
E) Collective epithelial migration.

1.2.2 Epithelial rearrangements: different cellular strategies to mold the epithelial tissues

The molecular and cellular changes described in the previous section support tissue level rearrangements and shape different epithelial 3-D architectures. These cellular modulations combined with proliferation and apoptosis ultimately result in combinations of changes in the size, shape, number or location of epithelial cells (Lecuit and Le Goff, 2007), which guide the shape and architecture of the epithelium. Here, I highlight the major epithelial rearrangements commonly seen in epithelial morphogenesis and describe how the cellular changes can shape the tissues with some examples (Figure 1.3). In addition, Table 1 enlists a few examples of well-studied epithelial organogenesis systems and the underlying tissue rearrangements that shape the distinct tissue architectures. The diverse ways in which epithelial sheets rearrange enable generation of the varied and distinct organ architectures.

1. Epithelial thinning or thickening: A uniform change in the shape of the cells in the plain of the epithelium can lead to epithelial thinning or thickening. These rearrangements commonly use modulations of the cortex and the plasma membrane across the whole epithelium. Based on the resulting organisation of the cells the epithelial tissues are classified as squamous, cuboidal, columnar or pseudostratified epithelia (Figure 1.3A). Such transformation of the epithelial organisation is often observed during development. For instance, during *Drosophila* egg chamber development, the outer follicle cell layer consisting of cuboidal cells undergoes different cell shape changes. On the anterior side the cells stretch to assume squamous morphology whereas on the posterior side the follicle cells adopt a columnar morphology (Horne-Badovinac and Bilder, 2005).

2. Epithelial convergence-extension: The epithelial tissue can also change dimensions in the plane of the epithelium by elongating in one direction (extension), while constricting in the other (convergence). Such convergent extension movements can involve various mechanisms including cell intercalation, oriented cell divisions and cell shape changes. The most studied system of convergent extension is that of germ band extension in *Drosophila*. In this case, the cells modulate their adherens junctions. The cell-cell contacts perpendicular to direction of extension shrink whereas new contacts are made and stabilized in the direction of extension. Such junctional modulation results in exchange of neighbours and the formation/resolution of multicellular rosette structures that drive the convergent extension process (Figure 1.3C) (Kong et al., 2017).

Table 1: Organogenesis based on epithelial rearrangements

System of epithelial organogenesis	Tissue architecture	Epithelial rearrangements	Cellular processes	References
***Drosophila* egg-shell appendages**	Tube	Epithelial bending and convergent extension	Apical constriction, ordered cell intercalation and basal filopodia-based crawling	(Dorman et al., 2004; Osterfield et al., 2017; Osterfield et al., 2013; Osterfield et al., 2015; Peters and Berg, 2016; Peters et al., 2013)
Vertebrate neural tube closure (anterior part)	Tube	Epithelial thickening, bending and convergent extension	Cell elongation, apical constriction, and cell intercalation	(Davidson and Keller, 1999; Haigo et al., 2003; Kinoshita et al., 2008; Nishimura et al., 2012; Nishimura and Takeichi, 2008; Rolo et al., 2009; Schoenwolf and Franks, 1984; Schroeder, 1970; Suzuki et al., 2012; Ybot-Gonzalez et al., 2007)
***Drosophila* egg chamber follicle cell layer morphogenesis**	Sheet	Epithelial thinning and thickening	Cell shape changes, posterior follicle cells: cuboidal to columnar, anterior follicle cells: cuboidal to squamous	(Gomez et al., 2012; Grammont, 2007; Kolahi et al., 2009; Ng et al., 2016; Wang and Riechmann, 2007)
Vertebrate ectodermal placodes (Molar dental placode or hair follicle placode)	placode/pit	Epithelial stratification and bending	Epithelial proliferation, migration and cell intercalation	(Ahtiainen et al., 2014; Li et al., 2016; Panousopoulou and Green, 2016; Prochazka et al., 2015)
Lens placode of vertebrates	Placode/pit	epithelial thickening and invagination	Cell elongation and apical constriction	(Chauhan et al., 2009; Gato et al., 2001; Greiling and Clark, 2009; Huang et al., 2011; Lang et al., 2014; Plageman et al., 2011; Plageman et al., 2010)
***Drosophila* wing imaginal disc**	Sac-like	Epithelial thinning and thickening	Cell shape changes: Peripodium: cuboidal to squamous, Disc proper: cuboidal to pseudostratified	(Dominguez-Gimenez et al., 2007; Eaton et al., 1995; McClure and Schubiger, 2005; Widmann and Dahmann, 2009a, b)
***Drosophila* trachea**	branched tubes	collective epithelial migration and convergent extension (tube elongation).	Tip cells: epithelial migratory motion, stalk cells: cell intercalations	(Caussinus et al., 2008; Ghabrial et al., 2011; Okenve-Ramos and Llimargas, 2014; Ribeiro et al., 2002; Ribeiro et al., 2004)
Vertebrate lung epithelium	branched network	Epithelial folding and tube elongation	Invagination, cell proliferation.	(Kadzik et al., 2014; Kim et al., 2013; Tang et al., 2011)

3. Epithelial-to-mesenchymal transition (EMT): Epithelial tissues can also be very plastic and modulate their epithelial features. At many instances during development epithelial cells born at one location move to different locations further away in the body. These movements are often supported by the loss of epithelial features to adopt migratory mesenchymal behaviour. It often involves downregulation of the components of adherens junction (Figure 1.3D). For instance, this is seen during development of vertebrate neural crest cells, where cells delaminate from the neural tube by undergoing EMT and then migrate away to give rise to tissues such as the facial cartilage and bone and the peripheral nervous system (Sauka-

Spengler and Bronner-Fraser, 2008). EMT is also observed in cancer cells and can aid in metastasis (Campbell and Casanova, 2016; Nieto, 2013).

4. Epithelial sheet movement: Epithelial sheets can also move to a new place without undergoing EMT. This movement could occur by active epithelial migration by modulating the focal adhesions (Figure 1.3E) or by passive displacement in response to external stress. More details are discussed in 1.2.4.

5. Epithelial bending: Unlike the epithelial arrangements mentioned so far, epithelial cells can also undergo out-of plane shape changes to mold into complex 3-D shapes by changing dimension of one face (apical or basal) of the sheet with respect to the other. Such apico-basally polarised dimension change results in the formation of wedge-shaped cells and enables bending of the epithelium (Figure 1.3B). The phenomenon of epithelial bending helps in shaping majority of diverse epithelial architectures; however, the underlying cellular mechanisms are diverse. More details are discussed in 1.2.3.

Two epithelial rearrangements important for my work are invagination and collective epithelial migration which are discussed below in detail.

1.2.3 Invagination: Epithelial bending

Epithelial bending is a significant epithelial rearrangement that transforms a flat sheet of cells into a fold or a pit or a tube through coordinated action of many cells. Depending on the direction of the bending with respect to the body/organ axis, the epithelial folding is called as invagination (inward bending) or evagination (outward bending). However, similar mechanisms can play a role in both the processes. Often, epithelial bending occurs via the apical side, where the apical area of the cells shrinks with respect to their basal areas resulting in wedge shaped cells (Figure 1.3B) (Martin and Goldstein, 2014). This has been extensively studied for the ventral furrow formation during gastrulation in *Drosophila* (Leptin and Grunewald, 1990). Now it is clear that some epithelial systems invaginate from the basal side where the cells adopt a wedge shape with shrunken basal side, e.g. the midbrain hindbrain boundary in the developing neural tube of zebrafish (Gutzman et al., 2008). However, the mechanisms of basal invagination remain elusive. In contrast, the process of apical invagination is extensively studied and commonly involves the interplay of apical junctions and the actomyosin cytoskeleton (Martin and Goldstein, 2014; Pearl et al., 2017). A few mechanisms observed in different morphogenetic systems are outlined below and combinations of these are used a system-specific way.

1. Apical constriction: One of the best-studied mechanisms of apical invagination is apical constriction. It involves action of apically localised contractile actomyosin that constricts the apical surface of the cells and creates wedge shaped cells. Although the upstream regulation of the process is tissue/species dependent, it ultimately regulates localised activation of the Rho GTPase RhoA and its effector Rho-kinase (ROCK) that regulate phosphorylation of the myosin regulatory light chain (MRLC) (Martin and Goldstein, 2014). MRLC phosphorylation activates myosin and is important for its contractile function (Bresnick, 1999). Thus, apically polarised Rho-ROCK mediated myosin contractility drives apical constriction. The apical contractile actomyosin can be arranged as circumferential actomyosin fibers, cortical actomyosin flows or actomyosin pulses (Martin and Goldstein, 2014). It is localised either medially in the apical cortex as seen for ventral furrow formation in *Drosophila* (Dawes-Hoang et al., 2005; Martin et al., 2009; Young et al., 1991) or laterally along the junctions as observed during chick neurulation (Nishimura et al., 2012; Nishimura and Takeichi, 2008). Eventually, as a crucial feature of apical constriction, the apical contractile actomyosin network is coupled with the adherens junctions to modulate cell-cell contacts and to ensure effective cell shape change (Martin and Goldstein, 2014).

2. Basal relaxation: Instead of active accumulation of contractile actomyosin on one side of the cell, this mechanism rather involves disassembly of actomyosin on the non-contracting side of the cells. Basal relaxation is reported for chick otic placode invagination (Sai and Ladher, 2008). However, such mechanism can also coexist with apical constriction. It has been proposed for *Drosophila* ventral furrow formation that basal relaxation helps in reducing the rigidity of the basal surface, while maintaining the cell volumes and is sufficient to drive ventral furrow formation in combination with the apical constriction (Polyakov et al., 2014).

3. Structural weakening: A different strategy towards invagination involves making a structurally weaker point in the epithelium that would facilitate buckling of the sheet. Such mechanism is reported during formation of tracheal pits, where mitotic cell rounding creates a weak point in the tissue (Kondo and Hayashi, 2013). On the other hand, during morphogenesis of the *Drosophila* leg epithelium, selective apoptosis of cells induces structural weakening and marks the sites of epithelial bending (Manjon et al., 2007; Monier et al., 2015). Both these mechanisms cause apical bending of the epithelium.

4. Crowding induced bending: When a less stiff epithelium is physically constrained within stiffer boundaries, increased proliferation or crowding of cells can cause bending of the sheet by passive buckling. Such mechanism is seen for *in vitro* optic cup morphogenesis

from mouse embryonic stem cells (Eiraku et al., 2012; Eiraku et al., 2011). In some other cases, the proliferation of cells can cause local stratification, which coupled with migratory action of the new cells drives invagination. In this scenario, the pushing force by the migrating cells causes bending of the stratified structure (similar to a punch in the dough). Such mechanism is observed during morphogenesis of the molar tooth placode and the hair follicle placode (Ahtiainen et al., 2014; Li et al., 2016; Panousopoulou and Green, 2016; Prochazka et al., 2015).

Thus, there are several ways in which an epithelium can bend. However, there are still many open questions. It is not clear how different mechanisms determine the speed of invagination. It is further not understood how different mechanisms determine the extent or depth of the invaginated structure and decide whether it should be a tube or a pit or a hemisphere. Moreover, although we now understand different mechanisms of apical invagination, basal invagination and the process of basal constriction still remain poorly understood. It would be interesting to investigate which basal cellular structures are involved in the basal invagination and if it is also dependent on the actomyosin cytoskeleton. Therefore, further research is required to understand the processes of epithelial bending in different model systems.

1.2.4 Collective epithelial migration

Epithelial cells can undergo movements as a sheet without losing their epithelial nature. Such epithelial movements are common during development (morphogenesis), homeostasis (wound healing) and can be reinitiated in mature tissues during cancer (Friedl and Gilmour, 2009; Haeger et al., 2015; Rorth, 2009). Although coordinated cell shape changes and addition/removal of cells can cause passive displacement of cells (Friedl and Gilmour, 2009), epithelial cells can also show active migratory behaviour by modulating their focal adhesions as described in 1.2.1. Such active migration of connected epithelial cells as a group is commonly called as collective epithelial migration. The mechanisms of single cell migration are quite well studied (Friedl and Wolf, 2010; Krause and Gautreau, 2014; Petrie and Yamada, 2012), however, the mechanisms underlying collective migration are diverse and hence less well understood (Friedl and Gilmour, 2009; Haeger et al., 2015; Rorth, 2009). Here, I discuss some of the common themes and variations in collective epithelial migration. Some prominent examples of collective epithelial migration phenomena are included in Table 2.

1. Cell-cell adhesion and epithelial organisation: In contrast to individual cell migration, collective cell migration features cell-cell adhesion, which coordinates the cellular behaviour

across the group of cells. Loss of adhesion leads to detachment of cells and can result in delamination/loss of cells or an EMT-like phenotype (Friedl and Gilmour, 2009). Nevertheless, depending upon the adhesion and arrangement of the cells, the migrating epithelia can adopt different architectures and different modes of collective migration. The different modes of collective migration include A) 2D sheet moving as a monolayer B) multilayered 3D strands and C) isolated group or cluster of cells (Friedl and Gilmour, 2009; Rorth, 2009) (Table 2). However, how the migratory behaviour is regulated in such diverse collective migration phenomena still remains an active area of research.

Table 2: Collective epithelial migration phenomena

Model system	Epithelial organisation	Guidance cue and polarisation	Important references
in vitro			
Scratch or gap induced migration in epithelial and endothelial cell cultures	Epithelial sheet	Growth factor-induced leader cell behaviour distinct from behaviour of follower cells.	(Poujade et al., 2007),(Vitorino and Meyer, 2008),(Block et al., 2004; Farooqui and Fenteany, 2005; Nikolic et al., 2006) (Simpson et al., 2008)
Mammary epithelial branching in 3D mammary gland cultures	Multilayered 3D strands	Extracellular matrix, tip/leader cells lack membrane protrusions	(Ewald et al., 2008)
in vivo			
Border cell migration in *Drosophila* egg chamber.	Isolated group of cells	Chemokine growth factors, cells migrate through the group of nurse cells	(Bianco et al., 2007; Duchek and Rorth, 2001; Duchek et al., 2001)
Follicle cell migration during *Drosophila* egg chamber rotation	Epithelial sheet	Planar cell polarity and ECM pattern, lack any specific leader cells	(Cetera et al., 2014; Diaz de la Loza et al., 2017; Haigo and Bilder, 2011; Viktorinova et al., 2009)
Posterior lateral line primordium in zebrafish	Isolated group of cells	Chemokine, Polarisation of primordium through combined action of FGF and Wnt signalling to restrict chemokine receptor expression to the leading edge.	(Aman and Piotrowski, 2008; Dambly-Chaudiere et al., 2007; David et al., 2002; Dona et al., 2013; Friedl and Gilmour, 2009)
Tracheal sprouting morphogenesis in *Drosophila*	Multilayered 3D strands	Chemokines, distinct tip cell and stalk cell behaviours	(Caussinus et al., 2008; Ribeiro et al., 2002)
Vascular sprouting during formation of vasculature in mouse	Multilayered 3D strands	Chemokines, distinct tip cell and stalk cell behaviours	(Gerhardt et al., 2003)

2. Guidance cues for migration, epithelial polarisation and the leader-follower model:

An important aspect of collective migration is directionality. External guidance cues polarise the migrating group of cells and ensure directional migration. The specific guidance cues used during migration are context specific and differ from system to system (Haeger et al., 2015). The cells can respond to specific chemical cues and exhibit directed migration by chemotaxis. For example, chemokine signalling regulates the directionality of migration of

the zebrafish lateral line primordium (Aman and Piotrowski, 2008; Dambly-Chaudiere et al., 2007; David et al., 2002) (Dona et al., 2013) and the border cell migration in *Drosophila* egg chamber (Bianco et al., 2007; Duchek and Rorth, 2001; Duchek et al., 2001). Alternatively, the polarised migration can also occur in response to a gradient of stiffness of the ECM, a process termed as durotaxis or haptotaxis. Experiments on various cultured epithelia showed that the cell collectives migrate faster and more persistently towards the stiffer edge (Sunyer et al., 2016). The different guidance cues used in some important examples of collective epithelial migration are summarised in Table 2.

Such guidance cues subsequently polarise the migrating epithelium into distinct cell populations, classically called as leader cells and follower cells. Leader cells are defined as the cells at the migrating front/ the leading edge that respond to the guidance cue and initiate the migratory response with prominent membrane protrusive activity. The follower cells form the bulk of the migrating tissue and follow the path of leader cells. However, in majority of scenarios, the follower cells are not passive but show active migratory features (Rorth, 2009). Such leader-follower module forms the functional unit of many collective migration phenomena. Nevertheless, there are also systems such as the follicle cell migration in the *Drosophila* egg chambers, in which cells undergo collective epithelial migration without any specific leader cells (Haigo and Bilder, 2011). Thus, the leader-follower model does not seem to be a common feature of all epithelial migration phenomena as previously thought and needs to be carefully addressed by studying more systems involving epithelial cell migration.

3. Membrane protrusions and dynamic cell-matrix contacts: Most of the collective epithelial migration phenomena share certain common features with systems of single cell migration (Friedl and Wolf, 2010; Krause and Gautreau, 2014; Petrie and Yamada, 2012). These include membrane protrusions and dynamic cell-matrix contacts. Indeed, the screens to identify regulators of collective cell migration revealed specific modules of core cell motility genes (cytoskeletal regulators and cell-matrix adhesion regulators), acting downstream of the guidance and polarising cues (Simpson et al., 2008; Vitorino and Meyer, 2008). The membrane protrusions of collective migrating cells are usually lamellipodial or filopodial in nature (Friedl and Gilmour, 2009; Rorth, 2009). The protrusive activity is enriched in the so-called ‘leader cells’. However, careful analysis has shown that often the follower cells also show protrusions, sometimes referred to as ‘cryptopodia’ (Farooqui and Fenteany, 2005). For productive cell movement, the protrusions are coupled with dynamic contacts of cells with the environment, the ECM or the peripheral cells (Friedl and Gilmour, 2009; Rorth, 2009). This is supported by the findings that many collective migration events such as the

follicle cell migration in the *Drosophila* egg chamber (Diaz de la Loza et al., 2017; Frydman and Spradling, 2001; Haigo and Bilder, 2011; Lewellyn et al., 2013) or the mammary gland morphogenesis (Klinowska et al., 1999) crucially depend on the function of ECM component laminin and its cellular receptor integrinβ1. Thus, the basic migration toolkit involving cytoskeletal organisation, membrane protrusions and modulation of the cell-matrix contacts is used similarly in different collective migration phenomena.

To conclude, in this section 1.2, I introduced various epithelial rearrangements used to shape epithelial structures. However, it remains challenging to understand how different organs and tissues adopt specific combinations of these strategies to achieve the unique tissue architectures and timely organogenesis. This has been the central theme of my work.

1.3 Shaping the retinal neuroepithelium: A case of epithelial morphogenesis

An interesting yet underexplored epithelial morphogenetic event is the formation of the vertebrate optic cup, which includes morphogenesis of the retinal neuroepithelium (RNE) and the retinal pigment epithelium (RPE) (Figure 1.4). The RNE forms the bulk of the optic cup and serves as the organ precursor for the neural retina (Figure 1.4). It consists of the retinal progenitor cells that later in development give rise to the different retinal neurons. Across vertebrates, RNE has a conserved characteristic hemispherical architecture, which is maintained even later in development in the neural retina. The developing lens is located in the curvature of the optic cup and this unit paves the way for building the vertebrate camera-type eye (Figure 1.4) (Fernald, 2000; Lamb et al., 2007). The hemispherical architecture of the retina is thought to have co-evolved with the lens. The earliest known invaginated RNE in the early craniate hagfish is correlated with the emergence of the lens placode. Later in evolution, the optic cup invagination and lens development were further elaborated, as seen even in the most primitive vertebrate, lamprey (Lamb et al., 2007). The curvature of the retina is proposed to provide visual acuity, improved sense of depth and better ability to detect light coming from different directions. This possibly also explains the advantage of the curved retina in cephalopods, although the cephalopod retina has a very different developmental origin (Fernald, 2000). Thus, morphogenesis of the hemispherical RNE and the optic cup has been an evolutionary milestone and serves as an important initial step for the vertebrate eye development. Additionally, defects in the optic cup architecture can cause structural eye defects such as microphthalmia (small eye) and coloboma (optic fissure closure defects) (Fuhrmann, 2010; Williamson and FitzPatrick, 2014). Therefore,

understanding OCM is not only an attractive model for developmental biology but is also important from a disease point of view to investigate the origin of ocular defects.

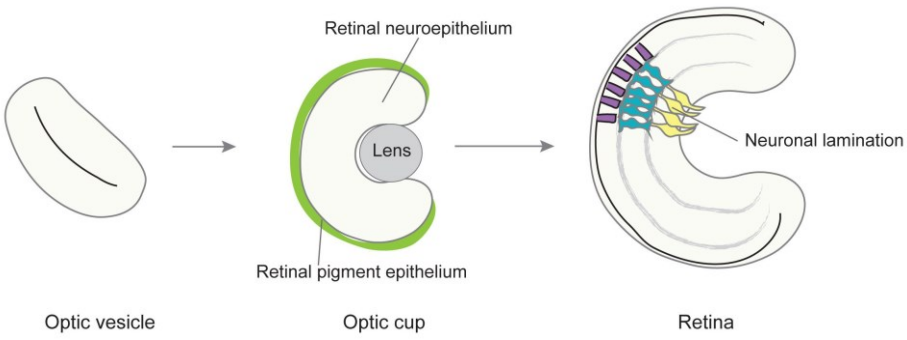

Figure 1.4: Vertebrate eye development
Optic vesicle undergoes morphogenesis to form the hemispherical optic cup that consists of the inner retinal neuroepithelium and the outer retinal pigment epithelium. The retinal neuroepithelium serves as an organ precursor to the neural retina.

Recently, it has also been possible to form such hemispherical optic cups from mouse and human embryonic stem cells under *in vitro* culture conditions (Eiraku et al., 2011; Nakano et al., 2012). These *in vitro*-formed optic cups further differentiate to give rise to the retinal neurons. This organoid culture approach is particularly useful to generate different retinal neurons for therapeutic research. Interestingly, these optic cups develop in absence of accessory structures in the developing eye such as the developing lens and the periocular mesenchyme. Hence, it is postulated that the retinal cells have the inherent property to self-organise into an optic cup (Eiraku et al., 2012; Eiraku et al., 2011). However, it is not understood if the *in vitro* RNE formation follows the same morphogenetic principles as that of the i*n vivo* situation. Therefore, to understand the principle of organogenesis, it is important to investigate how this hemispheric architecture comes into shape *in vivo* in the given developmental time window.

In this section, I will outline the current understanding of early eye development, with special focus on the morphogenetic processes, epithelial rearrangements and underlying cellular changes. Beginning with the formation of eye-field, I will describe the formation of optic vesicles and the subsequent the formation of the hemispherical optic cup. I will discuss the important literature on the organogenesis principles of optic cup mophogenesis (OCM) in the *in vitro* system as well as in different *in vivo* animal models and highlight the open questions.

1.3.1 Early eye development: From eye field to the optic vesicle

The cells that give rise to the future retina and the retinal pigment epithelium are set aside early on during forebrain development. Under the control of patterning cues, the expression of so-called 'eye-field transcription factors' (ET, Rx1, Six3, Pax6, Lhx2, Optx2) specifies eye-field cells and demarcates them from the rest of the forebrain tissue (Fuhrmann, 2010; Graw, 2010). The importance of some of these transcription factors is shown by the loss-of-function mutants that feature anophthalmia (absence of eyes) or microphthalmia (highly reduced eye) and ectopic expression studies that can induce ectopic eye-fields (Fuhrmann, 2010; Graw, 2010). As the development proceeds, the eye field splits along the midline into two parts, each of which gives rise to an optic vesicle. A failure to split the eye field results in cyclopia, formation of one big eye instead of two. Signaling pathways of Sonic hedgehog, TGF-β/nodal involved in midline/axis specification are important for this process (Fuhrmann, 2010; Graw, 2010). Alongside the patterned expression of the eye-field transcription factors, morphogenetic movements guide early eye development (England et al., 2006). In teleosts, it has been shown that the eye field transcription factor rx3 plays an important role in the process. Rx3 regulates expression of *ephs* and *ephrins*, which help in segregating the eye-field cells from the remaining cells of the anterior neural plate (Cavodeassi et al., 2013). Similarly, Rx3 downregulates the expression of cell adhesion molecule *nlcam*, which also helps in segregation of the eye-field cells and prevents them from converging at the midline (Brown et al., 2010). Thus, the early transcriptional programs in the eye-field also regulate the cell behaviours that lead to splitting of the eye-fields.

In case of mammalian early eye development, although the role of patterning and transcription factors has been established (Fuhrmann, 2010), the morphogenetic studies have been tricky due to the difficulty of *in vivo* imaging. The *in vitro* matrigel-based organoid cultures of mouse and human embryonic stem cells allow specification of the eye-fields (Eiraku et al., 2011; Nakano et al., 2012). However, due to the lack of global patterning cues the embryonic stem cell aggregates develop multiple eye fields which also do not split. As a result, little is known about the dynamics of mammalian eye field morphogenesis and this field requires further research.

After eye-field specification and splitting, each of the two groups of cells grows outwards from the anterior neural tube by a process called as evagination, which forms the optic vesicle. The mechanism of optic vesicle formation depends on the mode of neurulation, the formation of the neural tube. In case of amniotes, the anterior neural tube is formed by invagination of the epithelial neural plate to form a hollow epithelial tube. As a result, the

optic vesicle bulges out of the neural tube in the form of a hollow epithelial pocket (Figure 1.5) (Araya et al., 2016; Lowery and Sive, 2004). This phenomenon is also observed in the matrigel cultures of embryonic stem cells, however with low efficiency (Eiraku et al., 2011; Nakano et al., 2012). Currently, the evagination step is considered to be rate limiting for efficient *in vitro* optic cup formation (Volkner et al., 2016). Therefore, understanding the underlying molecular mechanisms might aid in improving the efficiency of *in vitro* optic vesicle evagination and optic cup formation. A few studies have investigated the cellular rearrangements that drive the optic vesicle evagination in amniotes. In case of mouse, analysis of cell shape changes by analysing electron microscopy images predicted that the evagination process involves apical constriction and associated remodelling of the ECM (Svoboda and O'Shea, 1987). A quantitative description of chick optic vesicle evagination using 3D imaging suggests that intercalation of epithelial cells drives evagination by deforming the tissue anisotropically in the mediolateral axis (Morishita et al., 2017). Interestingly, inhibiting cell proliferation had minimal effect on the process of evagination (Morishita et al., 2017). Nevertheless, the molecular mechanisms underlying optic vesicle formation in amniotes remain elusive.

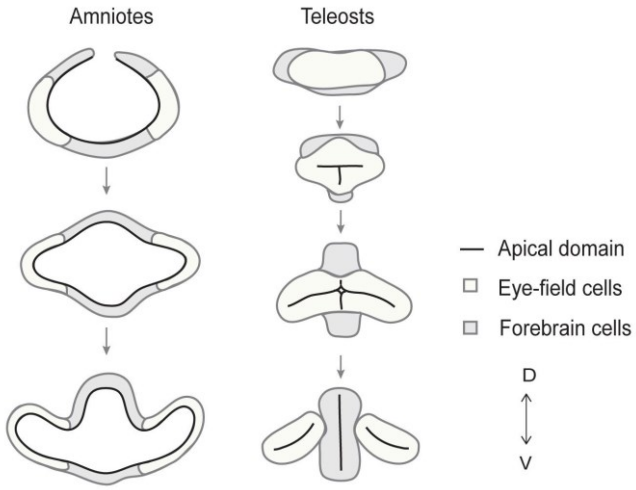

Figure 1.5: Optic vesicle evagination
Schematic drawing of optic vesicle evagination in amniotes and in teleosts. In amniotes, pre-polarised eye field cells form optic vesicle by cellular rearrangements. In teleosts, eye field cells simultaneously undergo epithelial polarisation and intercalations to form the optic vesicles.

In contrast to amniotes, optic vesicle evagination process has been extensively studied in teleosts due to the ease of *in vivo* imaging. However, it should be noted that teleost neurulation happens differently than in the higher vertebrates. The anterior neural tube forms by convergence of neural plate cells which are rather mesenchymal in morphology and lack epithelial polarity (Araya et al., 2016; Lowery and Sive, 2004). Based on live tracking of

nuclei, it was postulated that migration of these mesenchymal cells is responsible for the optic vesicle evagination (Rembold et al., 2006). However, it was later shown that the cells simultaneously undergo epithelial polarisation in response to the ECM component laminin. Interestingly, the eye field cells undergo this apicobasal polarisation prior to the remaining forebrain cells and a subset of them adopts the epithelial morphology (Ivanovitch et al., 2013). This prioritised polarisation of the eye-field cells helps the efficient segregation of eye fields and the development of the optic vesicles (Ivanovitch et al., 2013). Later, the cellular rearrangements of evagination involve cell intercalations similar to the chick optic vesicle. These intercalations, help in integrating more cells undergoing apicobasal polarisation into the optic vesicle epithelium (Ivanovitch et al., 2013). Thus, during teleost (zebrafish) development, neurulation, eye field specification, epithelial polarisation, and cell intercalations occur concurrently and drive the process of evagination (Figure 1.5).

1.3.2 Optic cup morphogenesis: Patterning and fate specification

The evaginated optic vesicles are exposed to different signals from the surrounding tissues: the forebrain, the surface ectoderm that later forms the lens placode, and the periocular mesenchyme. Under the influence of the signalling cues, the optic vesicle is patterned in the dorso-ventral, proximo-distal and naso-temporal axes (Table 3). Consequently, the equipotential cells of the optic vesicle adopt different fates either as RPE or RNE that form the optic cup or the optic stalk that connects the optic cup to the developing forebrain and later forms the optic nerve (Fuhrmann, 2010; Graw, 2010). A vast amount of research has contributed to our understanding of different signalling pathways involved in the induction and maintenance of these fates (summarised in Table 3) (Fuhrmann, 2010; Graw, 2010). These patterning and signalling events ultimately determine the expression patterns of specific transcription factors involved in cell fate determination (summarised in Table 3). FGF signalling is important for the RNE fate and induces expression of the homeobox transcription factor Vsx2 (Chx10), which is an established marker for the RNE (Liu et al., 1994; Zou and Levine, 2012). On the other hand, Wnt signalling is important for the RPE fate via suppression of the RNE fate and it activates expression of the RPE-specific transcription factor Mitf and its downstream effectors (Fuhrmann, 2010). As a result of these expression patterns, the distal domain of the optic vesicle develops into the RNE and dorsal proximal domain forms the RPE. Such subdivision is also recapitulated in the *in vitro* retinal organoid cultures (Eiraku et al., 2011; Hasegawa et al., 2016). However, how these patterning signals influence the behaviour of the cells and in turn OCM remains poorly understood. Conversely, it also needs to be investigated, if the morphogenetic processes themselves have a role to establish these patterned domains.

Table 3: Signaling pathways in optic cup morphogenesis

Signaling pathway	Role in optic cup morphogenesis	Reference
Fibroblast growth factor (Fgf) signaling	Specification of retinal neuroepithelial fate and **Vsx2** expression. Proliferation of the retinal neuroepithelium. Naso-temporal axis specification.	(Picker and Brand, 2005; Picker et al., 2009; Pittack et al., 1997) (Horsford et al., 2005; Nguyen and Arnheiter, 2000)
Wnt signaling	Specification of retinal pigment epithelial fate and **Mitf** expression. Repression of the retinal neuroepithelial fate.	(Fujimura et al., 2009; Hagglund et al., 2013; Schepsky et al., 2006; Veien et al., 2008; Westenskow et al., 2009; Yasumoto et al., 2002; Zhou et al., 2008)
Bone morphogenetic protein (BMP) signaling	Dorso-ventral patterning of the optic cup. Imparts dorsal identity and promotes **Tbx5** expression, inhibits **Vax2** expression.	(Adler and Belecky-Adams, 2002; Behesti et al., 2006; Heermann et al., 2015; Pandit et al., 2015; Sasagawa et al., 2002)
Sonic hedgehof (Shh) signaling	Dorso-ventral patterning of the optic cup. Imparts ventral identity. Regulates optic stalk development. Promotes **Pax2** expression.	(Ekker et al., 1995; Macdonald et al., 1995; Mui et al., 2005; Sasagawa et al., 2002; Schwarz et al., 2000; Zhao et al., 2010)
Retinoic acid (RA) signaling	Ventral retina invagination and morphogenesis	(Lupo et al., 2011; Mic et al., 2004; Molotkov et al., 2006; Sasagawa et al., 2002)
Hippo Pathway (Yap/Taz signaling)	Specification of the RPE fate	(Kim et al., 2016; Miesfeld et al., 2015)

1.3.3 Optic cup morphogenesis: Epithelial rearrangements and morphogenetic principles

Along with acquisition of the new fates, the initially similar looking cells of the optic vesicle also adopt new morphologies as they shape the optic cup. These epithelial changes are crucial for proper optic cup architecture and the subsequent eye development. The predominant epithelial rearrangement that occurs during OCM is the invagination of the distal part of the optic vesicle that forms the RNE. This invagination occurs by bending the epithelial layer from the basal side. There are various conflicting models proposed for this invagination process. 1) In case of mouse, it has been proposed that mechanical coupling between the developing lens and the future RNE through filopodia-like connections bends the RNE rather passively in response to the invagination of the lens (Chauhan et al., 2009) (Figure 1.6A). This proposal is based on the observation that optic cup invagination is weaker in *Cdc42* conditional mutant that lacks the filopodial connections (Chauhan et al., 2009). However, it does not explain the residual invagination still observed in the conditional mutant. Additionally, a previous study using chick showed that ablation of the lens placode does not affect the invagination of the optic cup and concluded that the role of the surface ectoderm is limited mainly as a signaling centre at early stages (Hyer et al., 2003). Furthermore, it has been shown in *in vitro* organoid cultures that the optic vesicle epithelium can self-organize into a hemispherical shape even in the absence of any lens-like structure (Figure 1.6B) (Eiraku et al., 2012; Eiraku et al., 2011). Thus, the role of the lens in

invagination seems to be limited than proposed before. 2) Alternatively, in the retinal organoid cultures, the RNE invaginates in response to high cell proliferation in the space confined by the stiff RPE (Figure 1.6B) (Eiraku et al., 2011; Nakano et al., 2012). However, work in zebrafish and *Xenopus* shows that RNE development continues even when cell proliferation is blocked (Harris and Hartenstein, 1991; Kwan et al., 2012). Thus, this model does not seem to function in the *in vivo* scenario. 3) An additional model proposed for mouse OCM is a bimetallic strip model, which proposes the RPE as a major driver of the process of invagination (Carpenter et al., 2015). This model is based on the observations that conditional loss of Wnt signals from the surface ectoderm reduces the proliferation of prospective RPE, affects the RPE architecture and results in perturbed RNE with mild invagination. However, the study also reports accompanying defects in periocular mesenchyme, an important signaling centre (McMahon et al., 2009) and retinoic acid signaling known to play a role in RNE invagination (Lupo et al., 2011; Mic et al., 2004). Therefore, it is not clear whether the observed defects can solely be attributed to the RPE. A new report using chick system predicts that the bimetallic strip model could work, but with the constraint being the ECM (Oltean et al., 2016). Given these conflicting observations, the biological mechanism of optic cup invagination and the underlying cellular dynamics still remain elusive.

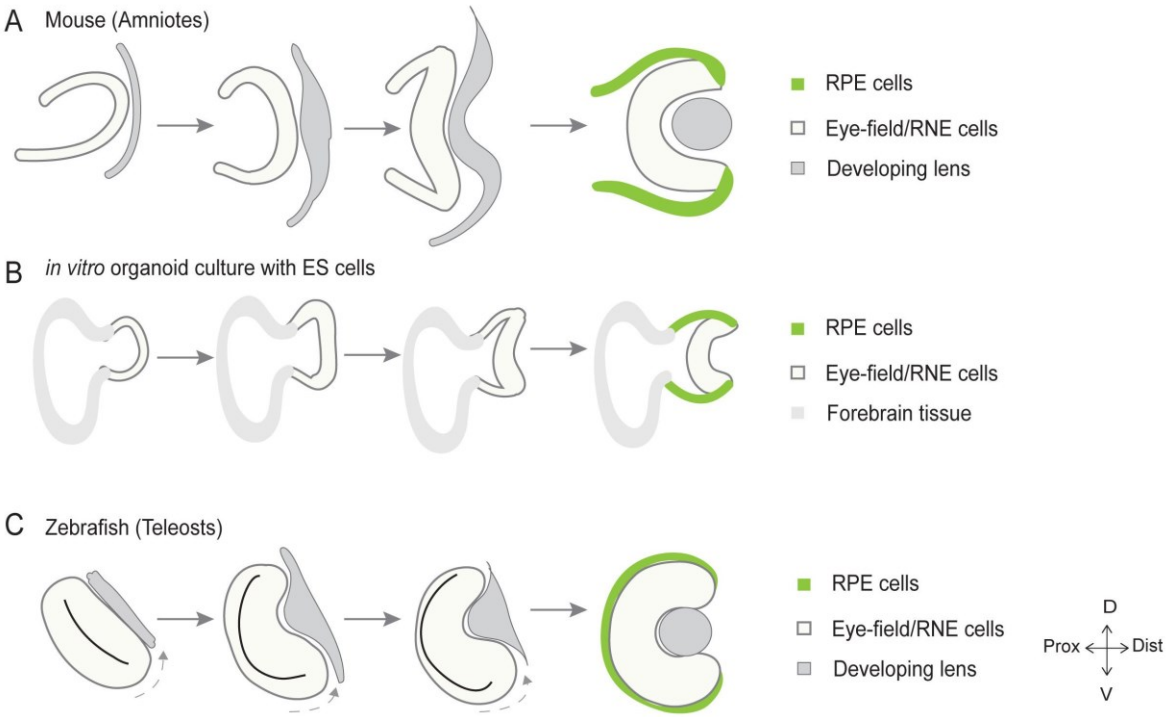

Figure 1.6: Optic cup morphogenesis
Schematic drawing of optic cup morphogenesis in amniotes (A), in *in vitro* cultures of embryonic stem cell aggregates (B), and in teleosts (C). In *in vitro* culture, optic cup forms in absence of the developing lens.

Furthermore, in all vertebrates the invagination of the optic cup is asymmetric. It starts at the dorsal side and progresses towards the ventral side. Such asymmetric invagination creates the choroid fissure and helps in formation of the optic stalk (Bazin-Lopez et al., 2015). However, none of the invagination mechanisms proposed so far can explain this asymmetry in invagination. Therefore, in order to investigate the mechanisms that shape the RNE into a hemisphere it is important to consider this asymmetry. To this end, it is important to study the regional differences in the cell behaviours across the developing optic up that could support such an asymmetric invagination.

An important aspect of studying morphogenesis is visualising the dynamic cell behaviours and the associated molecular changes. Studies based on lineage tracing in the chick and *Xenopus* system have reported occurrence of cell movements in RNE morphogenesis (Holt, 1980; Kwan et al., 2012). Nevertheless, so far, the teleost systems of zebrafish and medaka OCM have provided the most detailed cellular understanding of OCM (Figure 1.6C). Live imaging and cellular tracking of the whole morphogenetic event have revealed presence of several complex cell movements in the process (Heermann et al., 2015; Kwan et al., 2012; Li et al., 2000; Picker et al., 2009). It has been proposed that similar to the role of apical constriction in apical bending of the epithelium, the basal bending of the RNE could be supported by basal constriction of cells (Martinez-Morales et al., 2009). Indeed, cell-ECM contacts located at the basal side are shown to be important for this process. Integrins are the cellular receptors that bind to the ECM and form cell-matrix adhesion. Investigating the medaka mutant *ojoplano* revealed that perturbed trafficking of integrins affects the process of RNE invagination (Bogdanovic et al., 2012; Martinez-Morales et al., 2009). Additionally, a mutant allele for the basal lamina component laminin-α1 shows various defects in the optic cup architecture (Bryan et al., 2016). Both of these studies indicate a role of basal dynamics in the process of optic cup invagination. However, unlike higher vertebrates the teleost optic vesicle is not shaped as a hollow epithelial pouch but rather as an epithelial fold (Figure 1.6C). As a result, a subpopulation of prospective RNE cells is located in the proximal epithelial layer. Therefore, it is not clear whether basal constrictions in the distal part can alone drive RNE morphogenesis or whether the proximal cells play an additional role. These proximally located cells have been observed to move into the distal, invaginating neuroepithelium along the rim of the cup (Heermann et al., 2015; Kwan et al., 2012; Li et al., 2000; Picker et al., 2009). I refer to these cells as ‘rim cells’ and their movement as ‘rim involution’. These rim cells are shown to include the progenitors of the future retinal stem cells, which later localise to a special region in the teleost eye called the ciliary margin zone (Heermann et al., 2015; Tang et al., 2017). However, to date, it remains unclear which molecular mechanisms drive rim involution and whether it is actively involved in RNE

morphogenesis. Taken together, *in vivo* OCM is far from understood and requires further investigation using an experimentally amenable system.

1.4 Aims of the thesis

The main goal of this work is to understand how epithelial morphogenesis shapes complex architectures by investigating the formation of hemispherical RNE. I have approached this question from the morphogenesis angle to understand the cellular dynamics involved in the process. Due to its unmatched imaging potential, the zebrafish is an excellent model to understand *in vivo* organogenesis including OCM at both the cellular and the tissue level. Zebrafish system also allows easy genetic manipulation by microinjections of DNA/RNA constructs and reverse genetic approach by morpholino-mediated knockdown of genes. The ease of transgenesis, cell transplantations and small molecule treatment further make zebrafish an experimentally amenable model system. Lastly and importantly, the faster development of the zebrafish embryos enables easy imaging of the entire OCM event in a living embryo within one experiment. Therefore, I set out to investigate the process of RNE morphogenesis in developing zebrafish embryos.

Aim 1: Verifying the basal constriction hypothesis

The current prevalent hypothesis for zebrafish OCM proposes that basal constriction of neuroepithelial cells drives RNE invagination. Therefore, my first aim was to test the basal constriction hypothesis and if true to understand the cellular mechanisms that drive it.

Aim 2: Understanding rim involution and its potential role in OCM

Many cells move across the rim of the developing optic cup by process of rim involution. However, this process is understudied and it is not clear, if these cells move passively or actively, and if they move as individual cells or as a collective. Therefore, I aimed to characterise and to understand the cellular mechanism of rim involution. Furthermore, the role of such cell movement remains unknown. Hence my next goal was to decipher the role of rim involution by investigating the impact of perturbed rim involution on OCM.

Aim 3: Understanding collective effect of different epithelial rearrangements in OCM

Morphogenesis of many epithelial structures involves collective action of different epithelial rearrangements. Interestingly, the different epithelial rearrangements seen during OCM occur at different regions of a single continuous epithelium. Therefore, I aimed to understand how the different epithelial rearrangements that occur during zebrafish RNE morphogenesis cooperate to achieve efficient and timely OCM.

2. Results

The vertebrate retinal neuroepithelium (RNE) has a characteristic hemispherical architecture that shapes and defines the optic cup and lays the foundation for the subsequent eye development. Its formation involves complex epithelial morphogenesis. However, the cellular basis of the epithelial rearrangements is not yet completely clear. Therefore, using the developing zebrafish embryo as a model system, I set out to understand the cellular dynamics driving this morphogenetic event. My experimental workflow followed the common framework of morphogenesis studies aptly summarised in a review by Osterfield et al. (Osterfield et al., 2017). I began with documenting and measuring the cell and tissue level changes occurring in the developing RNE, followed by characterising the localisation of key components of the molecular toolkit of the cells (See section 1.2). Lastly, based on these observations, I investigated the underlying cellular mechanisms through genetic and chemical perturbations of the morphogenetic process.

2.1 Zebrafish optic cup morphogenesis: complex cellular rearrangements shape the retinal neuroepithelium.

The oviparous development and transparency of the developing zebrafish embryos allowed easy microscopic recording of the entire process of optic cup morphogenesis (OCM). In zebrafish embryos, OCM begins soon after the evagination of the optic vesicles at around 16 hours post fertilisation (hpf) or 15 somite stage (15 ss) (Kwan et al., 2012). The optic vesicle in the zebrafish embryos is shaped as an epithelial fold, with the eye-field neuroepithelium folded onto itself. This creates two tightly apposed layers with their apical sides facing inwards (Figure 2.1). During OCM, this epithelial fold transforms into a hemisphere through elaborate epithelial rearrangements (Kwan et al., 2012). A transgenic line, which labels the cells with a membrane marker (HRAS-GFP) allowed me to visualise these cellular rearrangements (Figure 2.1A, Movie 1). The cells in the distal layer (brown) began the epithelial folding or invagination (Figure 2.1). Simultaneously, the cells in the proximal layer also showed rearrangements. A group of cells (blue) located at the rim of the developing optic cup, hence called rim cells, moved along the rim into the invaginating layer. This movement is similar to the morphogenetic movement commonly referred to as involution (Solnica-Krezel, 2005), hence called ‘rim involution’ (Figure 2.1). It should be noted that the rim involution was more prominent on the ventro-temporal side of the optic cup than the nasal side (Figure 2.1, Movie 1). Simultaneously, a small group of cells underwent epithelial thinning and formed the outer layer of the squamous retinal pigment epithelium. Thus, I could capture the entire morphogenetic event, which is completed by 24 hpf or 30 ss and I

could observe the different epithelial rearrangements reported before (Heermann et al., 2015; Kwan et al., 2012; Picker et al., 2009). Importantly, the entire developmental event occurred in a timeframe similar to the wild-type development, using both the light sheet microscope as well as the spinning disk confocal microscope. Therefore, these initial experiments helped me to establish the sample mounting and imaging system and to choose the right developmental time windows to understand the cellular dynamics of this morphogenetic event.

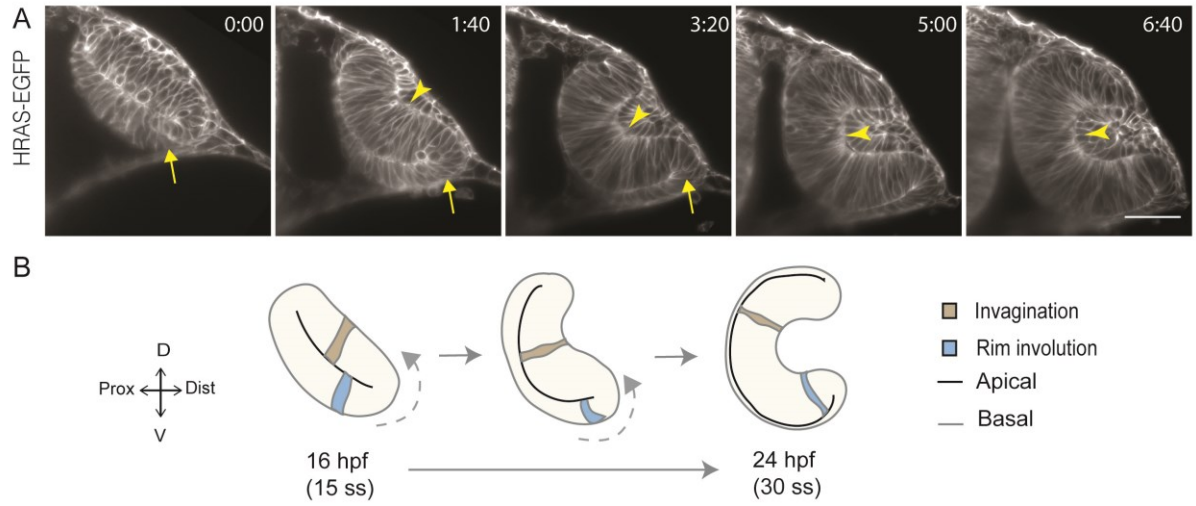

Figure 2.1: Epithelial rearrangements during RNE morphogenesis in zebrafish embryos.
A) Time-lapse imaging of RNE morphogenesis in membrane marker line Tg*(actb1:HRAS-EGFP).* Invagination (Arrowhead). Rim involution (Arrow). Movie started around 15 ss. Time in h:min. Frames from Movie 1. Scale bar = 50 µm.
B) Schematic representation of RNE morphogenesis from 15 ss to 30 ss showing RNE cells that undergo invagination (brown) and rim cells undergoing involution (blue). Direction of the rim involution (dashed arrow).

2.2 Invagination of the retinal neuroepithelium involves basal cell surface reduction

The major epithelial rearrangement occurring during OCM is the invagination or inward bending of the distal layer of the optic vesicle (Figure 2.2A). Invagination of epithelial sheets is driven by cell shape changes that expand/shrink one side of the epithelial layer with respect to the other (Davidson, 2012). Most of the well-studied invagination phenomena feature apical bending of the epithelial sheet guided by apical constriction of cells (Pearl et al., 2017). However, the morphogenesis of the RNE involves basal folding of the epithelium (Figure 2.2A). Therefore, it was proposed that basal constriction of cells drives retinal invagination and formation of the hemispheric optic cup (Martinez-Morales et al., 2009). To test this idea, I analysed the shape of the invaginating neuroepithelial cells during OCM. I labelled the cell outlines by staining the cell cortex with F-actin marker phalloidin to visualise and measure the apical and basal area of the invaginating cells. I found that the cell density

at the basal side of the neuroepithelium increased over time (Figure 2.2B,C). Accordingly, the average basal area of the cells reduced by about 45%. This reduction occurred during the initial phase of OCM until around 21 ss (Figure 2.2D). Concurrently, the average apical area of the cells increased (Figure 2.2E). Thus, the invaginating cells underwent an overall shape change from apically narrower to basally narrower wedge shape. Similar results were also recently reported by Martinez-Morales group using live imaging of the invaginating cells (Nicolás-Pérez et al., 2016). These observations confirmed that the invaginating RNE cells undergo basal shrinkage, which potentially drives retinal invagination and OCM.

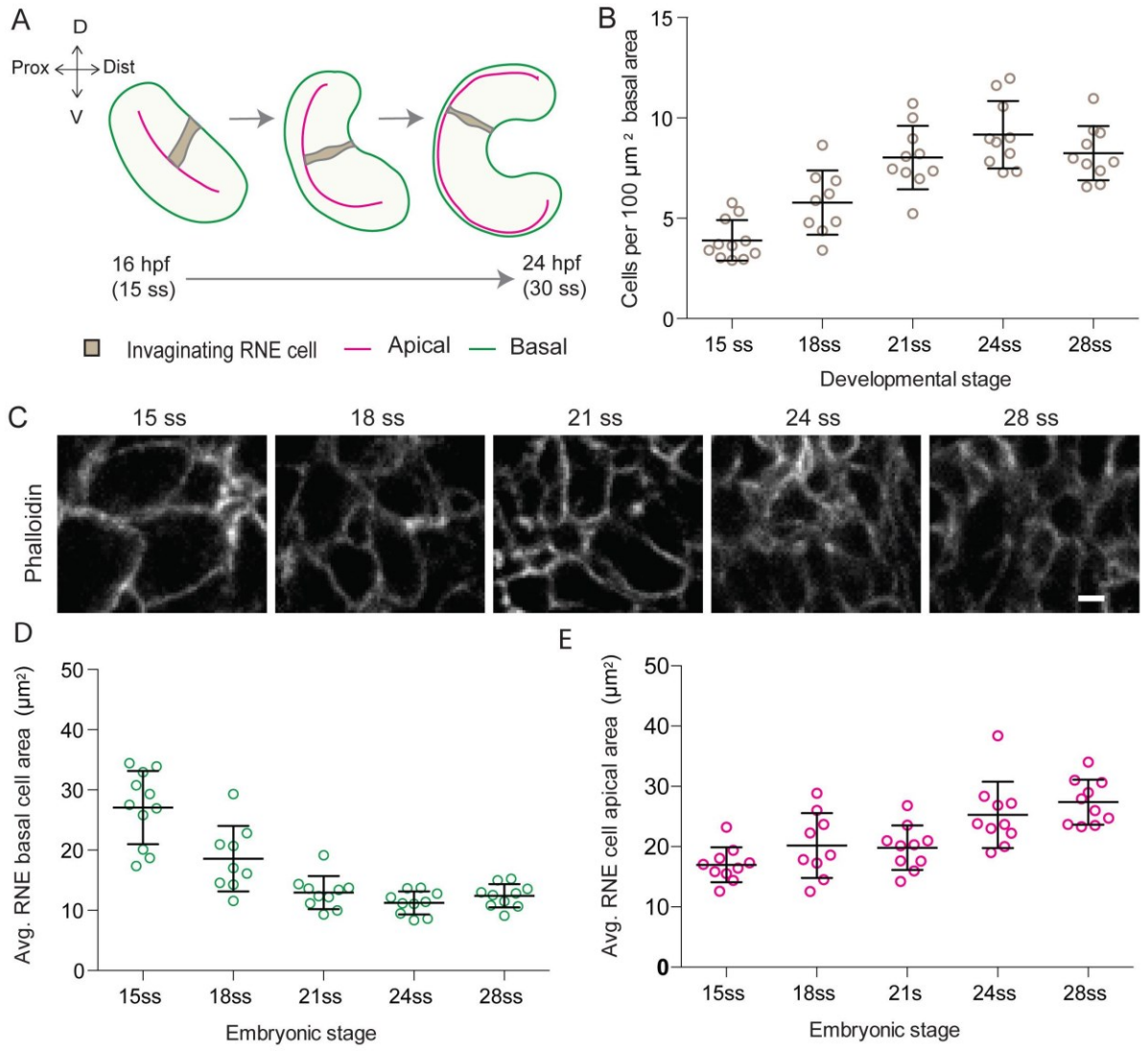

Figure 2.2: Analysis of basal and apical area of invaginating RNE cells

A) Schematic representation of RNE morphogenesis from 15 ss to 30 ss showing RNE cells that undergo invagination (brown).

B) Average number of cells per 100 µm^2 basal area of RNE at different stages of development. Mean±SD, N ≈ 10 embryos each.

C) Confocal scans of the basal side of the RNE cells stained with phalloidin at different developmental stages. Scale bar = 2 µm.

D,E) Average area of RNE cells at basal (D) and apical (E) sides during RNE morphogenesis with mean±SD. N ≈ 10 embryos.

2.3 Invagination of the retinal neuroepithelium involves basal accumulation of contractile actomyosin

Next, I investigated which molecular mechanisms could drive the basal cell shrinkage and in turn the invagination of the RNE. Constriction mechanisms often involve preferential localisation and action of contractile actomyosin at the shrinking side of the epithelial cells (Davidson, 2012; Martin and Goldstein, 2014). To check if there was any preferential localisation of actomyosin at the basal side of the RNE cells, I visualised actomyosin dynamics during OCM. Live imaging of embryos expressing F-actin marker GFP-UtrophinCH (Burkel et al., 2007) or myosin marker myl12.1-GFP (Iwasaki et al., 2001) revealed an enrichment of both markers at the basal side of the cells, specifically in the invaginating zone (Figure 2.3A,B, Movie 2). Such basal enrichment was not observed in other parts of the developing optic cup, such as the developing RPE or the rim zone, where the epithelium folded (Figure 2.3A,B, Movie 2). This observation was corroborated by immunostainings using the F-actin marker phalloidin and anti-phosphomyosin antibody (Figure 2.4A). The anti-phosphomyosin antibody marks the phosphorylated form of myosin that is active and contractile (Matsumura, 2005). Thus, the staining further confirmed that the basally enriched actomyosin was contractile. A quantification of the intensity distribution of the actomyosin markers in a 3D tissue volume showed that the actomyosin enrichment was localised to about 15% of the cell height from the base (Figure 2.4B-D). Taken together, these results showed that the invaginating RNE cells accumulate contractile actomyosin at their basal side as they undergo basal shrinkage and as the tissue invaginates.

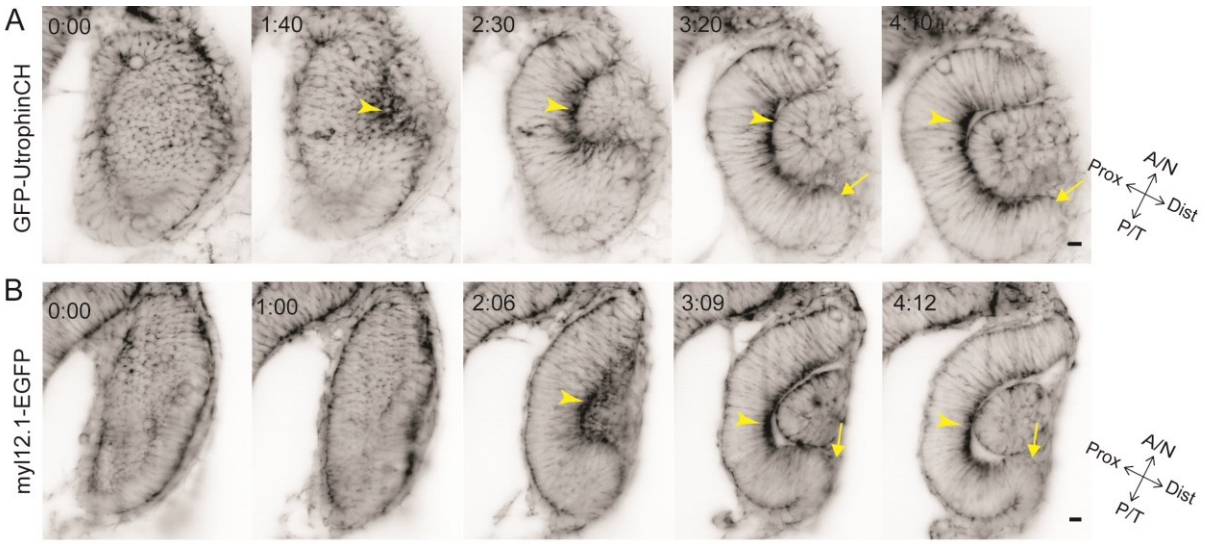

Figure 2.3: Analysis of actomyosin localisation during RNE morphogenesis.
A,B) Time-lapse imaging of RNE morphogenesis in actin marker line Tg(*bactin::GFP-UtrophinCH*) (A) and myosin marker line Tg(*bactin::myl12.1-EGFP*) (B). Basal enrichment in RNE (Arrowhead). Rim zone lacking basal enrichment (Arrow). Movies started around 15 ss. Time in h:min. Frames from Movie 2. Scale bar = 10 µm.

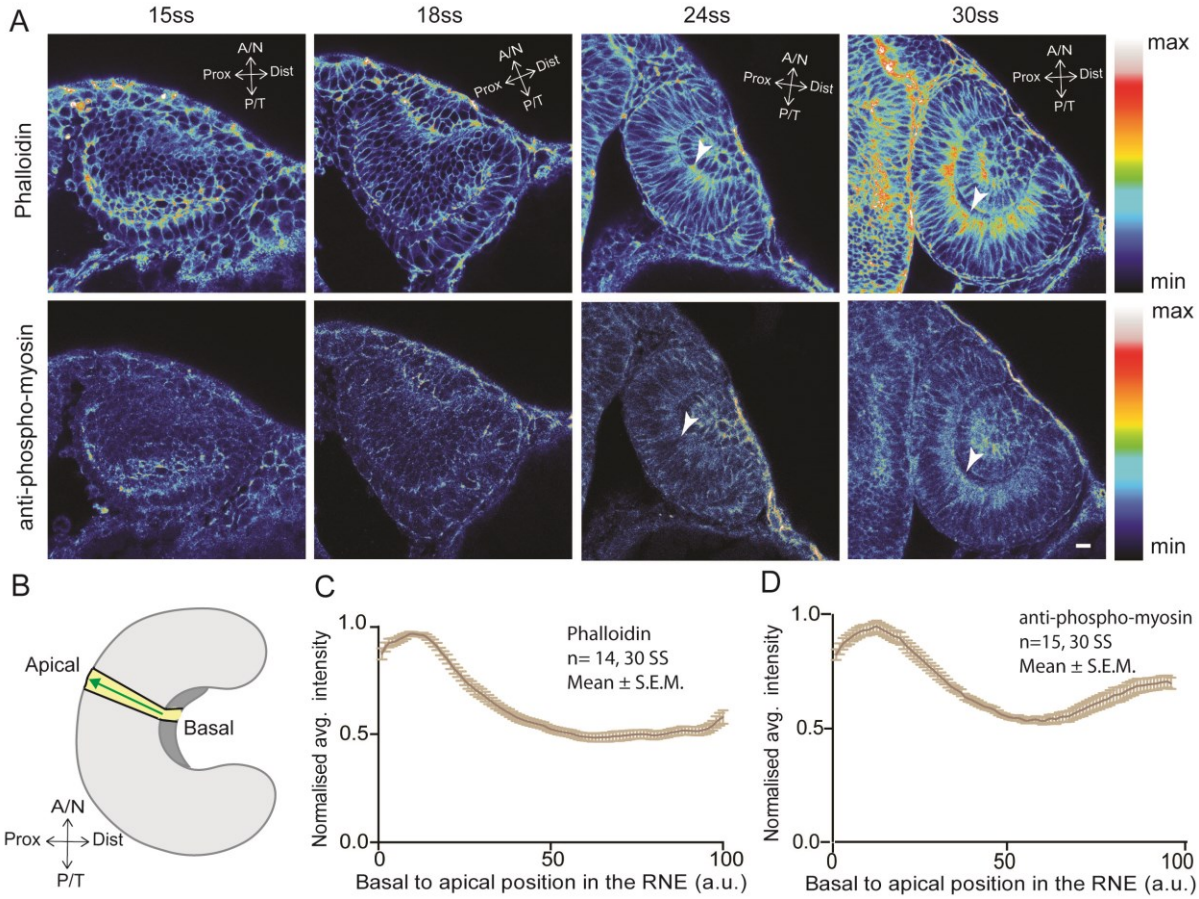

Figure 2.4: Analysis of actomyosin distribution during RNE invagination.
A) Confocal scans of different stages of RNE morphogenesis stained for phalloidin and phosphomyosin. Basal enrichment (Arrowhead). Scale bar = 10 µm.
B) Schematic drawing of a typical tissue volume used for actomyosin intensity distribution analysis (yellow). The average intensity was measured from basal to apical side of the tissue volume (green arrow) and normalised to the highest intensity value along the axis.
C,D) Normalized average intensity distributions of phalloidin (C) and phosphomyosin (D) in the tissue volume along the apicobasal axis of the RNE at 30 ss. Mean±SEM. Tissue sections, n = 14 for phalloidin and n = 15 for phosphomyosin; N = 5 embryos.

2.4 Actomyosin driven basal constriction accelerates invagination process but is not the main driver of RNE morphogenesis

Asymmetric actomyosin contractility is shown to sufficiently drive various invagination phenomena (Pearl et al., 2017). Therefore, I hypothesized that the basal enrichment of contractile actomyosin drives retinal invagination and OCM. Accordingly, a disruption of the basal actomyosin network should inhibit invagination and OCM. To test this hypothesis, I treated the embryos with 50 µM blebbistatin, a potent inhibitor of myosin-II contractility (Straight et al., 2003), that blocks myosin in an actin-detached state (Kovacs et al., 2004). However, the prolonged blebbistatin treatment severely affected the overall embryonic

development, including the developing eye (data not shown). Not surprisingly, such broad myosin-II inhibition induced severe cell death (data not shown), given the role of actomyosin in interkinetic nuclear migration in the neuroepithelium (Norden et al., 2009; Strzyz et al., 2015) and its requirement for cytokinesis (Straight et al., 2003). Therefore, this is not a good approach to investigate the role of basal actomyosin in the retinal invagination.

Hence, instead of broad inhibition of overall myosin activity, I focused on the specific rho-kinase (ROCK) regulated actomyosin contractility. ROCK phosphorylates the regulatory light chain of myosin II and thus activates the actomyosin contractility (Amano et al., 1996). I used a chemical inhibitor of ROCK, Rockout, that acts as a competitive inhibitor of myosin phosphorylation by competing with ATP (Yarrow et al., 2005). A dose-response experiment at different concentrations of Rockout revealed that low concentration of 50 µM did not have obvious morphological phenotypes. In contrast, treatment with 150 µM concentration resulted in severe cell death. Therefore, 100 µM concentration was chosen for the treatment. The treatment was started around 13–14 ss, a timepoint when the optic vesicle is evaginated, so as to give sometime for the drug to penetrate and act at the right stages of retinal invagination. Upon 7 h long Rockout treatment, the basal actomyosin enrichment was markedly reduced, without disrupting the whole tissue architecture (Figure 2.5A,B,C,D). The overall anti-phosphomyosin staining was also weaker in the treated embryos, confirming the action of the drug (Figure 2.5B,D). In spite of the reduction in the basal actomyosin enrichment, the effect on the morphology of the optic cup was surprisingly weak. When I scored the embryos for the phenotypic effects, I observed that 40% of embryos showed an accumulation of cells at the rim of the cup, whereas 30% of embryos showed a milder optic cup phenotype (n=30 embryos per experiment, N=5 experiments) (Figure 2.5A). Remaining 30% of embryos showed stalled development and were thus excluded from the analysis. To assess the effect of basal actomyosin perturbation on the extent of invagination, I measured the angle of invagination: the angle held by the inner lips of the optic cup at the centre of the RNE (see schematic, Figure 2.5E). The invagination angle was moderately wider in the Rockout treated embryos than the control embryos (Figure 2.5E), indicating that the invagination process was not as efficient in the Rockout treated embryos. Nevertheless, RNE invagination was initiated and was not inhibited upon marked reduction in the basal actomyosin enrichment.

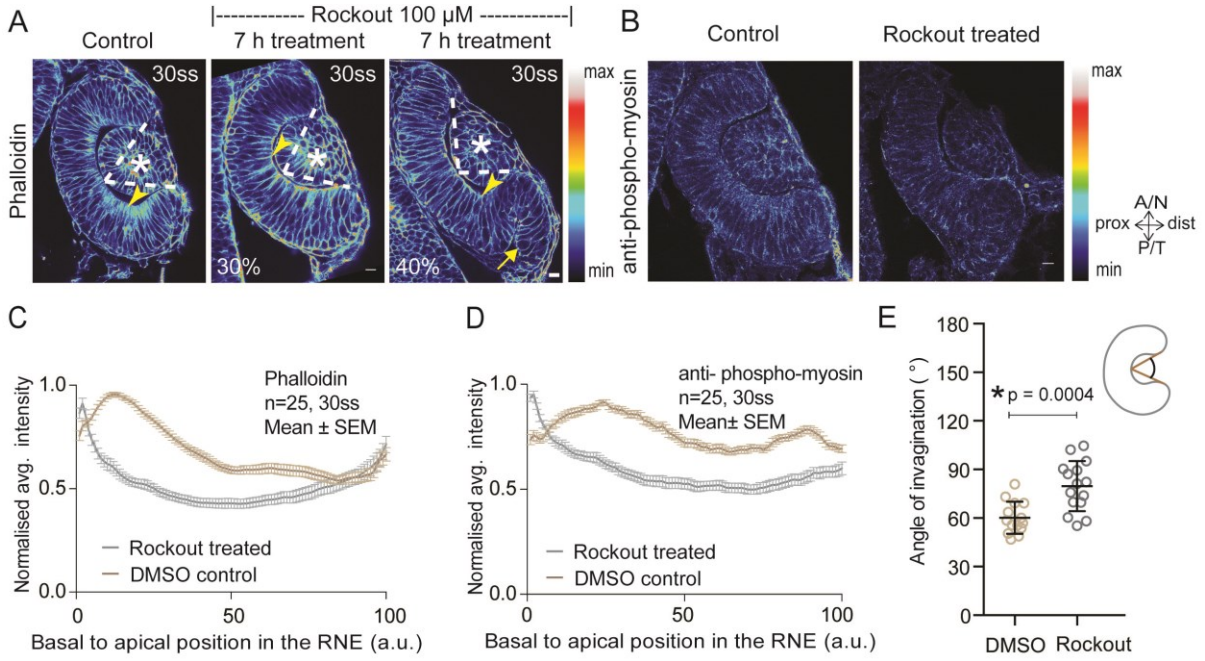

Figure 2.5: Effect of Rockout treatment on the RNE

A) Confocal scan of optic cup at 30 ss stained for phalloidin. Control (left), phenotypes after 7 h of Rockout treatment: mild invagination defect in 30% embryos (middle), invagination defect with epithelial accumulation in 40% embryos (right), (n = approx. 30 embryos, N = 5 experiments). Basal side of the RNE (Arrowhead). Epithelial accumulation outside the RNE (Arrow). Developing lens (Asterisk). Angle of invagination (Dashed line).

B) Confocal scan of 30 ss RNE in control (left) and Rockout treated (right) embryo stained for phosphomyosin.

C,D) Normalized average intensity distributions of phalloidin (C) and phosphomyosin (D) in the tissue volume along the apicobasal axis of the RNE at 30 ss. Mean±SEM. Control (brown), Rockout treated (grey). Tissue sections, n = 25; N = 5 embryos.

E) Invagination angle at 30 ss. Mean±SD. The schematic shows the invagination angle as the angle held at the base of central RNE by the inner lips of the optic cup. Mann-Whitney test, p = 0.0004.

All scale bars = 10 µm. Rockout treatment was performed for 7 h starting from 13-14 ss.

To better understand the effect of reduced basal actomyosin enrichment on invagination, I performed live imaging of RNE morphogenesis in control and Rockout treated embryos labelled with GFP-UtrophinCH. Use of a chambered glass-bottom dish allowed me to mount the Rockout treated and control embryos in separate chambers of the same dish and to treat them with the respective media, while being imaged simultaneously on the same microscope set-up. The simultaneous imaging revealed that in spite of the reduced basal enrichment of actomyosin, the RNE did invaginate in the Rockout-treated embryos, although with slower kinetics (Figure 2.6A, Movie 3). Similar slower kinetics were also revealed upon analysing the change in the basal cell surface area over different stages of OCM using fixed samples (Figure 2.6B). However, the cell area analysis indicated that at the end of OCM (30ss), the basal surface area of the invaginated cells was similar in control and Rockout-treated embryos (Figure 2.6B). Thus, these results indicated that the basal actomyosin mainly makes the process of invagination faster and efficient to ensure timely morphogenesis

(Figure 2.6C). However, it is not the sole driver of invagination. This argued for the role of additional factors that guide the invagination of the RNE.

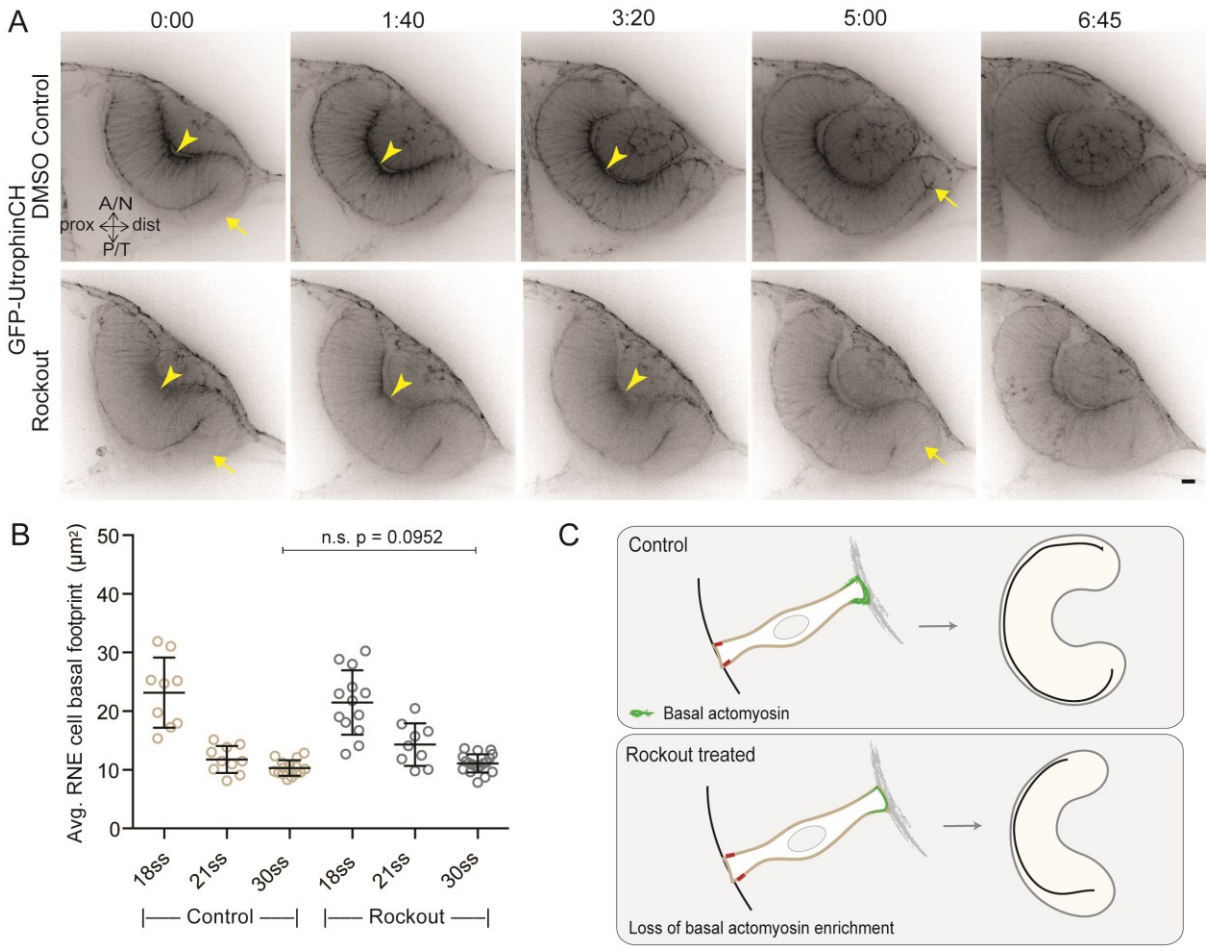

Figure 2.6: Effect of Rockout treatment on progression of RNE morphogenesis
A) Time-lapse of RNE morphogenesis in DMSO Control (upper) and Rockout-treated (lower) embryos expressing actin marker GFP-UtrophinCH. N = 5 embryos each. Rockout treatment was started 2 h before imaging around 13–14 ss. Imaging started at around 18 ss. Both movies were imaged simultaneously and under identical imaging conditions. Scale bar = 10 µm. Time in h:min. Frames from Movie 3.
B) Average basal area of RNE cells with mean±SD. Each dot represents an embryo. Mann-Whitney test for 30 ss p = 0.0952.
C) Schematic drawing showing role of basally enriched actomyosin in regulating timing of invagination.

2.5 Cell proliferation has limited role in RNE morphogenesis

Alternative to the cell intrinsic contractile mechanism, cell shape changes and invagination can also be aided passively by crowding-induced compaction by the neighbouring cells in the epithelial layer (Davidson, 2012). An increase in the number of cells inhabiting the RNE could support such crowding and hence compaction. One way to increase the number of cells in the sheet is cell proliferation. Indeed, development of the RNE is accompanied with

high cell proliferation (Kwan et al., 2012). Furthermore, such proliferation based mechanism has been suggested to drive optic cup formation in *in vitro* retinal organoids (Eiraku et al., 2012; Eiraku et al., 2011). In the proposed mechanism, high proliferation in a physically confined space forces the epithelial sheet to buckle and bend. Indeed, blocking proliferation inhibits the process of the *in vitro* optic cup formation (Eiraku et al., 2011). However, experiments in zebrafish and *Xenopus* have shown that inhibition of proliferation influences the size of the optic cup but does not prevent the invagination of the RNE (Kwan et al., 2012; William A. Harris, 1991).

Nevertheless, the previous studies did not analyse the basal shrinkage of the RNE cells. Therefore, it is not clear if the proliferation based mechanism influences the basal shrinkage during invagination of the RNE. To test this, I analysed the effect of proliferation inhibition on the basal shrinkage of the RNE. Cell proliferation was blocked using hydroxyurea (HU) and aphidicolin (Aphi), known cell cycle blocking agents (Ikegami et al., 1978; Young and Hodas, 1964), from 10ss onwards. The efficacy of the treatment was assessed by staining with mitotic marker pH3. The treated embryos indeed showed a marked reduction in pH3 staining (Figure 2.7A). In line with the previous report (Heermann et al., 2015; Kwan et al., 2012), the neuroepithelium still underwent invagination and the angle of invagination was comparable to that of the control, in spite of the reduced proliferation (Figure 2.7B,C). Additionally, this treatment did not affect the basal actomyosin enrichment, which was similar to the controls (Figure 2.7F,G). This raised the question of what makes RNE invagination robust? To test if basal actomyosin and proliferation were acting together to make the process robust, I combined the Rockout and HU + Aphi treatment. However, the combined treatment was lethal for the embryos and therefore, I could not assess the role of basal actomyosin in the cell proliferation inhibition condition.

Nevertheless, upon taking a closer look at the cellular morphologies of the RNE cells in the HU and Aphi treated embryos, I observed that the cells exhibited rather columnar morphology with an average basal area wider than the control condition (Figure 2.7B,D,E). This observation indicated that the cell shapes and basal surface area are not solely dependent on the actomyosin enrichment at the basal side of cells but are also influenced by the total number of cells in the invaginating RNE. It further suggests that the basal shrinkage of the neuroepithelium includes contribution by crowding-induced compaction. However, in the reduced proliferation condition, RNE can invaginate even when cells show broader basal area. Therefore, it was important to test the crowding-induced compaction hypothesis using other methods. It raised the question, if any other process could support crowding and compaction of the RNE.

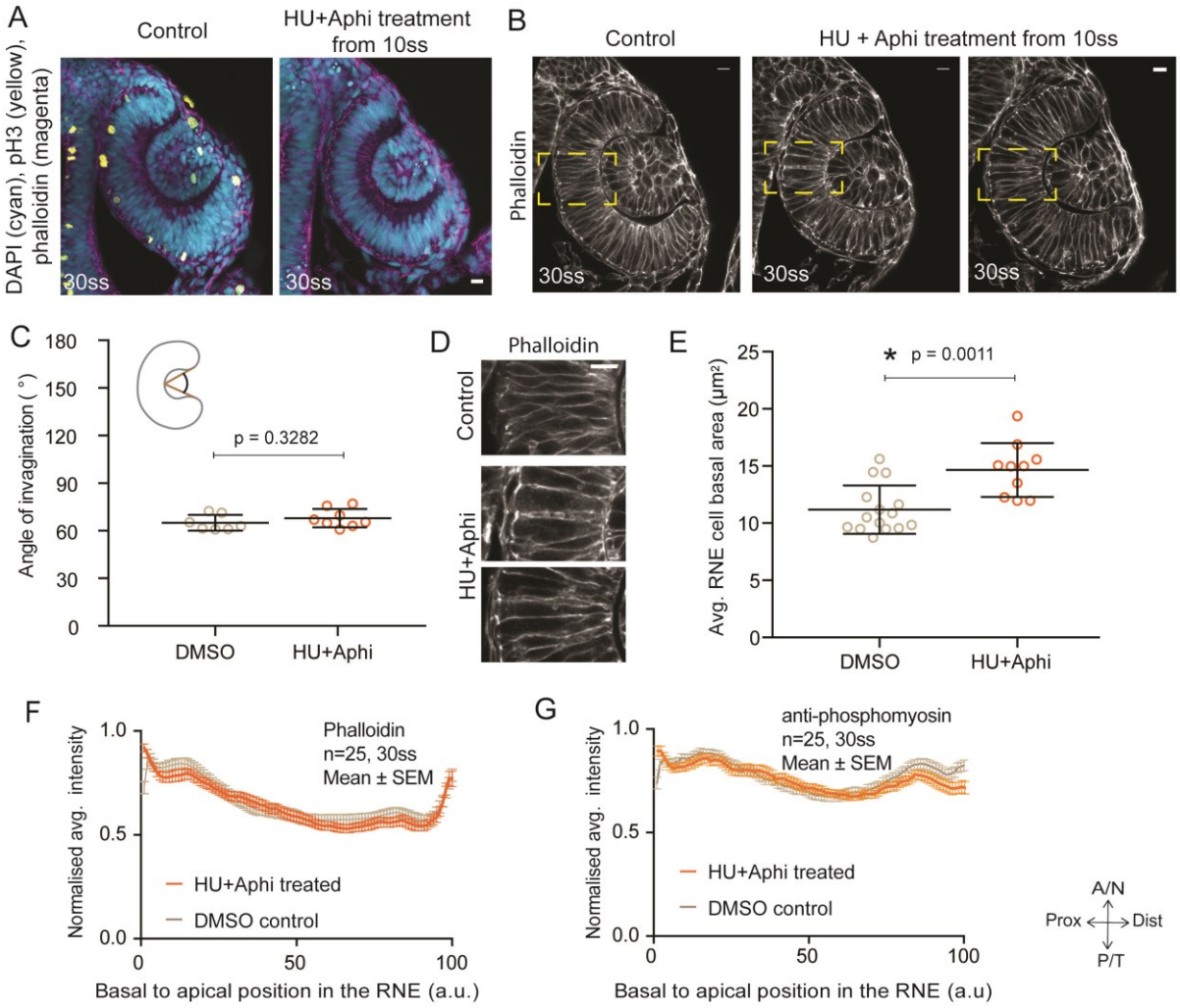

Figure 2.7: Effect of Hydroxyurea and aphidicolin treatment on RNE morphogenesis

A) Confocal scans of 30 ss RNE in control (left) and HU+Aphi treated (right) embryos stained for DAPI (cyan), mitotic marker phosphohistone-3 (yellow) and phalloidin (magenta).

B) Confocal scans of 30 ss RNE in control (left) and HU+ Aphi-treated (middle and right) embryos stained with phalloidin. Areas marked by yellow box are shown in D.

C) Invagination angle at 30 ss. Mean±SD. The schematic shows the invagination angle as the angle held at the base of central RNE by the inner lips of the optic cup. Mann-Whitney test p = 0.3282.

D) Confocal scans of RNE cells stained with phalloidin (zoomed images of regions marked in B. Control (top), HU+Aphi treated (middle and bottom).

E) Average basal area of RNE cells with mean±SD. Each dot represents an embryo. Mann-Whitney test p = 0.0011.

F,G) Normalized average intensity distributions of phalloidin (F) and phosphomyosin (G) in the tissue volume along the apicobasal axis of the RNE at 30 ss. Mean±SEM. Control (brown), HU+Aphi treated (orange). Tissue sections, n = 25; N = 5 embryos.

All scale bars = 10 µm.

2.6 RNE morphogenesis involves active cell migration at the rim of the optic cup

Next, I investigated which additional mechanisms could support the crowding and compaction in the RNE. Apart from proliferation, the number of cells can also be increased by displacing more cells into the invaginating layer. Indeed, previous studies have reported movement of cells from the proximal layer to the distal layer along the rim of the developing optic cup, a process called rim involution (Figure 1, Figure 2.8A) (Heermann et al., 2015; Kwan et al., 2012; Li et al., 2000; Picker et al., 2009). Rim involution does not occur uniformly along the rim of the developing optic cup but predominantly along the ventral and temporal rim (Heermann et al., 2015; Kwan et al., 2012; Picker et al., 2009). This suggests that rim involution is not merely a passive response to the symmetric pulling force of invagination. Supporting this argument, rim involution continued in the Rockout treated embryos, which lacked basal actomyosin enrichment (Figure 2.6A, Movie 3). Rim involution has been shown to translocate a substantial number of cells to the invaginating neuroepithelium (Picker et al., 2009). Furthermore, rim involution is also shown to continue in embryos treated with the cell proliferation inhibitors (Heermann et al., 2015). Therefore, rim involution may support the crowding-induced compaction and invagination of the RNE. Furthermore, it could possibly explain the continued invagination in Rockout-treated and proliferation-inhibited embryos. However, the cellular dynamics underlying rim involution were unknown and needed to be investigated in order to address the role of rim involution in the process of optic cup formation. Therefore, I first set out to characterise the cellular dynamics during rim involution.

During the process of optic vesicle formation, cells attain the epithelial polarity and form a fold of opposing short pseudostratified epithelia (Ivanovitch et al., 2013). In line with this observation, the rim cells at the fold localised the centrosomes and primary cilia at the apical side, which formed the interface between the two epithelial layers (Figure 2.8B). Additionally, these cells were proliferative and underwent apical mitoses as seen for other pseudostratified epithelia (Strzyz et al., 2016) (Figure 2.8B, C). Live imaging of rim cells marked with apical marker Par3-GFP showed that the cells were apico-basally polarised and the polarity was maintained throughout the involution process (Figure 2.8D, Movie 4). Furthermore, the cells maintained an apical actin pool associated with the adherens junctions as revealed by live imaging using the actin marker GFP-Utrophin (Figure 2.8E, Movie 4), indicating that these cells were part of a continuous epithelial sheet. Thus, rim cells exhibited pseudostratified epithelial morphology, epithelial cell-cell adhesion and polarity.

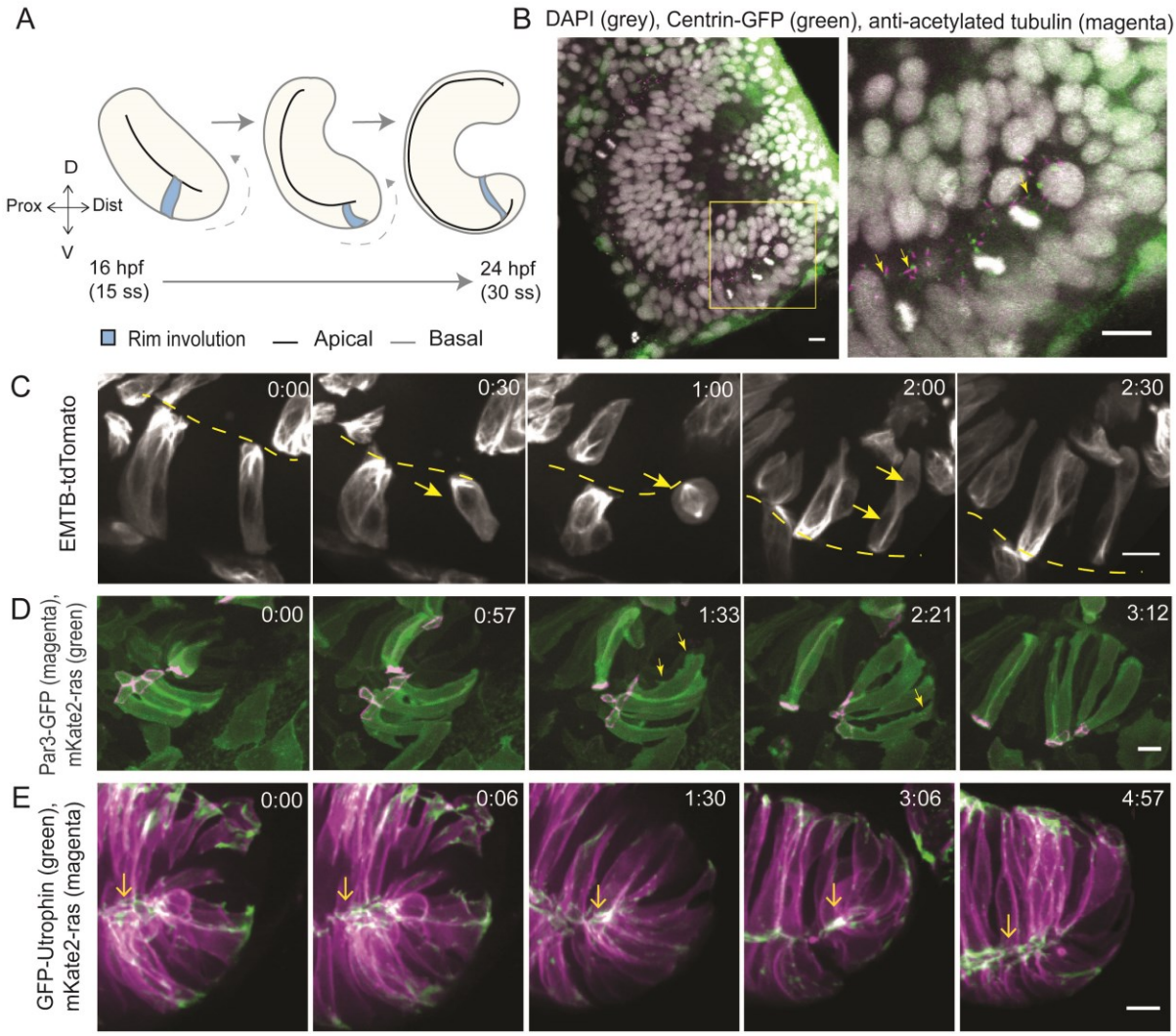

Figure 2.8: Cellular characterisation of rim cells.
A) Schematic representation of RNE morphogenesis from 15 somite stage (ss) to 30 ss showing cells that undergo rim involution (blue). Direction of involution (dashed arrow).
B) Confocal scans of rim zone in 21 ss embryo stained for DAPI (grey), centrosome marker centrin-GFP (green) and acetylated tubulin (magenta). Zoom-in image of the area marked by yellow box (right). Primary cilia (arrow).
C) Time-lapse imaging of rim zone with mosaic expression of EMTB-tdTomato. Cell dividing during rim involution (Arrow). Apical side (Dashed line). N = 4.
D) Time-lapse imaging of rim zone with mosaic expression of Par3-GFP and mKate2-ras. Membrane protrusions (Arrow). Frames from Movie 4. N = 5.
E) Time-lapse imaging of rim zone with mosaic expression of GFP-UtrophinCH and ras-mKate2. Apical actin localization at adherens junctions (Arrow). Frames from Movie 4. N = 6.
All scale bars = 10 µm. All movies started around 17–18 ss. Time in h:min.

The above observations showed that rim cells were epithelial in nature. But it remained unclear how they moved along the rim of the cup. To answer this question, I investigated the potential cellular features that could move these polarised epithelial cells along the rim of the cup. mRNA injections at 16–32 cells stage allowed me to sparsely label the cells in the optic

vesicle and to visualise the dynamics of the marked cellular components. Live imaging of the membrane dynamics during rim involution using mKate2-ras marker showed that in comparison to the apical side, the basolateral side of the rim cells was highly dynamic and cells formed dynamic basal membrane protrusions (Figure 2.8D, movie 4). In order to understand the molecular basis of these basal dynamics, I investigated the cytoskeletal dynamics during rim involution. Microtubules did not show any major rearrangement during the involution process, suggesting a limited role in rim involution (Figure 2.8C). In contrast, live imaging of actin marker GFP-UtrophinCH revealed that the basal protrusion in rim cells were actin rich, similar to the lamellipodial/filiopodial protrusions (Figure 2.9A, Movie 5). This suggested that the epithelial rim cells use basal protrusive activity to move along the rim and involute. Therefore, I asked if these protrusions were polarised in any direction. To this end I counted the number of protrusions at the basal side of the cell at the leading edge facing the invaginating region and the opposite trailing edge (Figure 2.9C). The analysis revealed that the basal protrusions were indeed preferentially extended in the direction of movement, at the leading edge of the cell (Figure 2.9C,D). Notably, the directed protrusive activity was not affected in the Rockout-treated embryos (Figure 2.9E,F, Movie 6). These results indicated that the rim cells use directed membrane protrusions to support their directional movement during rim involution. Directed actin-based protrusions and rearward myosin contractility are used by variety of actively migrating cells for their locomotion (Vicente-Manzanares et al., 2009). Therefore, I probed the myosin dynamics at the basal side of rim cells. Indeed, myosin marker DD-myl12b-GFP formed dynamic foci at the basal side (Figure 2.9B, Movie 7). Thus, while being integrated in the epithelial layer, rim cells exhibited migratory behaviour and actively extended directed protrusion in the direction of migration.

Importantly, the migratory behaviour was restricted only to the rim zone. Upon entering the invaginating layer, the basal dynamics of these cells changed dramatically. The protrusive activity ceased and actomyosin markers localised stably at the basal side similar to the invaginating RNE cells (Figure 2.9A, B, Movie 4, 5,7).

Taken together, these results suggest that the rim cells use active migratory behaviour to move along the epithelial fold or rim of the cup as a collective to reach the inner invaginating layer. This indicates a collective epithelial migration-like phenomenon. At this stage, these cells showed epithelial features of polarity and adhesion as well as mesenchymal-like active migratory behaviour. However, this behaviour changed once the cells resided in the RNE where they attained a stable epithelial state.

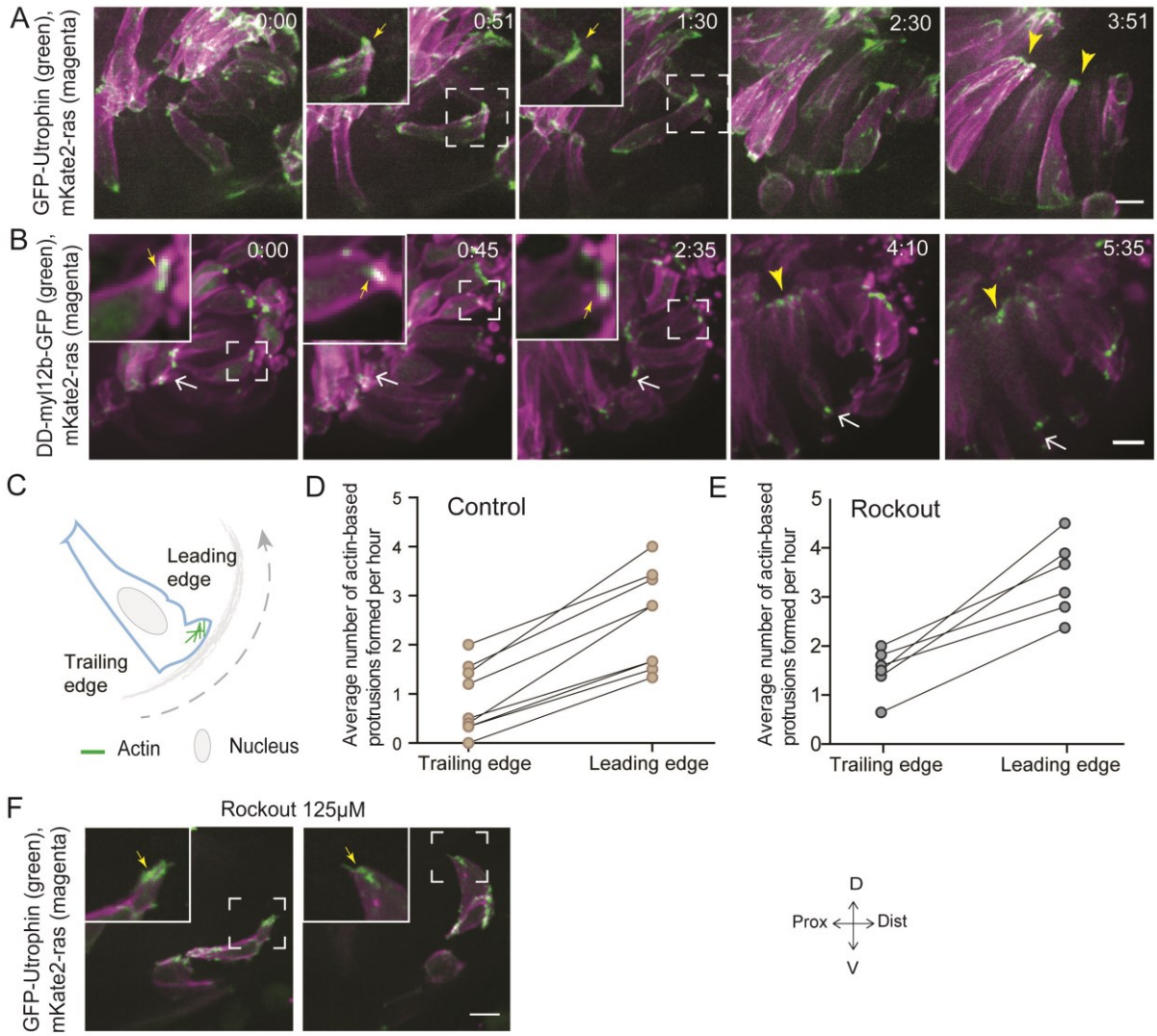

Figure 2.9: Cellular characterisation of rim cells and the protrusive activity.
A) Time-lapse imaging of rim zone with mosaic expression of GFP-UtrophinCH and ras-mKate2. Inlays show zoomed marked area. Actin localization in the protrusions (Arrow). Basally enriched stable actin pool in the RNE (Arrowhead). Frames from Movie 5. N = 6.
B) Time-lapse imaging of rim zone with mosaic expression of DD-myl12b-GFP and mKate2-ras. Inlays show zoomed marked area. Basal myosin punctae in the rim cells (Yellow arrow). Adherens junctions (White arrow). Basally enriched stable actin pool in the RNE (Arrowhead). Frames from Movie 7. Imaging started at 15–16 ss. N = 5.
C) Schematic of a rim cell exhibiting actin-based protrusions at the basal side. The arrow marks the direction of involution. The leading and lagging edges indicate the sides referred in (D) and (E).
D) Number of actin protrusions observed per hour in the rim cell in control condition. Each pair of datapoints represents two sides of the same rim cell. n = 9 cells from 6 different embryos.
E) Number of actin protrusions observed per hour in the rim cell in Rockout treatment condition. Each pair of datapoints represents two sides of the same rim cell. n = 6 cells from 6 different embryos.
F) Confocal scan of rim zone in Rockout-treated embryos with mosaic expression of GFP-UtrophinCH and ras-mKate2. Inlays show enlarged marked area. Actin localization in the protrusions (Arrows). Frames from Movie 6. N=6
Scale bars = 10 µm, Movies started around 17–18 ss. Time h:min.

2.7 Rim cell migration involves dynamic cell-ECM adhesion

My results so far suggest that while being integrated in an epithelium, rim cells exhibit collective migratory behaviour driven by directed basal lamellipodial activity. It is known that lamellipodial migration often depends on dynamic contacts with the underlying extracellular matrix (ECM) (Friedl and Wolf, 2010). Most epithelia, including the epithelium of the optic cup, are lined basally by ECM in the form of the basal lamina (Kwan, 2014; Mouw et al., 2014). Therefore, to assess if similar phenomenon also occurs during rim involution, I assessed the spatial distribution of ECM components during RNE morphogenesis by immunostaining for the basal lamina components Laminin, Chondroitin sulfate and Fibronectin. The stainings revealed that all three components were present already since the optic vesicle stage and weakly localised under the developing RPE (Figure 2.10A, B). Laminin and chondroitin sulfate were enriched in the rim zone, under the invaginating RNE and the lens placode (Figure 2.10A). On the other hand, Fibronectin was preferentially enriched in the rim zone and under the lens placode but was weakly localised under the invaginating RNE (Figure 2.10B). Furthermore, over development the fibronectin staining showed a shift in the localisation pattern correlating with the shift and shrinking of the rim zone. Thus, the rim cells were exposed to various components of ECM that could serve as a scaffold for migration.

Cells adhere to the ECM by focal contacts or focal adhesion, using cell surface molecules integrins. Integrins are transmembrane proteins that bind directly to the ECM components on the extracellular side. On the intracellular side, they bind indirectly to the actin cytoskeleton via scaffolding proteins such as vinculin, talin and paxillin (Berrier and Yamada, 2007; Iskratsch et al., 2014). During migration, cells make transient contacts with the ECM and these focal contacts show fast turnover (Berrier and Yamada, 2007; Iskratsch et al., 2014). Therefore, if the rim cells indeed underwent active migration, rim cells would not be stably attached to the underlying basal lamina. Instead, rim cells would have dynamic contact to the basal lamina. To test this idea, I analysed the dynamics of components of focal contacts. Time-lapse imaging revealed that both markers, Integrin b1b-mKate2 and paxillin-mKate2, localised as transient foci during rim movement (Figure 2.11A,B, Movie 8). However, when the rim cells reached the inner invaginating layer of the cup, the localisation pattern changed and both markers were stably enriched at the basal side indicative of stable attachment (Figure 2.11A,B, Movie 8). This finding was corroborated by simultaneous imaging of markers of actin and paxillin. While the cells in the rim zone lacked basal enrichment of actin and paxillin, cells in the invaginating region showed stable basal enrichment of Paxillin coinciding with the basal accumulation of actin (Figure 2.11C, Movie 9). This suggested that

the rim cells use dynamic contacts to reach the invaginating layer, strengthening the active migration hypothesis. In addition, these results showed that upon reaching the inner layer of the optic cup, the cells become stably attached to the basal lamina and enrich basal actomyosin to participate in the ongoing invagination. This further highlighted that the migratory behaviour was restricted to the rim zone and was absent in the other regions of the optic cup.

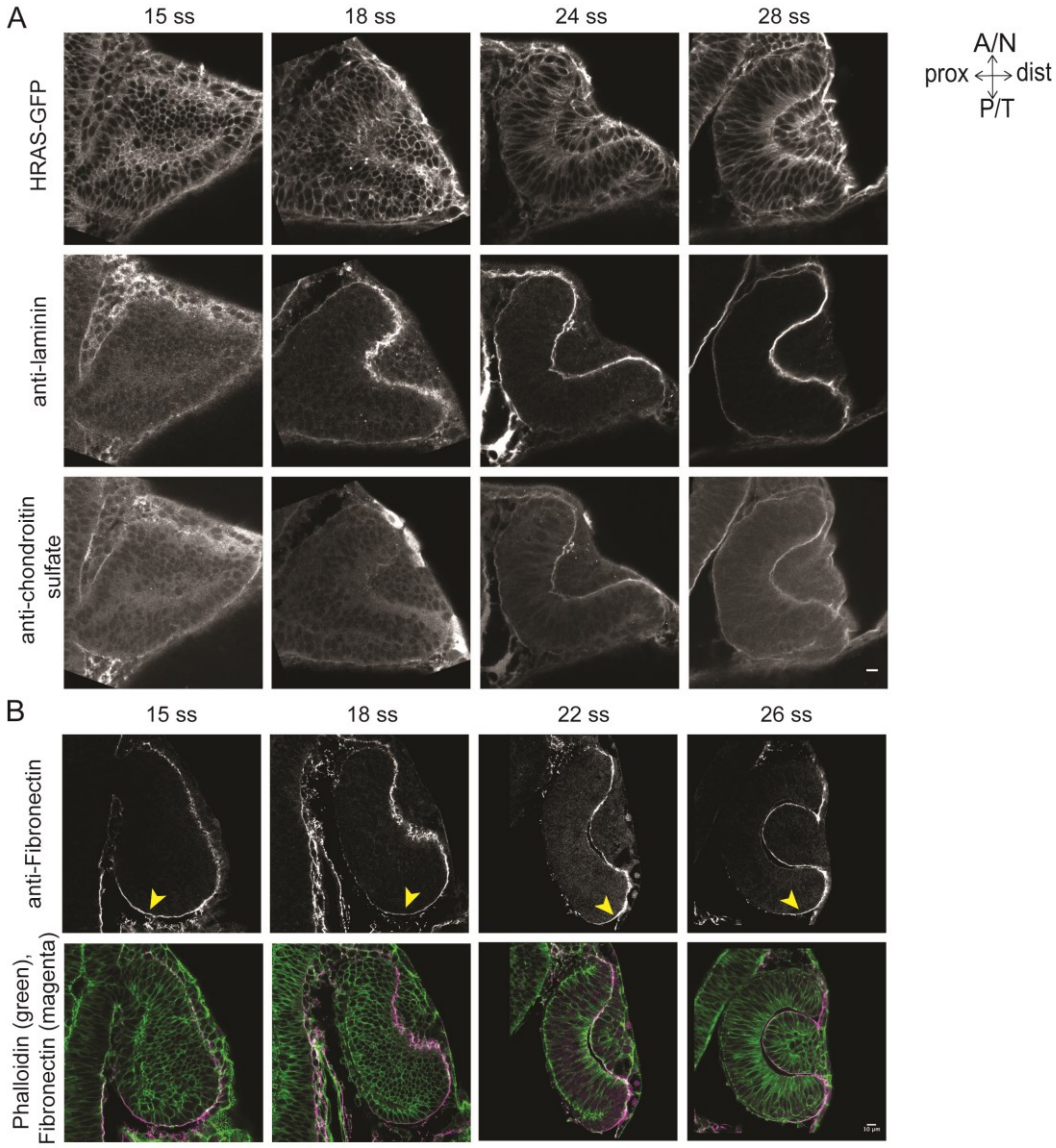

Figure 2.10: Analysis of ECM distribution during optic cup morphogenesis.
A) Confocal scans of immunostainings for laminin (middle), chondroitin sulfate (bottom) and GFP(top) in Tg*(actb1:HRAS-EGFP)* embryos across different stages of RNE morphogenesis.
B) Confocal scans of immunostainings for Fibronectin (top) and phalloidin across different stages of RNE morphogenesis. Merge (bottom). Shifting rim zone localisation of fibronectin (Arrowhead)
All scale bars = 10 µm.

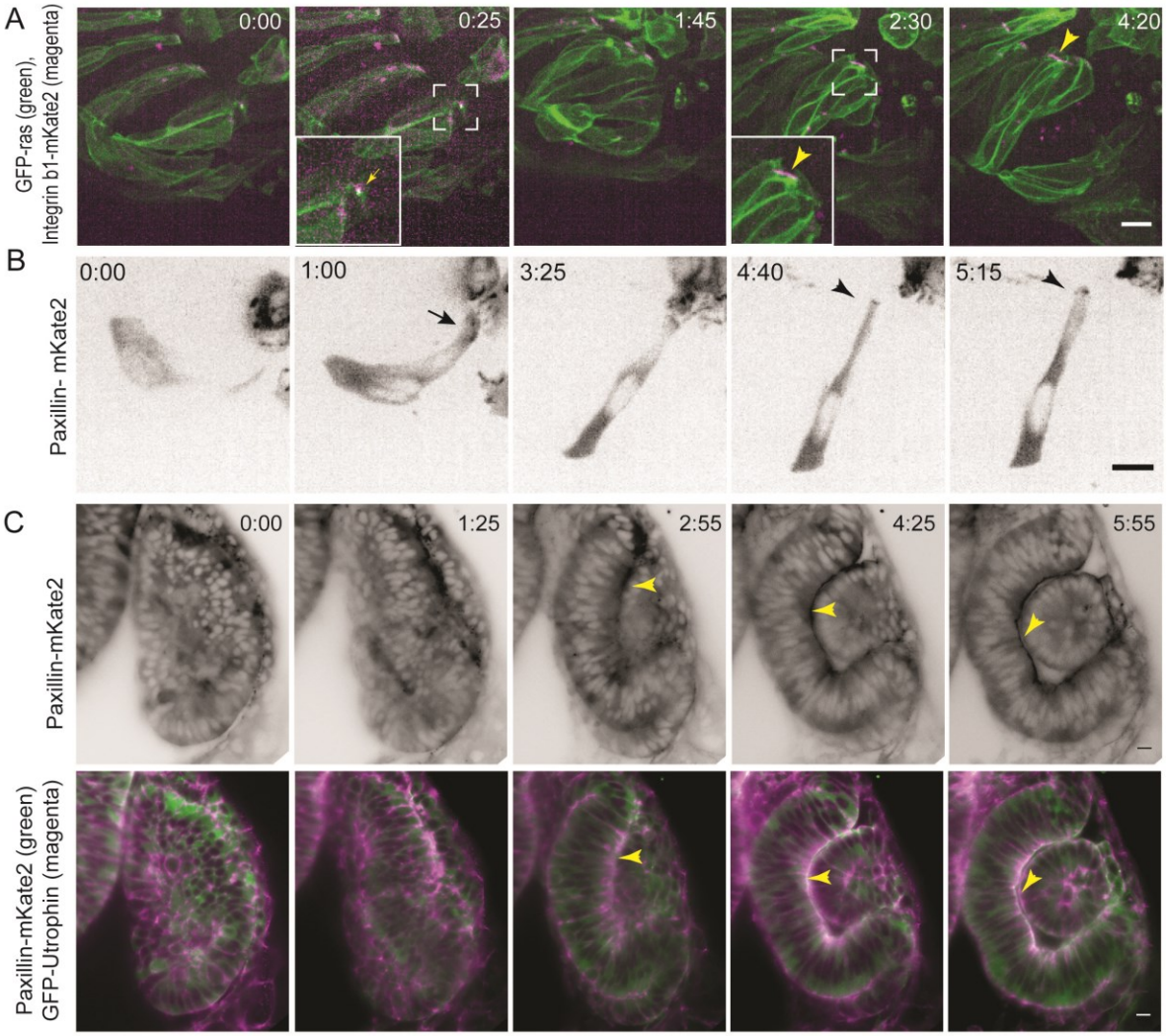

Figure 2.11: Analysis of cell-matrix adhesion during RNE morphogenesis

A) Time-lapse imaging of rim zone with mosaic expression of GFP-ras and Integrin-b1b-mKate2. Inlays show enlarged marked area. Integrin foci during migration (Arrow). Basally enriched stable integrin pool in the RNE cell (Arrowhead). Frames from movie 8. N = 4. Imaging started at 17–18 ss.

B) Time-lapse imaging of rim zone with mosaic expression of paxillin-mKate2. Short-lived paxillin foci (Arrow). Stable basal paxillin localization in the RNE (Arrowhead). Frames from movie 8. N = 6. Imaging started at 17–18 ss.

C) Time-lapse imaging of RNE morphogenesis in embryos expressing Paxillin-mKate2 and GFP-UtrophinCH. Paxillin enrichment coinciding with UtrophinCH enrichment (Arrowhead). Frames are from Movie 9. Imaging started at 15 ss.

All scale bars = 10 µm. Time h:min.

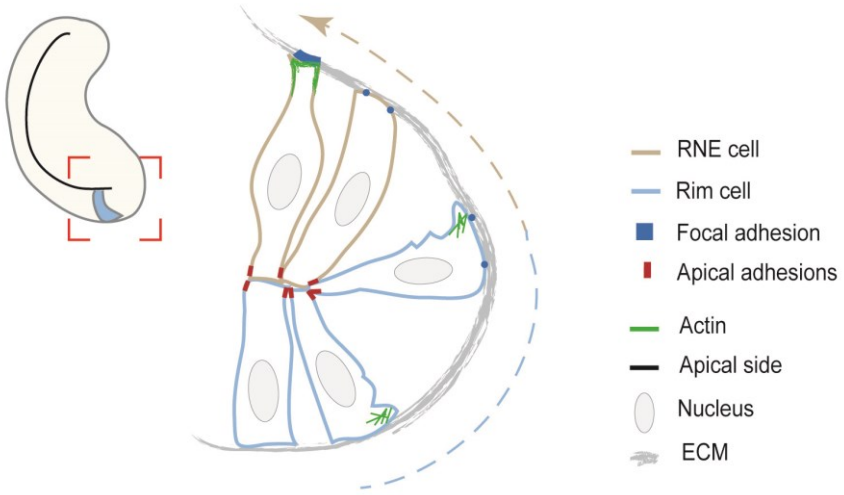

Figure 2.12: Working model of rim involution
Schematic drawing of the working model of rim involution showing the cellular dynamics occurring when rim cells migrate along the rim of the optic cup and become part of the invaginating layer.

2.8 Rim cell migration depends on dynamic cell-ECM adhesion

Next, I investigated if the dynamic cell-ECM adhesion was indeed important for rim cell movement. The requirement of cell-ECM attachment has been established before for the process of optic vesicle evagination, where role of laminin is critical for the polarisation of the eye field cells (Ivanovitch et al., 2013). Additionally, cell-ECM adhesion is also important for the RNE invagination in zebrafish and medaka (Bogdanovic et al., 2012; Bryan et al., 2016; Martinez-Morales et al., 2009). These reports were based on the phenotypes of loss-of-function mutants for *laminin-α1* (Bryan et al., 2016) and integrin regulator *opo* (Martinez-Morales et al., 2009). However, the role of cell-ECM attachment in rim migration remains elusive. It is known that *laminin-α1* and *opo* are expressed at mRNA levels throughout the optic vesicle, including the rim zone (Gago-Rodrigues et al., 2015; Pickering, 2012). Therefore, it is tempting to speculate that Laminin-α1 and opo could also play a role during rim involution.

In case of laminin-α1, three different alleles of the mutant *bashful* have been described before (Paulus and Halloran, 2006; Semina et al., 2006). However, earlier investigations of the alleles were focused on the role of laminin in lamination of retinal neurons and did not investigate the effect of loss of laminin on early eye development. A recent study investigated one of the alleles during OCM and reported profound polarity defects resulting in a very severe optic cup phenotype (Bryan et al., 2016). Such drastic phenotype would not allow to study the role of laminin in other cellular processes during OCM. Therefore, I opted for morpholino-mediated knockdown of *laminin-α1* and *opo* using previously published

morpholinos (Martinez-Morales et al., 2009; Pollard et al., 2006). The efficacy of the morpholino-mediated laminin-α1 knockdown was checked using antibody staining and western blot using anti-laminin antibody. Both experiments confirmed efficient knockdown (Figure 2.13A,C). In case of *opo* morphants, due to unavailability of a commercial anti-opo antibody, I performed a functional test for integrin localisation. Indeed, concurrent with the original study (Martinez-Morales et al., 2009), *opo* morphants showed reduced basal integrin localisation, confirming efficient knockdown (Figure 2.13B,D).

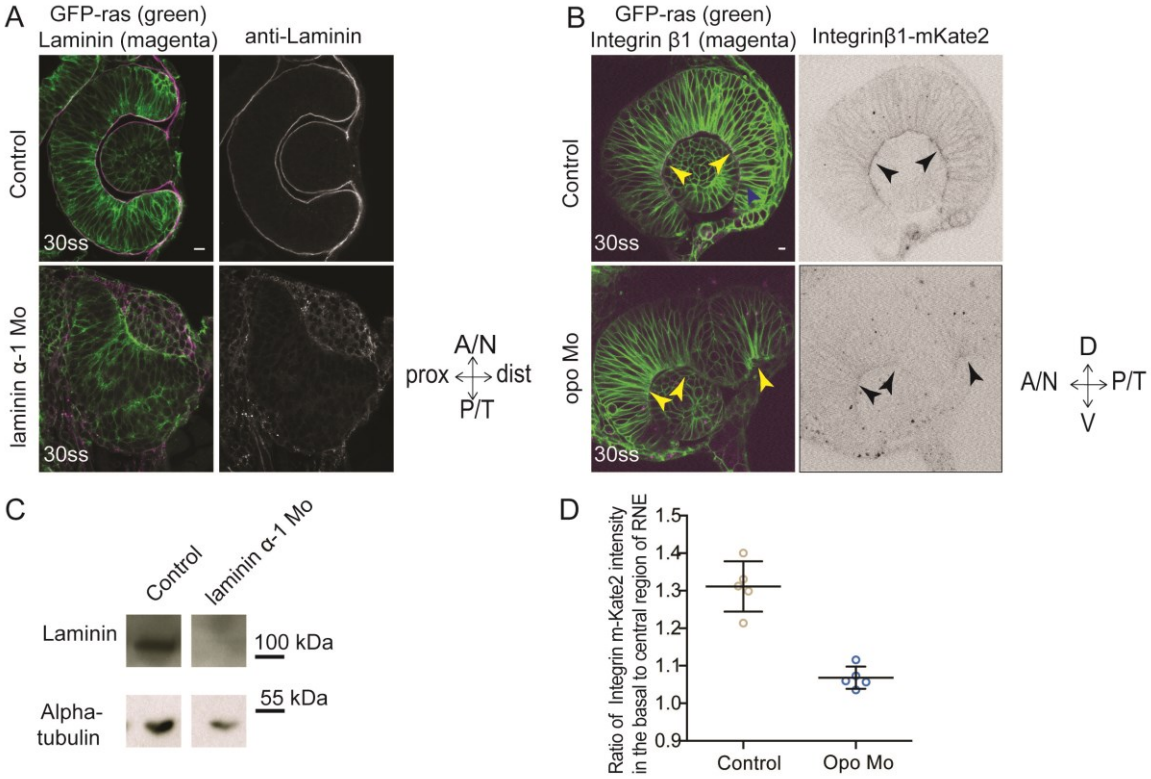

Figure 2.13: Analysis of knockdown efficiency of *laminin-α1* and *opo* morpholinos.
A) Confocal scan of 30 ss RNE in control (top) and *laminin-α1* morphants (bottom) marked with GFP-ras stained for laminin. Morphant shows S-shaped RNE and reduced laminin staining.
B) Confocal scan of side view of 30 ss RNE in GFP-ras and Integrin-β1-mKate2 RNA injected control (top) and *opo* morphant (bottom) embryo. Morphant shows S-shaped RNE with secondary invagination zone and highly reduced basal localization of integrin. N = 5.
C) Western blot for laminin and alpha-tubulin in control and *laminin-α1* morphant.
D) Ratio of average integrin β1-mKate2 signal at the basal to central region in the RNE in optical section along the apicobasal axis of the RNE at 30 ss. Mean±SD, N = 5 embryos.
All scale bars = 10 µm.

Laminin acts as a cross-linker molecule in the basal lamina and organises the other matrix components (Hohenester and Yurchenco, 2013; Mouw et al., 2014). Therefore, I analysed the distribution of the other ECM component fibronectin in *laminin-α1* morphants. Interestingly, I observed that upon laminin knockdown, fibronectin distribution changed. Fibronectin, which in control embryos stained the basal lamina in the invaginating zone very weakly, showed overall enrichment upon *laminin-α1* knockdown in the rim zone as well as

the invaginating zone (Figure 2.14A). Thus, *laminin-α1* knockdown provided a condition to assess the effect of altered ECM composition on rim involution and OCM. On the other hand, knockdown of *opo*, a regulator of integrin trafficking, affected basal integrin localisation in the developing RNE without strong effect on fibronectin localisation (Figure 2.13B,D,14B). Thus, it provided an additional tool to address the role of cell-ECM attachment in rim migration and OCM.

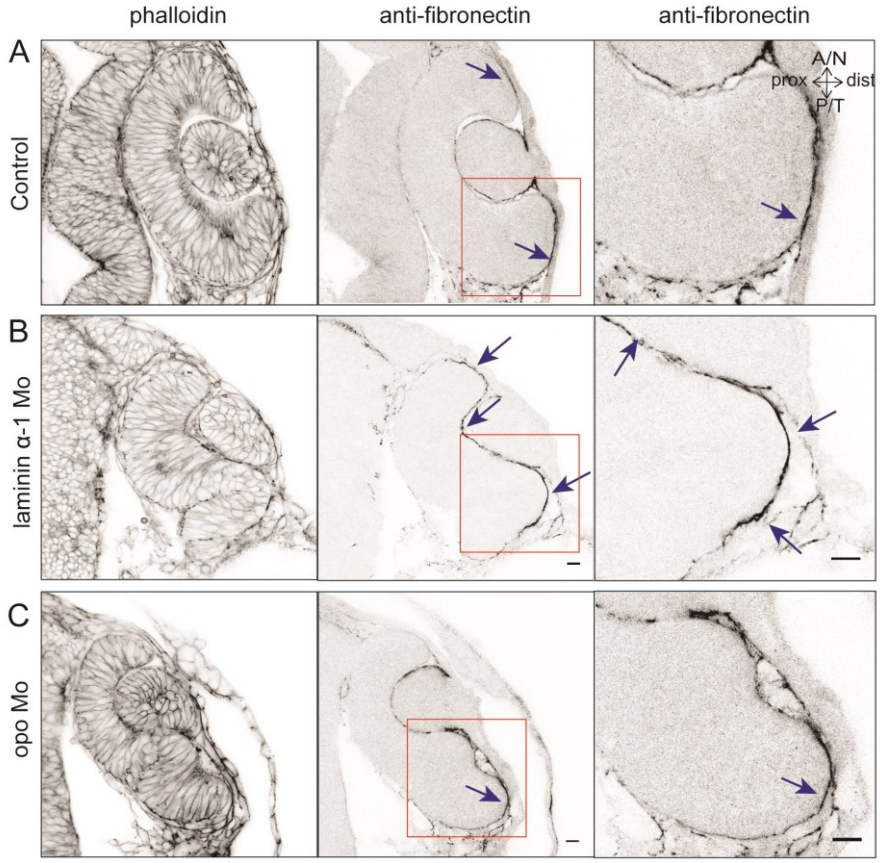

Figure 2.14: Analysis of fibronectin distribution in laminin and opo morphants.
Confocal scan of 30 ss RNE in control (A) and *laminin-α1* morphant (B) and *opo* morphant (C) stained for phalloidin and fibronectin. Enhanced fibronectin staining (Arrows). The right panels show a zoomed image of the area marked by the red box. N = 6. Scale bar = 10 µm.

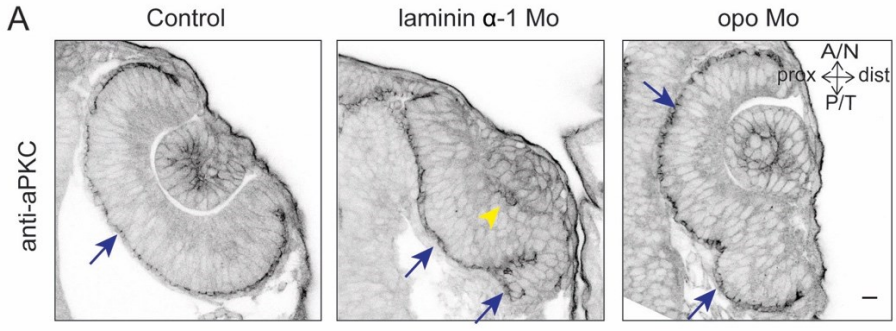

Figure 2.15: Analysis of polarity marker aPKC localisation in *laminin-α1* and *opo* morphants.
A) Confocal scan of 30 ss RNE in control (left), *laminin-α1* morphant (middle) and *opo* morphant (right) stained for aPKC. apical domain marked by aPKC (blue arrow). Delaminated cells in the *laminin-α1* morphant (yellow arrowhead). N = 5. Scale bar = 10 µm.

Importantly, unlike the mutant phenotype described before (Bryan et al., 2016), *laminin-α1* morphants did not show a very severe polarity defect. A few delaminated cells showed ectopic localisation of apical markers, but the overall tissue polarity was not severely perturbed (Figure 2.15A). Similarly, the *opo* morphants did not show any polarity defects (Figure 2.15A). Therefore, the morpholino-mediated knockdown allowed me to address the role of ECM composition and cell-ECM attachment in rim migration.

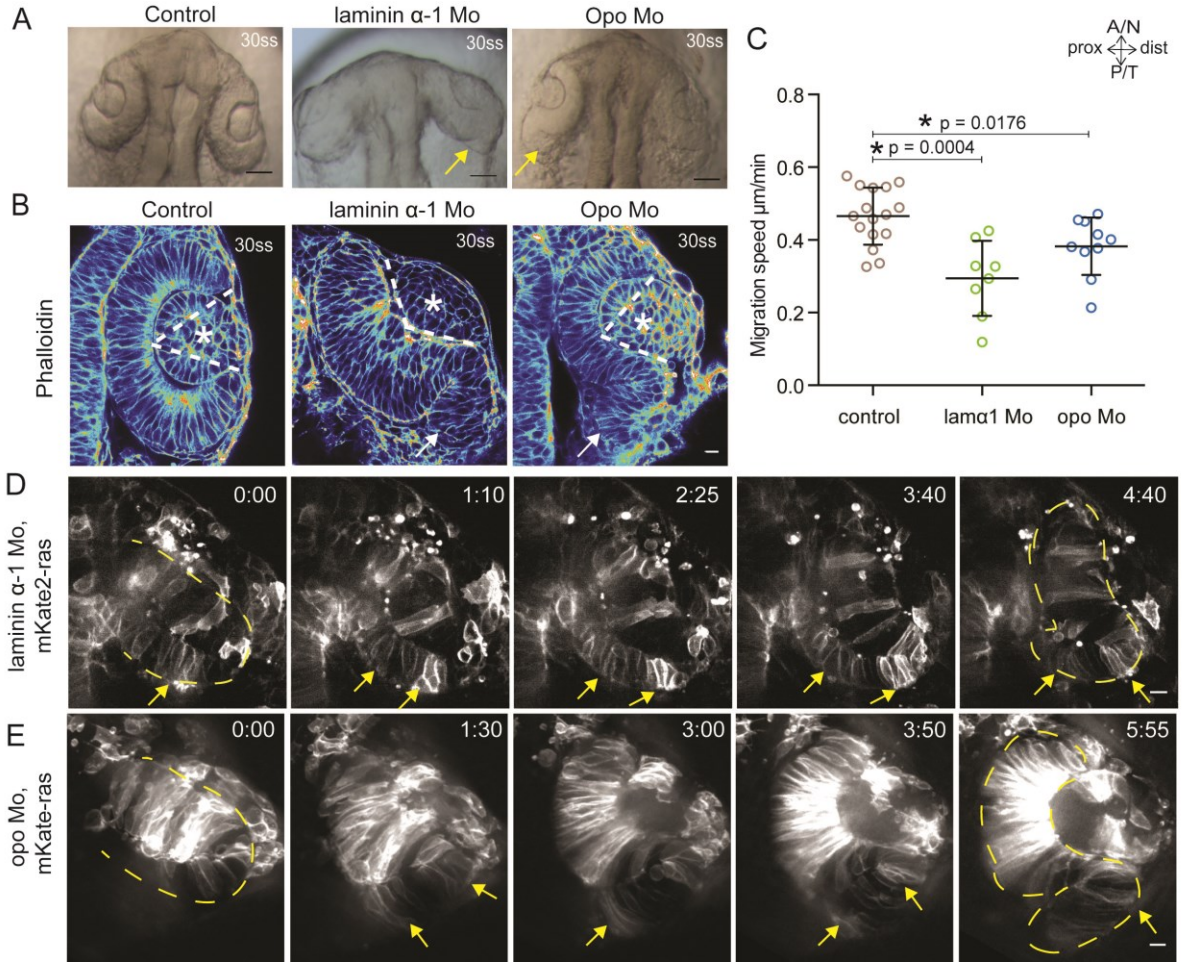

Figure 2.16: Analysis of RNE morphogenesis in *laminin-α1* and *opo* morphants.
A) Brightfield images of dorsal view of 30 ss embryo head. Control (left), *laminin-α1* morphant (middle) and *opo* morphant (right). Epithelial accumulation outside the RNE (Arrow). Scale bar = 50 µm.
B) Confocal scan of optic cup at 30 ss stained for phalloidin. Control (left), *laminin-α1* morphant (middle) and *opo* morphant (right). Epithelial accumulation outside the RNE (Arrow). Angle of invagination (Dashed line). Developing lens (Asterisk). Scale bar = 10 µm.
C) Migration speed of rim cells (Mean±SD). Mann Whitney test, *laminin-α1* Mo p = 0.0004, *opo* Mo p = 0.0176.
D,E) Time-lapse imaging of RNE morphogenesis in *laminin-α1* morphant (D) and *opo* morphant (E) injected mosaically with mKate2-ras RNA. Rim cells that failed to move (Arrow). Outline of the developing RNE (dashed line). Frames from movie 10. Time in h:min. Scale bar = 10 µm. Movies started at 16–17 ss.

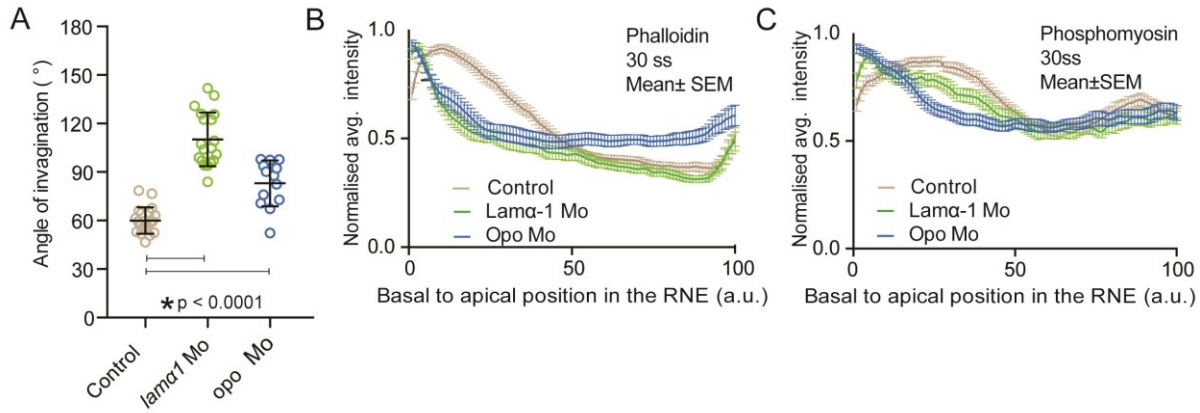

Figure 2.17: Analysis of RNE invagination in *laminin-α1* and *opo* morphants.
A) Invagination angle at 30 ss. Mean±SD. Mann-Whitney test p < 0.0001
B,C) Normalized average intensity distributions of phalloidin (B) and phosphomyosin (C) in tissue volume along the apicobasal axis of the RNE at 30 ss. Mean±SEM. Control (brown) n = 25, *laminin-α1* Mo (green) n = 19 and *opo* Mo (blue) n = 20. Tissue sections (n); embryos, N = 5.

Having established the two experimental systems, I assessed the effect of perturbed cell-matrix attachment on overall RNE architecture. Loss of Laminin-α1 and loss of Opo both resulted in a RNE with perturbed architecture. Instead of the C-shaped RNE morphology seen in controls, the morphant RNEs exhibited a shape that rather appeared like an S, due to an accumulation of epithelial cells at the ventro-temporal side (Figure 2.16A, B). It should be noted that the ventro-temporal side of the optic cup is the part where rim involution is predominant (Figure 2.1). This suggested a possible defect in rim migration that perturbed RNE morphogenesis. To test this, I performed time-lapse imaging of the morphant RNE development. Indeed, rim migration was defective in the morphant conditions with the average speed of the rim cells being lower than the control (Figure 2.16C). Some migration defective rim cells did not undergo rim involution and accumulated outside the invaginating region (Figure 2.16D,E, Movie 10).

Previous studies have established the role of laminin and opo in invagination of the RNE (Bogdanovic et al., 2012; Bryan et al., 2016; Martinez-Morales et al., 2009). Hence, I analysed if in my experiments, the rim involution defect was accompanied with perturbed invagination. Analysing the angle of invagination revealed that the invagination angles were wider in the *laminin-α1* and *opo* morphants than the controls (Figure 2.17A). This observation confirmed a defect in invagination. The previous results using Rockout treatment had shown that the perturbation of the basal actomyosin lead to slowed invagination and wider invagination angles (Figure 2.5). Therefore, I tested if this defect in invagination was due to similar effect on basal actomyosin enrichment. Analysis of the actomyosin distribution in *laminin-α1* and *opo* morphants revealed a reduction in the basal enrichment of the actomyosin in the RNE (Figure 12.17B,C). This suggests that the basal

actomyosin enrichment is dependent on cell-matrix adhesion. The effect on invagination was more severe in the laminin condition, possibly due to the combined defect in ECM composition, and cell-ECM attachment. Additionally, opo being a regulator of integrin trafficking, the *opo* knockdown condition is possibly a milder perturbation of cell-ECM attachment. Nevertheless, these results suggested that the observed S-shaped optic cup phenotype was probably due to combined effect on invagination as well as rim migration.

2.9 Perturbed cell-matrix adhesion correlates with perturbed basal lamellipodial activity

To understand the contribution of rim involution to RNE morphogenesis without directly affecting invagination, I needed a condition that perturbs rim migration selectively. Therefore, to identify the cellular process that selectively affects the rim migration, I analysed the single cell behaviour of the rim cells in the migration-defective conditions of *laminin-α1* and *opo* morphants. Characterisation of rim cells showed that in the control condition, these cells form lamellipodia-like protrusions (Figure 2.8D, Movie 4) and exhibit transient paxillin foci (Figure 2.11B, Movie 8). Interestingly, these cellular features were perturbed in both the morphants. In *laminin-α1* morphants, the cells did not possess dynamic foci of paxillin, instead paxillin localised stably to the basal side of the cell (Figure 2.18A, Movie 11). Such paxillin localisation could possibly result from the fibronectin enrichment in *laminin-α1* morphants (Figure 2.14B). Additionally, the lamellipodial protrusive activity was replaced by bleb-like protrusive activity at the basal side of the cell (Figure 2.18A, Movie 11). Blebs are plasma membrane protrusions resulting from detachment of the plasma membrane from the underlying actomyosin cortex. They are devoid of myosin and contain actin only during retraction phase (Charras and Paluch, 2008). I observed similar localisation of actomyosin markers in the bleb-like protrusion in the morphants. Myosin did not localise in the membrane protrusion but was restricted at the base of the protrusion, whereas actin marker localised to the protrusion in the retraction phase (Figure 2.18B). This confirmed that the aberrant protrusions in the *laminin-α1* morphant were true blebs. It is known that certain cells undergo bleb-based migration (Charras and Paluch, 2008). However, the rim cells with basal blebs did not show productive movement upon loss of lamellipodial protrusions (Movie 11). The lamellipodial protrusions were also affected in the *opo* morphants. Although, the paxillin foci remained dynamic in opo condition, the lamellipodial activity was replaced by formation of blebs at the basal side of the cells and the cells did not show any productive movement (Figure 2.18C, movie 12). Importantly, these bleb-like protrusions were also observed in *opo* morphant cells transplanted into WT embryos, suggesting that the perturbed cell-matrix attachment lead to the blebbing phenotype in a cell-autonomous manner (Figure 2.18D,

Movie 13, N=4 out of 5 transplanted embryos). These results suggest that perturbed cell-matrix adhesion also perturbs the normal lamellipodial protrusive activity of the rim cells, which in turn affects their migration (Figure 2.18E).

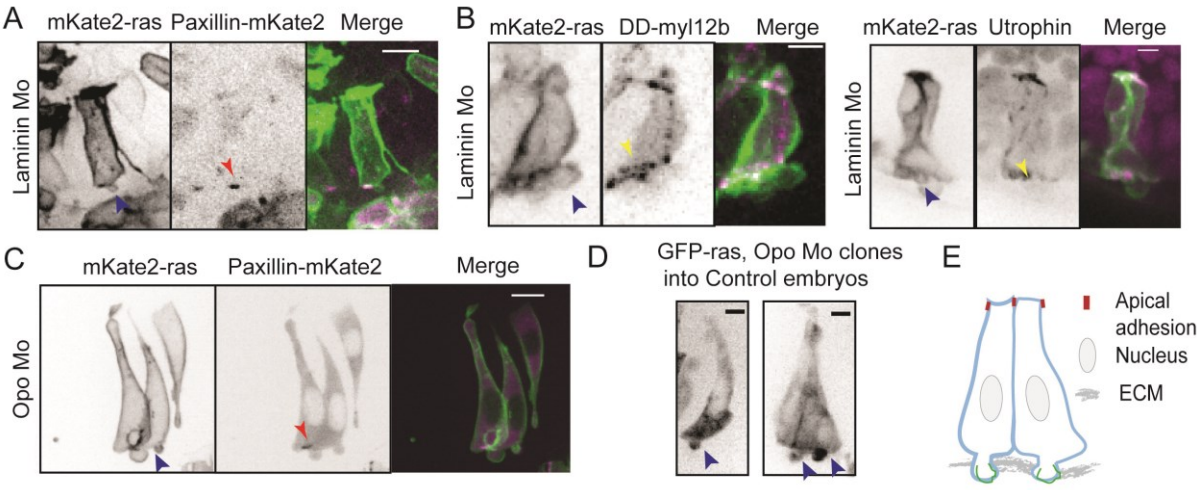

Figure 2.18: Analysis of rim cell protrusive activity in *laminin-α1* and *opo* morphants.
A) Confocal scan of rim cell in *laminin-α1* morphant embryos with mosaic expression of mKate2-ras and paxillin-mKate2. Bleb (blue arrowhead). Stable paxillin localization (Red arrowhead). Frames from Movie 11. N = 3. Scale bar = 10 µm.
B) Confocal scan of rim cells exhibiting blebs (blue arrowhead) in *laminin-α1* morphants mosaically labelled by mKate2-ras with DD-myl12b-GFP (left) and GFP-UtrophinCH (right). Yellow arrowhead marks the localization of DD-myl12b-GFP outside and UtrophinCH inside the bleb. Scale bar = 2 µm.
C) Confocal scan of rim cell in *opo* morphant embryos with mosaic expression of mKate2-ras and paxillin-mKate2. Bleb (blue arrowhead). Transient paxillin localization (Red arrowhead). Frames from Movie 12. N = 3. Scale bar = 10 µm.
D) Confocal scans of rim zone showing GFP-ras-expressing *opo* morphant clone in control embryos. N=4 out of 5 transplanted embryos. Basal blebs exhibited by the transplanted morphants cells (blue arrows). Frames from Movie 13. Scale bar = 5 µm.
E) Schematic drawing of membrane blebbing in the *laminin-α1* and *opo* morphant rim cells.

2.10 Perturbed basal lamellipodial activity affects migration of rim cells and leads to defects in RNE architecture

The finding that the cells that failed to undergo active rim migration exhibited blebs instead of lamellipodia raised the question if the perturbation of the normal protrusive activity could by itself interfere with rim migration. Rac proteins, members of Rho GTPase family, are important lamellipodial regulators that activate Arp2/3-mediated actin polymerisation and formation of lamellipodial protrusions or membrane ruffles (Heasman and Ridley, 2008). Therefore, in order to disrupt the lamellipodia formation in rim cells, I opted to use a dominant negative version of Rac1 (DN-Rac, Rac1-T17N), which traps the activating partner GEF proteins and thus hampers the function of endogenous Rac (Subauste et al., 2000).

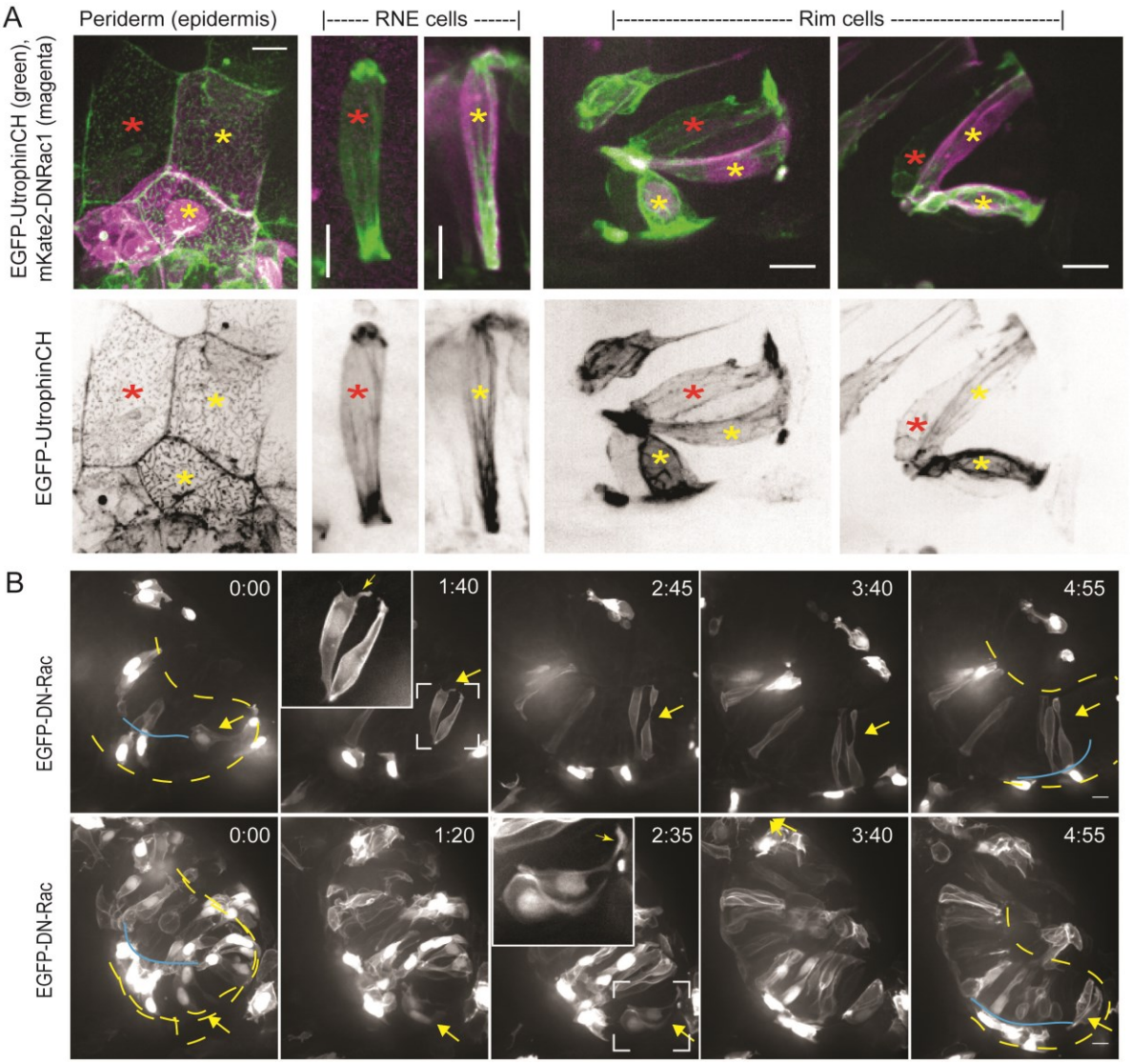

Figure 2.19: Analysis of cellular phenotypes upon expression of DN-Rac
A) Confocal scans of F-actin distribution marked by heat shock induced EGFP-Utrophin in peridermal cells of the epidermis (left), RNE cells (middle) and rim cells (right). Cells expressing heat shock-induced mKate-DN-Rac (Yellow asterisk). Control cells (Red asterisk). Note that upon DN-Rac expression, the pattern of actin microridges is affected in the epidermis and actin organisation shows filamentous arrangement in the RNE and rim cells.
B) Time-lapse imaging of RNE morphogenesis in embryos showing mosaic expression of hsp70::EGFP-DN-Rac. Inlays show the abnormal protrusions in DN-Rac expressing cell. Outline of the developing RNE (Yellow dashed line). Apical side (Blue line). Heat-shock at 12 ss. Imaging started 3 hours after heat shock. Time in h:min.
All scale bars = 10 µm.

Results

I expressed the DN-Rac under the heat-shock promoter, to precisely activate its expression during OCM. To evaluate the efficiency of the construct, I assessed its effects on the actin cytoskeleton in different cell types. I noted that actin arrangements were altered in both RNE cells and epidermal cells (Figure 2.19A). Thus, I concluded that the construct was functional and can be used to interfere with lamellipodia formation. However, expression of DN-Rac induced milder effect on the protrusions and rim involution. The DN-Rac-expressing rim cells formed aberrant filopodia-like protrusions, which could still support the movement of cells and the effect on rim involution was weaker even in the embryos expressing larger clones of DN-Rac (Figure 2.19B). Therefore, the formation of filopodia-like protrusions made it difficult to interpret the results.

As expression of DN-Rac did not allow efficient disruption of migration of rim cells, I opted for another strategy to perturb the lamellipodial protrusions and rim cell migration. Ezrin is a member of ERM family of proteins that link the actin cortex to the plasma membrane (Fehon et al., 2010). Ezrin knockdown has been shown to cause increased blebbing and reduced migration rates of zebrafish prechordal plate precursor cells (Schepis et al., 2012). As the cells in the *laminin-α1* and *opo* morphants also featured membrane blebs at the basal side, I decided to mimic the blebbing phenotype by ezrin knockdown. For ezrin knockdown, I used previously published morpholinos (Link et al., 2006). The efficiency of knockdown was assessed by western blot with the phospho-ERM antibody which showed a reduction in the protein levels (Figure 2.20A). However, it should be noted that I used a milder knockdown of ezrin as severe knockdown of ezrin resulted in gastrulation defects (Link et al., 2006) and high cell death in the neural tube. Indeed, knockdown of ezrin changed the protrusive dynamics and resulted in basal blebbing in the rim cells (Figure 12.20B). These blebs were seen only at the basal side of the cells and the lateral edges were not affected. Furthermore, similar blebbing was observed in *ezrin* morphant cells transplanted into WT embryos (Figure 12.20C, N=2 out of 4 transplanted embryos). This variability in the blebbing could be due to varying morpholino concentration within transplanted cells as they come from different donors. ERM proteins are also known to play a role in regulating the epithelial polarity (Fehon et al., 2010). However, immunostainings for apical marker aPKC did not show any defect in the polarity of the tissue (Figure 2.20D). Thus, ezrin knockdown provided me a tool to perturb the rim cell protrusive activity.

Next, I asked if the perturbation of rim cell activity had any impact on rim involution and RNE morphogenesis. Indeed, phenotypic observation of the *ezrin* morphants revealed that the RNE architecture was affected. This phenotype resembled what was seen in *laminin-α1* and *opo* morphants, an S-shaped optic cup with epithelial cells accumulated at the ventro-

temporal side (Figure 2.21A,B). Live imaging of the *ezrin* morphants confirmed that defective rim migration lead to the observed accumulation of cells (Figure 2.21C, Movie 14). The average speed of rim migration was also lower in the *ezrin* morphants as compared to the controls (Figure 2.21D). However, unlike *laminin-α1* and *opo* morphants, the basal accumulation of actomyosin was not affected in the *ezrin* morphants (Figure 2.21E,F). To confirm this, I compared the instantaneous slopes of phalloidin intensity distribution in the different conditions. Rockout, *laminin-α1* morphant and *opo* morphant conditions, which caused a reduction in the basal actomyosin showed a similar pattern of the instantaneous slope curve. On the other hand, *ezrin* morphants showed a pattern closer to the control condition (Figure 2.21G). Also, the angle of invagination was only mildly affected in *ezrin* morphant and was not as severe as seen in *laminin-α1* morphants (Figure 2.21H). Thus, the defect in optic cup architecture upon loss of *ezrin* was mainly due to perturbed rim migration and was not due to a defect in basal actomyosin accumulation.

Taken together, my results highlight the importance of dynamic cell-matrix adhesion and lamellipodial activity in rim migration. Furthermore, the data show that rim migration plays an important role in shaping the RNE.

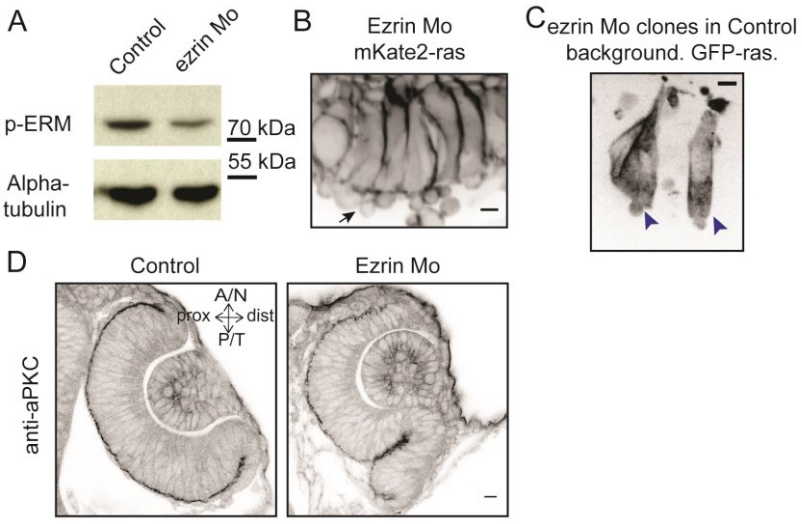

Figure 2.20: Analysis of *ezrin* morphants.
A) Western blot for p-ERM and alpha tubulin in control and *ezrin* morphant.
B) Confocal scan of rim cells in mKate2-ras injected *ezrin* morphant. Basal blebs (arrow). Scale bar = 5 µm.
C) Confocal scan of rim zone showing GFP-ras expressing *ezrin* morphant clone in a control embryo. N = 2 out of 4 transplanted embryos. Basal blebs (arrowhead). Scale bar = 5 µm.
D) Confocal scan of 30 ss RNE in control (left), *ezrin* morphant (right) stained for aPKC. N = 5. Scale bar = 10 µm.

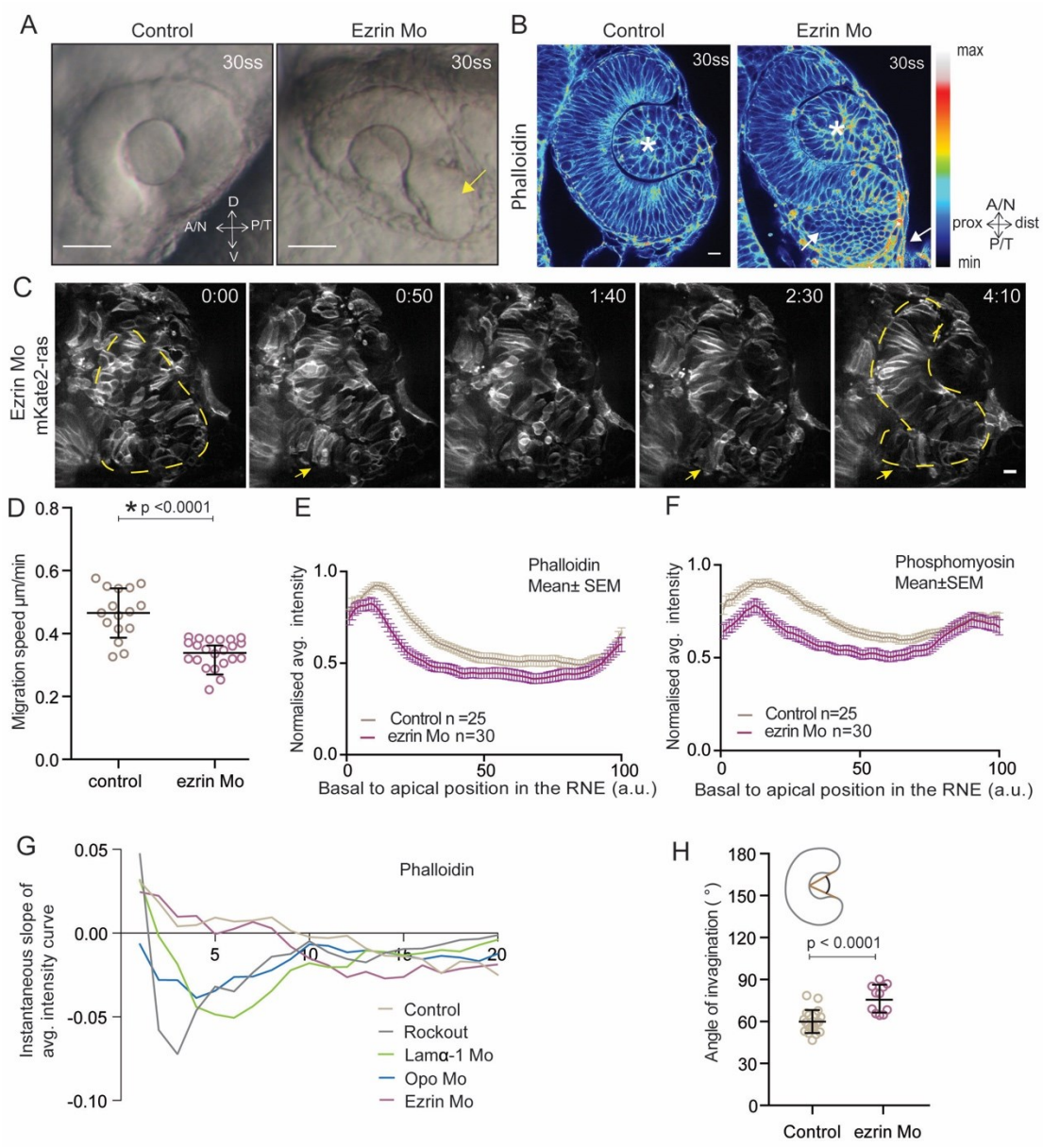

Figure 2.21: Analysis of RNE morphogenesis in *ezrin* morphant.

A) Brightfield images of side view of 30 ss optic cup. Control (left) and *ezrin* morphant (right). Epithelial accumulation outside the RNE (Arrow). Scale bar = 50 µm.

B) Confocal scan of optic cup at 30 ss stained for phalloidin. Control (left) and *ezrin* morphants (right). Epithelial accumulation outside the RNE (Arrows). Lens (Asterisk). Lookup table indicates the minimum and maximum intensity values. Scale bar = 10 µm.

C) Time-lapse imaging of RNE morphogenesis in *ezrin* morphant injected mosaically with ras-mKate2 RNA. Rim cells that failed to move (arrow). Outline of developing RNE (dashed line). Frames from movie 14. Time in h:min. Scale bar = 10 µm. Imaging started at 17–18 ss.

D) Migration speed of rim cells (Mean±SD). Mann Whitney test. $p < 0.0001$.

E,F) Normalized average intensity distributions of phalloidin (E) and phosphomyosin (F) in the tissue volume along the apicobasal axis of the RNE at 30 ss. Mean±SEM. Control (brown) *ezrin* Mo (magenta). Tissue sections, n = 25 for control and n=30 for *ezrin* Mo; N = 5 embryos.

G) Instantaneous slope of the average intensity curves for phalloidin plotted for the basal 20% height of the neuroepithelial volume. The position on the X-axis marks the position along the apicobasal axis. The analysis was performed using the data from Figure 2.4C, 2.5C, 2.17B and 2.21E.

H) Invagination angle at 30 ss. Mean±SD. The schematic shows the invagination angle as the angle held at the base of central RNE by the inner lips of the optic cup. Mann-Whitney test $p < 0.0001$.

2.11 Rim cell migration ensures timely entry of RNE cells into the optic cup

The results so far revealed that the rim cells involute by collective epithelial migration to reach the invaginating layer, and a failure in rim involution perturbs the RNE architecture. This raises the question, what happens to the cells that failed to undergo rim involution and accumulated at the ventro-temporal side of the optic cup? In the control situation, the rim cells form stable focal adhesions marked by paxillin only upon reaching the inner invaginating layer, where they attained the RNE morphology (Figure 2.11, 2.22A). In contrast, the rim cells in *ezrin* morphants that failed to undergo rim migration featured stable paxillin staining prematurely, before reaching the invaginating layer (Figure 2.22A,B). This is similar to the observation in *laminin-α1* morphants, where the blebbing cells exhibited stable paxillin localisation even without reaching the RNE (Movie 11). This suggested that the cells attained RNE-like morphology at an ectopic location. Such RNE-like stable adhesion to the basal lamina might additionally hamper their movement, adding to the severity of the phenotype. In some embryos, depending upon how many cells accumulated outside of the invagination zone, the migration defect had profound effects. These phenotypes persisted until 36 hpf, when neurogenesis in the RNE is known to start (Weber et al., 2014), resulting in abnormal architecture of the optic cup (Figure 2.23A). In some *ezrin* morphants, these displaced RNE cells even initiated a second invagination zone (Figure 2.23B). This observation again highlighted that the migration defective cells showed RNE-like behaviour and underwent a similar morphogenetic program but at a wrong location.

The premature attainment of RNE-like morphology suggested presence of a developmental timer in the cells. Even when the cells are not at their right location, the developmental timer induces the cells to attain RNE-like morphology. Such a developmental timer could be acting through the fate determination program, that determines the fate of the cells in the developing optic cup as RNE or RPE. Therefore, I asked if the ectopic attainment of RNE-like morphology was also accompanied by determination of RNE fate. Homeobox transcription factor Vsx2 is a well-known marker specifically expressed in the retinal progenitors and responsible for their fate determination (Kimura et al., 2006). Live imaging of the fate determination using a reporter line Tg(*vsx2*::GFP) showed that in controls, the rim cells showed very weak GFP signal outside the invaginating layer. However, the GFP signal became brighter as the rim cells involuted and became part of the invaginating layer (Figure 2.24A, Movie 15). This indicated that the cell fate determination was intricately linked with rim involution. Upon following the fate determination in the rim involution-perturbed condition of *ezrin* morphant, it was observed that in the cells that failed to migrate the GFP signal of

vsx2::GFP was brighter already outside the invaginating layer (Figure 2.24A, Movie 15). As a result, *vsx2*::GFP positive cells accumulated ectopically. This was observed in *ezrin* as well as *laminin-α1* and *opo* morphants (Figure 2.24B). Together, these results showed that the cellular determination occurred independent of their position. As a result, failed rim migration resulted in ectopic accumulation of cells determined to be part of the RNE.

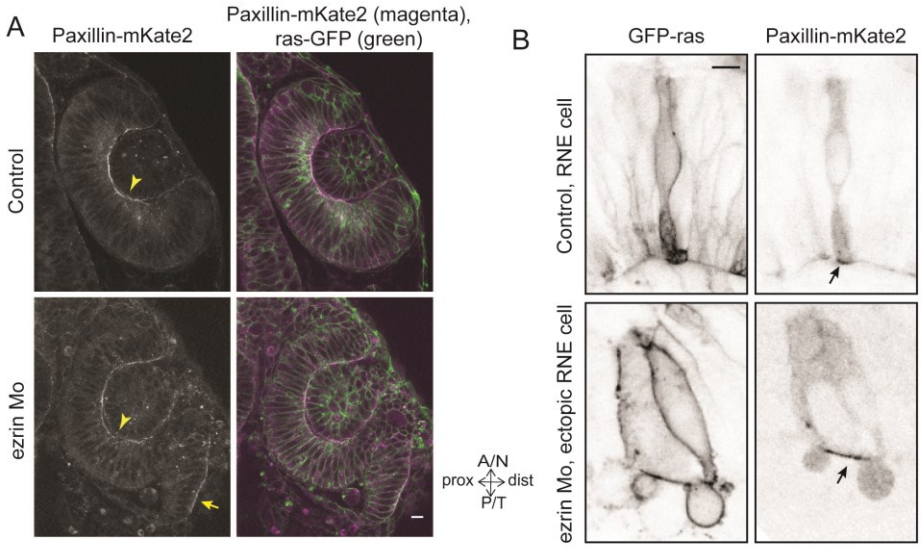

Figure 2.22: Analysis of rim cells that failed to undergo involution in *ezrin* morphant.
A) Confocal scan of 30 ss optic cup expressing paxillin-mKate2 and GFP-ras. Control (top), *ezrin* Mo (bottom). Paxillin enrichment at the basal side of the invaginating layer (Arrowhead). Premature paxillin enrichment (Arrow). N = 7. Scale bar = 10 µm.
B) Confocal scan of paxillin-mKate2 and GFP-ras expressing cells. Control RNE cells (top), ectopic RNE cell in *ezrin* morphant (bottom). Paxillin enrichment at the basal side (Arrow). Scale bar = 5 µm.

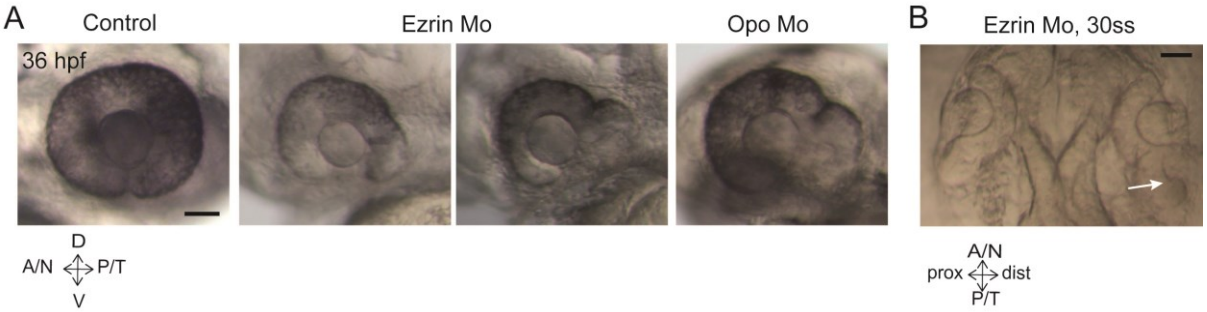

Figure 2.23: Analysis of late optic cup morphology upon failed rim cell migration.
A) Brightfield images of 36 hpf control embryos, *ezrin* morphants and *opo* morphant.
B) Brightfield image of 30 ss *ezrin* morphant showing secondary optic cup phenotype. Arrow marks secondary invagination zone.
Scale bars = 50 µm.

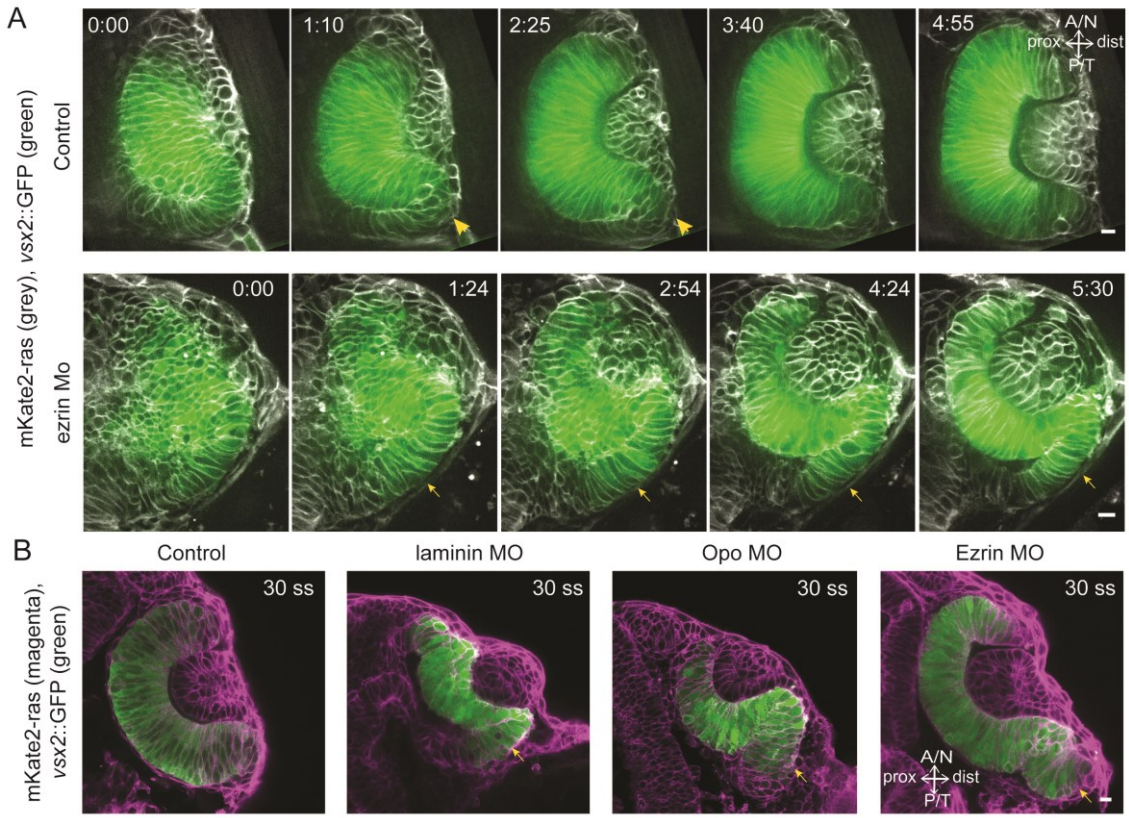

Figure 2.24: Analysis of RNE fate determination
A) Time-lapse imaging of control and *ezrin* morphant condition in Tg(*vsx2*::GFP, *bactin*::mKate2ras) background. Rim zone in control (Arrowheads). Rim cells that failed to migrate in *ezrin* morphant (Arrows). Frames from movie 15. Time in h:min. Movies started at 16–17 ss. N = 9.
B) Confocal scans of optic cups at 30 ss in control, *laminin* morphant, *opo* morphant and *ezrin* morphant conditions in Tg(*vsx2*::GFP, *bactin*::mKate2-ras). Embryos were stained for GFP and mKate2. Ectopic RNE cells (Arrow). N = 7.
Scale bars = 10 µm.

A previous study has suggested that the cell behaviours in the optic cup are regulated by the upstream signalling events and developmental patterning of the optic vesicle (Picker et al., 2009). The naso-temporal patterning of the optic vesicle has been proposed to underlie the behavioural difference at the nasal and temporal sides (Picker et al., 2009). In this study, the rim cells were shown to express markers of the temporal retina and to contribute to the temporal retina development (Picker et al., 2009). This raised the question, if the defects in rim migration were due to naso-temporal patterning defects in the optic vesicle. To investigate this, I analysed the expression of naso-temporal markers in the *ezrin* morphant condition, where rim involution is perturbed. To this end, I used the transgenic lines for the nasal marker Tg*(-8.0 Cldb::lyn-GFP)* (Haas and Gilmour, 2006; Picker et al., 2009) and the temporal marker Tg*(HGn42A::EGFP)* (Nagayoshi et al., 2008; Picker et al., 2009). I observed that the *ezrin* morphants were correctly patterned along the naso-temporal axis. The migration-defective rim cells could not reach their destination, nonetheless they

expressed the right markers (Figure 2.25A,B). These results highlighted that the defects observed in the *ezrin* morphants were not due to patterning defects, but due to genuine defects in morphogenetic movements.

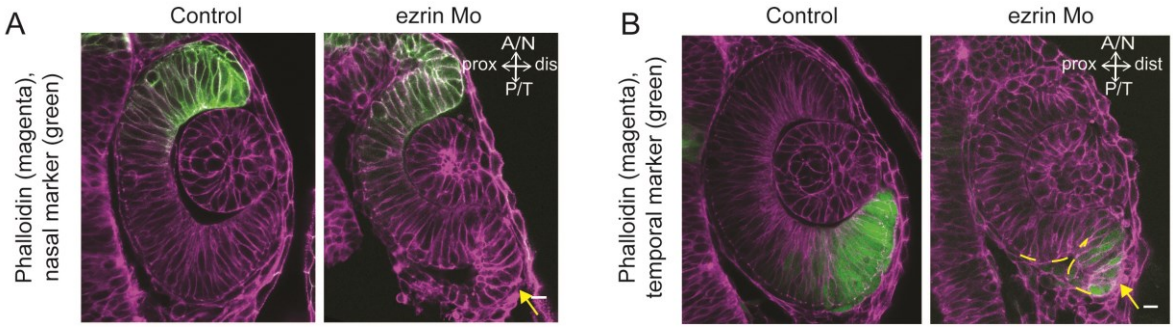

Figure 2.25: Analysis of naso-temporal patterning
A) Confocal scans of optic cups at 30 ss in control (left) and ezrin morphant (right) conditions in Tg(–*8.0 ClaudinB*::lyn-GFP) stained for GFP and phalloidin. Ectopic RNE cells (Arrow). N = 7.
B) Confocal scans of optic cups at 30 ss in control (left) and ezrin morphant (right) conditions in Tg(*HGn42A*::GFP) stained for GFP and phalloidin. Ectopic RNE cells (Arrow). N = 7.
Scale bars = 10 µm.

Taken together, my results show that rim involution is a crucial process in RNE morphogenesis that links morphogenetic and cell fate programs in the developing optic cup. It functions as a mechanism to ensure that initially 'misplaced' prospective RNE cells are moved to their correct location before they adopt RNE fate, making it a crucial step for subsequent retinal development.

3. Discussion

My work presented here has revealed important insights into the cellular dynamics during morphogenesis of the retinal neuroepithelium (RNE) of the zebrafish embryos. I show that basal shrinkage of the neuroepithelial cells and rim involution shape the RNE collectively. Basal shrinkage and RNE invagination are partly accelerated by an enrichment of contractile actomyosin at the basal side of the cells. However, the major contributor to RNE morphogenesis is rim involution. My work has revealed the so far unknown cellular mechanism of rim involution. I show that rim involution is a process of active collective epithelial migration. This collective rim migration translocates the prospective RNE cells to their right location in the invaginating neuroepithelium and contributes more cells to the ongoing invagination. A failure in rim migration results in perturbed RNE architecture. Thus, rim involution is important for the spatial organisation of the RNE. Furthermore, rim involution ensures that the prospective RNE cells reach their destined location at the right time. A defect in rim migration results in ectopic cell determination of the prospective RNE cells and has long-lasting effect on the RNE architecture. Therefore, rim involution couples the morphogenetic program with cell fate determination and coordinates timely development of RNE, the organ precursor of the retina. Overall this work highlights how morphogenetic processes coordinate epithelial organogenesis both in space and time to shape an epithelial organ precursor efficiently (summarised in Figure 3.1).

In this chapter, I discuss the significance and implications of my findings and also the new exciting questions they raise.

3.1 Multiple morphogenetic strategies ensure efficient morphogenesis

3.1.1 Basal RNE cell shrinkage and active rim migration together ensure efficient hemispheric RNE formation

My work highlights the importance of the combined action of two epithelial rearrangements to drive efficient and timely optic cup morphogenesis (OCM) in the zebrafish embryo. The shape of the optic vesicle as an epithelial fold might influence the choice of the epithelial rearrangements for invagination. The initial ‘proximal layer’ localisation of many presumptive RNE cells, possibly makes basal shrinkage in the distal layer a less efficient way to achieve RNE morphogenesis in the given developmental time window. This is suggested by the *ezrin* morphant phenotype, in which in spite of having actomyosin enrichment at the basal side, rim cells fail to involute on time (Figure 3.1Cii). Therefore, an interplay of cell shape changes

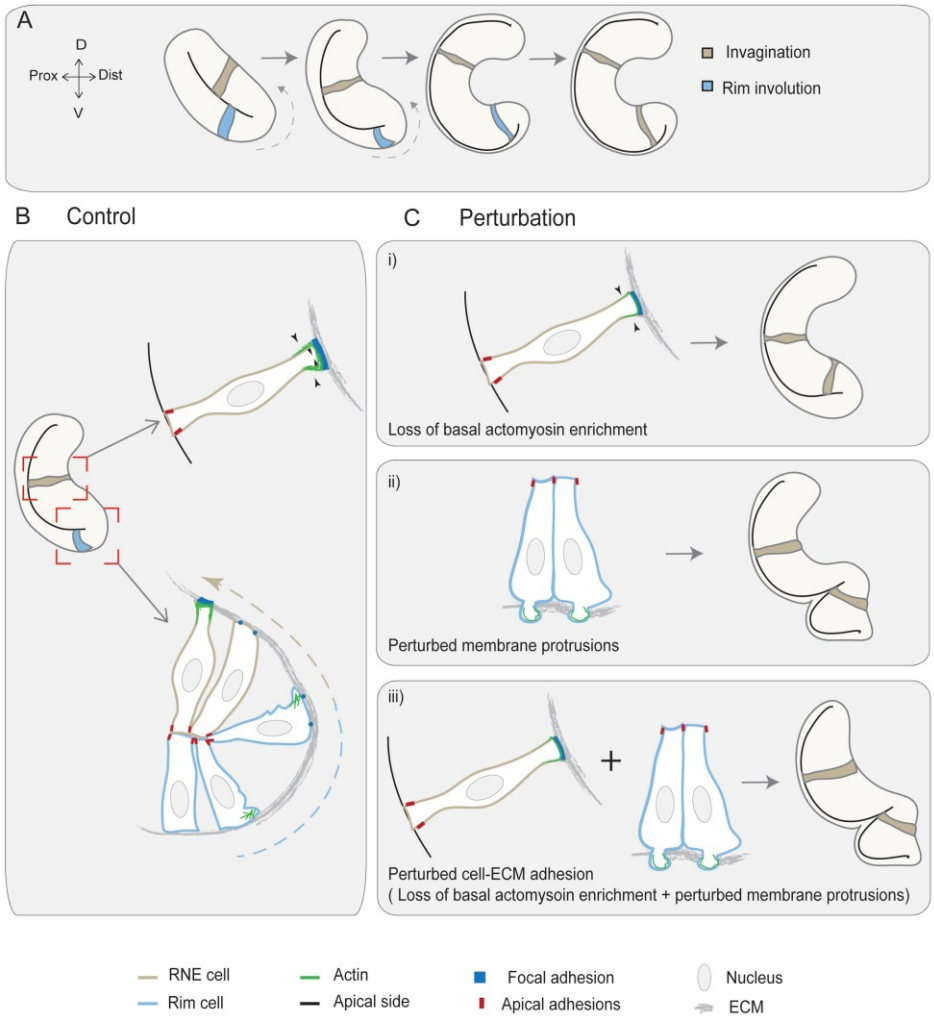

Figure 3.1: Concerted action of basal cell shrinkage and rim involution shapes the hemispheric RNE.
A) Schematic representation of RNE morphogenesis. The cells in the optic vesicle shape the RNE into a hemispheric cup. RNE cells in the distal layer (brown) contribute to invagination and prospective neuroepithelial cells (blue) undergo rim involution to reach the inner layer of the cup.
B) In control conditions, invagination is driven by basal area reduction that is guided by basally enriched actomyosin-driven constriction and overall compaction by increasing number of cells. Rim involution is driven by collective and directed migration of the epithelium at the rim of the developing optic cup. Protrusive migratory dynamics of rim cells change to adherent behaviour when cells reach the inner layer.
C) Effect of cellular perturbations on the RNE architecture. i) Loss of basal actomyosin enrichment slows the invagination process, which can result in a wider optic cup. ii) Perturbation of lamellipodial membrane protrusions affects the migratory behaviour and the optic cup architecture, resulting in an S-shaped optic cup. iii) Perturbation of cell-ECM adhesion results in both loss of basal actomyosin accumulation in the invaginating zone and perturbed lamellipodial membrane protrusions in the rim zone. Such combined effect leads to a severe optic cup phenotype.

and epithelial migration transforms the optic vesicle into an optic cup efficiently. When either basal actomyosin enrichment or rim involution were affected alone (Rockout-treated and *ezrin* morphant conditions) the effect on invagination was weak (Figure 3.1Ci,ii). However, when both the processes are perturbed (*laminin-α1* morphant condition), it resulted in a severe phenotype with very wide angle of invagination (Figure 3.1Ciii). Thus, both the epithelial rearrangements contribute to the process of morphogenesis individually, and their crosstalk determines the final architecture of the organ precursor.

Such combinations of epithelial rearrangements are possibly important to achieve organogenesis in short developmental time windows and are observed in other developmental events. For instance, during zebrafish posterior lateral line development, a group of cells in the form of a primordium migrates collectively across the body of the larva. On its way, subsets of cells form small rosettes, leave the primordium, and get deposited along the path. In this system, the coordination in epithelial rearrangements of rosette formation and the primordium migration determines the spacing between rosettes and in turn the lateral line architecture (Durdu et al., 2014). As an additional example, *Drosophila* germ band extension was thought to be driven solely by intercalation of cells using tissue-autonomous mechanisms. However, a recent study has revealed the additional importance of posterior midgut invagination that exerts a pulling force on the germ band and thus helps in oriented growth of junctions and tissue extension (Collinet et al., 2015). Such collective effort of different epithelial rearrangements possibly makes developmental processes more efficient and robust. The redundancy of approaches ensures that a defect in one of the processes does not completely block the organogenesis event. Furthermore, the collective effort possibly accelerates the process of organogenesis and regulates the timing of organ formation. Thus, the collective action and interplay of diverse cell behaviours is a common developmental strategy that orchestrates various organogenesis events.

3.1.2 Role of RPE morphogenesis: A riddle in RNE morphogenesis

Apart from basal shrinkage and rim involution, the optic vesicle epithelium undergoes an additional epithelial rearrangement that could play a role in RNE morphogenesis: formation of the retinal pigment epithelium (RPE). Although the biology of the mature RPE and the gene regulatory network involved in determination and specification of the RPE is well-understood (Fuhrmann et al., 2014; Kim et al., 2016; Miesfeld et al., 2015), we still lack an understanding of RPE morphogenesis. The RPE morphology differs between amniotes (columnar) and teleosts (squamous), however the morphogenetic strategies in both the groups involve cell shape changes. The teleost RPE morphogenesis involves epithelial

thinning, a drastic cell shape change from columnar to squamous shape. However, the cellular mechanisms of RPE flattening remain unknown, which makes it difficult to address its role in OCM. Nevertheless, I would like to discuss two important points revealed from my work that could be useful in this direction. 1) None of the perturbations described here (Rockout, *laminin-α1* morphant, *opo* morphant, and *ezrin* morphant) affected RPE morphogenesis. Neither have the previous *opo* and *laminin-α1* mutant studies reported any RPE phenotype (Bryan et al., 2016; Martinez-Morales et al., 2009). This argues that cell-matrix adhesion or actomyosin-dependent mechanisms probably do not play a role in RPE morphogenesis. 2) The developing RPE is a part of the continuous epithelium in the optic vesicle and thus it is physically linked to the developing RNE. Therefore, RPE morphogenesis could possibly exert a pushing force, which induces rim cell involution. Nevertheless, in *laminin-α1, opo,* and *ezrin* morphants, which show rim involution defects, RPE morphogenesis occurred normally. Thus, the pushing force from RPE flattening is probably not sufficient for rim involution and rim cells require active collective migration to involute. Future studies need to address the mechanism of RPE morphogenesis and its possible role in RNE invagination.

3.1.3 Role of accessory tissues in RNE formation

The vertebrate eye also contains other accessory tissues that develop in parallel with the RNE. These structures include the lens and the periocular mesenchyme (POM). The concurrent development of these structures is important for timely eye development and possibly influences RNE morphogenesis. Interestingly, under *in vitro* culture conditions it is possible to form an optic cup and the hemispherical RNE in absence of any lens or POM (Eiraku et al., 2011). This argues against the requirement of these accessory structures for RNE morphogenesis and highlights the self-organising power of the RNE. However, their presence and possible influence in the *in vivo* scenario cannot be ignored and needs more attention.

Multiple studies have shown the role of the lens as a signaling center but whether it also plays an active role in driving RNE invagination is debated (Chauhan et al., 2009; Hyer et al., 2003; Pandit et al., 2015). Nevertheless, the invagination of the lens and the RNE are highly coordinated and occur simultaneously (Fuhrmann, 2010). Therefore, I speculate that *in vivo* the lens placode might play a mechanical role in the invagination process. It could boost the kinetics of RNE invagination and thus contribute to the temporal regulation of OCM. In future, it would be interesting to compare the speeds of invagination with and without the developing lens placode. It has been proposed for mouse and medaka that the lens and the RNE are linked through filopodial connections (Chauhan et al., 2009;

Porazinski et al., 2015). However, I did not observe such filopodia in any of my experiments and this mechanism has not been tested for zebrafish OCM. It is possible that the filopodial mechanism is species specific. Therefore, to understand OCM in a holistic manner, more research is required to dissect the role of the lens.

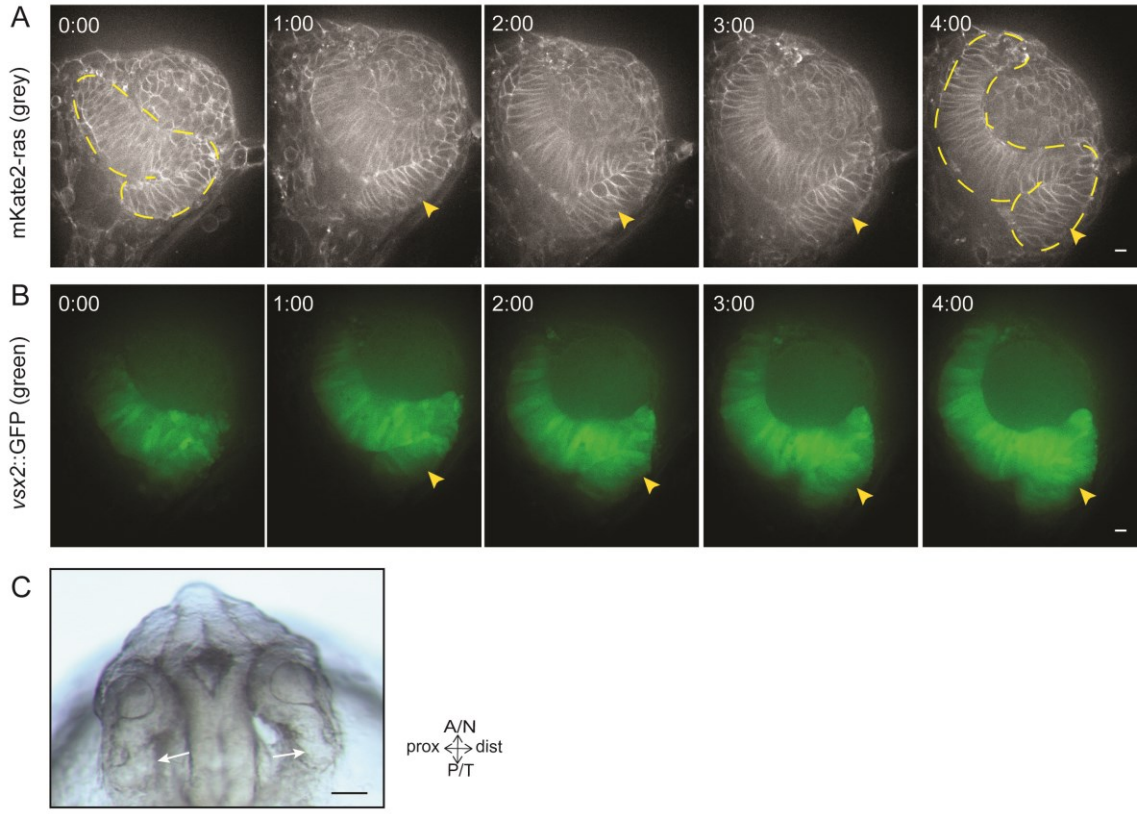

Figure 3.2: RNE morphogenesis in *lmx1b* double morphant
A,B) Time-lapse imaging of *lmx1b.1, lmx1b.2* morphant condition in Tg(*vsx2::GFP, bactin::mKate2ras*) background. Membrane marker (A) and *vsx2::*GFP signal (B). Rim cells with ectopic vsx2 expression (Arrowhead). Outline of the developing optic cup (dashed line). Time in h:min. Movies started at 17–18 ss. N = 5. Scale bar = 10 µm.
C) Brightfield image of 30 ss *lmx1b* morphant showing secondary optic cup phenotype. Arrows mark secondary invagination zone. Scale bar = 50 µm.

The second accessory tissue in the developing eye is the periocular mesenchyme (POM). It originates from the cranial neural crest-derived population of cells that migrates adjacent to the optic cup to reside initially near the rim zone and later near the ciliary margin zone. It later gives rise to the accessory structures such as the cornea and the iris. These cells are shown to be important signaling centers that regulate the FGF-mediated retinal patterning and the morphogenesis of the ventral optic cup including the choroid fissure closure (Lupo et al., 2011; McMahon et al., 2009; Sedykh et al., 2017). The Lmx1b transcription factor is shown to be crucial for survival of cranial neural crest cells and POM (McMahon et al., 2009). Morpholino-mediated knockdown of Lmx1b isoforms *lmx1b.1* and *lmx1b.2* in

zebrafish results in optic cups with very little POM and causes coloboma (McMahon et al., 2009). My preliminary data show that combined morpholino-mediated knockdown of *lmx1b.1* and *lmx1b.2* leads to a rim involution defect. It results in ectopic RNE cells that can initiate a secondary invagination zone (Figure 3.2). These observations further support the role of POM in RNE morphogenesis. Interestingly, also the severe *ezrin* morphants showed significant cell death in the region where cranial neural crest cells reside, which could possibly affect the POM organisation. However, it remains unknown if the role of the POM would be merely signaling based or if the POM also secretes some ECM molecules. Therefore, in the future it would be interesting to study the role of POM and its influence on rim cell behaviour and RNE morphogenesis.

3.2 Distinct dynamics at the basal side of the epithelium drive RNE morphogenesis

A highlight from my work is the importance of the basal membrane domain dynamics in epithelial morphogenesis of the RNE. During both, rim involution and invagination, the cells modulate the membrane and cell-matrix adhesion dynamics at their basal side. During rim involution cells extend basal lamellipodial protrusions and exhibit transient contacts with the matrix. During invagination, the cells accumulate contractile actomyosin at the basal side and form stable focal adhesions. The phenotypes of *laminin-α1*, *opo,* and *ezrin* knockdown show that perturbed basal dynamics affect RNE morphogenesis. Similar role for basal dynamics also seems to be important for *in vitro* OCM. The addition of matrigel or purified ECM components laminin and enactin to the culture medium is crucial to generate optic cups from the aggregates of embryonic stem cells (Eiraku et al., 2011). Thus, RNE morphogenesis provides an example of how epithelial morphogenesis can be guided by modulating the basal domain dynamics of the cells.

Other known systems where basal domain dynamics drive epithelial morphogenesis include the formation of the zebrafish midbrain-hindbrain boundary, where the ECM is important for basal shrinkage of the boundary cells (Gutzman et al., 2008), the *Drosophila* follicular epithelium, where cell-ECM adhesion plays a crucial role in follicle rotation and egg elongation (Diaz de la Loza et al., 2017; Haigo and Bilder, 2011) and the *Drosophila* wing imaginal disc, where the cell-matrix interaction also crucially shapes the tissue architecture (Dominguez-Gimenez et al., 2007; Ma et al., 2017; Pastor-Pareja and Xu, 2011). Additionally, now it is becoming clear that systems such as gastrulation movements in *Drosophila* embryogenesis, for which apical dynamics were considered as the main morphogenetic drivers, also involve interesting dynamics at the basal side. For instance, a

recent study on germ band extension shows the importance of basal membrane dynamics (Sun et al., 2017). The cells in the germ band often form rosette, by shrinking their specific apical contacts. The new study now shows that these cells feature basal protrusions, which are also important for rosette formation and the subsequent convergent extension. Interestingly, these basal protrusions precede the known apical changes of rosette formation and open an exciting series of new questions on basal dynamics (Sun et al., 2017). All these examples highlight that to understand the cellular mechanisms of epithelial morphogenesis, it is important to consider the cellular dynamics at the apical as well as the basal side.

Below I discuss a few points related to the basal dynamics in RNE morphogenesis.

3.2.1 Basal shrinkage: a combination of constriction and compaction

My work shows that the invaginating neuroepithelial cells shrink the basal area and adopt a basally narrower cone shape. However, this raises the question whether the basal shrinkage occurs by active contraction, compaction or a combination of both phenomena. The accumulation of basal contractile actomyosin argues for an active contractile force in the invaginating cells. A parallel study from the Martinez-Morales group (Nicolás-Pérez et al., 2016) has reported that the invaginating cells exhibit basal membrane fluctuations similar to the apical pulsatile behaviour observed during other processes of epithelial cell shape changes (Martin and Goldstein, 2014). This further supports presence of active contractile basal constriction. However, my results showed that the effect of the loss of basal actomyosin accumulation on invagination was surprisingly weak. The loss of basal actomyosin only affected the kinetics of the invagination but did not grossly perturb the final RNE architecture. This observation argues that apart from basal constriction, additional mechanisms drive RNE invagination. My data suggest that rim involution and cell proliferation together increase the cell density in the invaginating layer. Additionally, the flattening RPE and the involuting rim cells could create a stiffer boundary that inhibits a within-plane expansion of the neuroepithelial layer. Such crowding within a stiff boundary could result in the compaction of cells and shrinking of the basal processes of the neuroepithelial cells. Thus, the process of invagination is possibly a combination of constriction and compaction mechanisms. Thus, both of the previously proposed mechanisms, basal constriction (Martinez-Morales and Wittbrodt, 2009) and crowding-induced invagination (Eiraku et al., 2012; Eiraku et al., 2011) play a role to a certain extent. The coupling of the actomyosin contractility, rim migration and cell proliferation possibly supports an efficient, faster, and robust way to invaginate the RNE.

3.2.2 Epithelial feature to support basal contractility: a form of actin stress fiber assembly?

I showed that the invaginating cells accumulate actomyosin at the basal side. However, the cellular structure of the basal contractile actomyosin remains elusive. Based on the basal localisation close to the focal adhesions and its contractile nature, it is tempting to speculate that the basal actomyosin structure is similar to the actin stress fibers (Burridge and Wittchen, 2013; Tojkander et al., 2012). The dependency of this actomyosin localisation on cell-ECM attachment and Rho-Rock pathway supports this hypothesis. Furthermore, a treatment with CK-666, a chemical inhibitor of actin nucleator Arp2/3 complex, did not disrupt the basal actomyosin enrichment (data not shown). Such independence from Arp2/3 complex is in line with the dorsal stress fiber hypothesis (Hotulainen and Lappalainen, 2006). Unlike the well-studied apical actomyosin networks involved in apical constriction (Martin and Goldstein, 2014), the actomyosin structure playing a role in basal constriction remains elusive. Therefore, to understand the epithelial feature that could support basal contractility, it would be important to investigate the structure and composition of this basally enriched actomyosin network.

3.2.3 The role of apical components in RNE morphogenesis seems limited.

So far, I mentioned the role of basal dynamics in RNE morphogenesis. However, majority of epithelial morphogenetic phenomena such as gastrulation movements in *Drosophila*, and vertebrate neurulation involve modulation of apical components (see section 1.2), importantly the polarity complexes and the adherens junctions. This raises the question if apical components play any role in RNE morphogenesis. For *in vitro* optic cup formation, it is proposed that the apical constriction of the so called ‘hinge cells’, the cells at the boundary between the RPE and RNE is crucial for RNE invagination (Eiraku et al., 2012; Eiraku et al., 2011). Such apical constriction is accompanied with apical enrichment of phospho-myosin in the hinge cells. However, my work shows that there are no specific hinge cells in the teleost optic cup. Due to rim involution, the rim cells turnover continuously. Hence it is not clear how the apical constriction mechanism should work in this case. Imaging of the apical marker Par3-GFP showed that rim cells undergo a transient apical surface area reduction as the cells reach the fold of the epithelium (Figure 2.8D, Movie 4). Once, the rim cells turned around the fold and reached the invaginating layer, the apical area expanded again (Figure 2.8D, Movie 4). However, the molecular mechanism of such transient apical constriction remains unknown. Nevertheless, different studies aimed at understanding the role of apical components in eye and retinal development indicate that the apical components seem to be

mainly important for the epithelial integrity, regulation of neuronal differentiation and lamination of the retina. Studies using mutants/morphants for important polarity regulators *aPKC* (Horne-Badovinac et al., 2001), *crumbs* (Malicki and Driever, 1999; Omori and Malicki, 2006), *stardust*, (Wei and Malicki, 2002; Yamaguchi et al., 2010), *lgl* (Clark et al., 2012), and *pac* mutant of junctional component N-cadherin (Masai, 2003) have not reported any OCM defect but rather defects in retinal lamination. The only reports of apical components affecting optic cup architecture are that of mutants for *par3* (Wei et al., 2004) and the *glass onion* mutant of N-cadherin (Malicki et al., 2003; Pujic and Malicki, 2001). However, these mutants also show rather early defects. In *par3* mutant, the polarity defect already affects eye-field splitting and evagination process resulting in cyclopia (Wei et al., 2004). This phenotype is consistent with the role of Par3 in establishing polarity during optic vesicle evagination (Ivanovitch et al., 2013). In case of the *glass onion* mutant for N-cadherin, all neuroepithelia in the embryo disintegrate due to adhesion defects and hence its role in driving RNE morphogenesis is difficult to interpret (Malicki et al., 2003; Pujic and Malicki, 2001). Thus, the role of apical components as drivers of RNE morphogenesis seems limited. In contrast, the major mutants with well-described RNE morphogenesis defects include *laminin-α1* (Bryan et al., 2016) and *opo* (Martinez-Morales et al., 2009), both regulating basal dynamics of cells. All these studies indicate that RNE morphogenesis seems to be mainly driven by basal epithelial morphogenesis.

3.3 Rim cells migrate collectively

My work has revealed that rim involution is a new example of collective epithelial migration. Rim cells involute using migratory behaviour while being apically connected to each other via adherens junctions. Interestingly, cellular movements in RNE morphogenesis are not only seen in zebrafish, but have also been reported using cellular tracing in chick (Kwan et al., 2012) and *Xenopus* (Holt, 1980). Therefore, it would be interesting to see if collective migration phenomena are a conserved feature of vertebrate RNE morphogenesis.

There are several interesting points about the collective migration of rim cells.
1) This collective migration occurs only in the rim zone of the optic vesicle epithelium. Therefore, how the migratory behaviour is limited to the rim zone is an interesting question in itself. Nonetheless, such selective migratory behaviour only in a part of a continuous epithelial sheet represents a novel mode of collective epithelial migration. This mode is different from the known systems of collective epithelial migration, which include migration of entire 2D sheets, multi-layered 3D strands and isolated group or cluster of cells (Friedl and Gilmour, 2009; Rorth, 2009).

2) As the optic vesicle epithelium is continuous, it does not have a specific leading edge. This means that rim cells do not have any specially demarcated leader cells, which are common to many collective migration phenomena (see section 1.2.4). Lack of leader cells is also seen in case of follicle cell migration in the *Drosophila* egg chamber, where the follicle cells form a continuous sheet that encapsulates the germ cells and the future oocyte (Haigo and Bilder, 2011). Therefore, the presence of leader cells does not seem to be universal to all the collective epithelial migration phenomena as thought before (Friedl and Gilmour, 2009).

3) Even though the rim cells lack leader cells, they are still polarised in the direction of migration as revealed by the directed protrusions. However, the guidance cues that facilitate directed rim involution still remain unknown. In case of follicle cells, the directionality is given by planar cell polarity (PCP) that results in polarised distribution of cytoskeletal regulators and actomyosin cytoskeletal components in the plain of the epithelium (Lewellyn et al., 2013; Viktorinova et al., 2009). However, it is not known if PCP plays a role in OCM. Alternatively, the direction could also be given by the force distribution in the tissue. The pulling force of invagination and a mechanical barrier from the flattening RPE could possibly guide the cells to move into the invaginating region. Additionally, the basal lamina could also play a role in guidance by durotaxis. The patterns and mechanical properties of the ECM influence the migration of cells in variety of systems (Charras and Sahai, 2014). Similarly, migrating cells can also influence and change the underlying matrix (Loganathan et al., 2016). Indeed, the cells of the optic vesicle actively secrete ECM components, such as laminin (Pickering, 2012) and thus the whole morphogenetic process probably involves complex ECM remodelling. Therefore, the micropatterns in the basal lamina architecture and composition might guide the cellular movement and need to be investigated (See section 4.1).

Thus, rim involution is not only important to understand eye development, but offers an epithelial system to understand the cellular mechanisms of collective epithelial migration.

3.4 RNE morphogenesis occurs by spatio-temporal transition of cell behaviour from a migratory to an adherent epithelial state

During development, cells rarely exhibit archetypal epithelial or mesenchymal characteristics but rather a mixture of both. This is well-described by the emerging concept of a continuum between the mesenchymal and epithelial state (Bernadskaya and Christiaen, 2016; Campbell and Casanova, 2016). For example, during zebrafish gastrulation, the mesendodermal cells lack obvious apicobasal polarity but require cadherin based cell-cell adhesion for the gastrulation movements (Solnica-Krezel, 2006). The mesendodermal cells exhibit an intermediate state between the epithelial and mesenchymal archetypes. Thus,

cells resort to different states along this continuum in a context and morphogenetic process-dependent manner. My work shows that rim cells represent such an example and exhibit both epithelial (apicobasal polarity and cell-cell adhesion) and mesenchymal properties (directed protrusive activity and dynamic cell-matrix contacts). However, when the rim cells involute and become part of the invaginating RNE they stop their protrusive activity, adhere stably to the ECM and attain the archetypal epithelial state. Thus, rim cells traverse along the continuum of cellular states by modulating their cell behaviour in space and time to shape the RNE. Furthermore, the spatiotemporal regulation of this transition seems crucial, as a premature transition to the stably attached epithelial state perturbs subsequent retinal morphogenesis. However, the cue for the behavioural change in rim cells remains unknown and further research is required to understand how the cell behaviour is modulated in space and time (see section 4.2). Interestingly, similar cellular transitions are observed at earlier stages of teleost eye development. During optic vesicle evagination, the eye field cells, which are mesenchymal in nature, change their morphology and acquire apicobasal polarity to form the optic vesicle (Bazin-Lopez et al., 2015; Ivanovitch et al., 2013). Thus, the teleosts early eye development from the eye field to hemispherical retina utilizes gradual transition from the mesenchymal to epithelial state. Such strategy of parallel progression of neurulation, epithelial polarisation and evagination or that of parallel rim involution and invagination sets the timing of organogenesis and possibly makes the whole process suitable for the fast development of the zebrafish embryos.

3.5 Defects in rim migration cause ectopic RNE fate specification and interfere with future retinal development

I show that rim migration is indispensable for shaping the RNE, the organ precursor that gives rise to the retina. Rim involution positions the prospective RNE cells to their right location at the right time before they acquire the RNE fate and change their cellular behaviour. A defect in rim migration leads to ectopic determination and change of cell behaviour of prospective RNE cells. As a result, the migration-defective cells attach stably to the matrix prematurely, outside the primary invagination zone of the RNE. Such stable adhesion to the matrix possibly further hampers their movement and in turn the RNE architecture. This suggests that RNE cell behaviour is independent of the cellular position and is guided by some internal developmental timer. Similar observations were made for zebrafish neural tube development, where it was shown that the schedule of epithelial polarisation depends on the developmental time rather than the local environment (Girdler et al., 2013). The developmental timer in this process remains unknown and the effect is attributed to the number of cell cycles in the developmental history of the cells (Girdler et al.,

2013). However, I would like to speculate that since laminin is shown to be important for the polarisation of the neural tube cells (Ivanovitch et al., 2013), local cell-autonomous secretion of ECM could be the timer for the polarisation. As for the rim cells, it should be noted that rim cells also originate from the neural tube and similarly undergo the gradual transition from mesenchymal to epithelial morphology (Section 3.4). Therefore, the ectopic determination of RNE fate observed upon defective rim migration might be induced by prolonged exposure to the locally secreted ECM. Hence, it would be interesting to investigate if the local secretion of ECM by the optic vesicle cells and the duration of exposure to the local ECM could act as the developmental timer for RNE-like fate and behaviour. Overall, my work shows that rim involution serves as an important morphogenetic program to correctly localise the 'pre-programmed' presumptive RNE cells. It highlights that although developmental patterning and signalling are crucial, the morphogenetic movements are equally important drivers of organogenesis.

3.6 Developmental patterning of cell behaviours is a conserved theme in vertebrate optic cup morphogenesis

Interplay of morphogenesis and developmental patterning is crucial for successful organogenesis. Developmental patterning is commonly studied in terms of expression of specific transcription factors and downstream genes. However, at the most downstream level, such pattern can also be seen in the cell behaviours (Bernadskaya and Christiaen, 2016; Levine and Davidson, 2005). A pattern of cell behaviours is also apparent during OCM. The dorsal or distal layer of the optic vesicle starts invagination whereas the ventral region contributes to rim involution, predominantly in the ventral-temporal part of the retina (Schmitt and Dowling, 1994; Heermann et al., 2015; Picker et al., 2009; Kwan et al., 2012). In line with this, the phenotypes I observed upon perturbation of rim migration result in accumulation of rim cells specifically at the ventral-temporal side of the optic cup. In contrast, cells at the dorsal and nasal side are much less affected. In addition to the dorso-ventral pattern, patterning by FGF signaling also distinguishes the cell behaviours along the naso-temporal axis and makes the nasal cells more cohesive (Picker et al., 2009). This raises the question if such behavioural pattern is limited to the teleost optic vesicle or whether it is also conserved in higher vertebrates. Ventral-temporal cell movements have not only been observed in teleosts but also during *Xenopus* and chick RNE morphogenesis (Holt, 1980; Kwan et al., 2012). Furthermore, studies in mouse have indicated that the invagination of the dorsal and ventral RNE can be uncoupled (Molotkov et al., 2006). Therefore, I speculate that the specific cell behaviour at play might depend on the species and the shape of the optic vesicle. However, the use of differential morphogenetic strategies

for dorsal and ventral retinal morphogenesis seems a conserved feature of the vertebrate eye development.

It is possible that such 'pattern' of morphogenetic strategies segregates cells into distinct domains that experience different environments. It is tempting to speculate that such segregation of cells in the optic vesicle could help the cells to attain the RNE fate in a stepwise manner to prepare for the later retinal developmental programs. Interestingly, the early patterning of the retina already specifies the expression domains of the axon guidance molecules required later in the retinal development (Harada et al., 2007; Picker and Brand, 2005). Thus, the morphogenetic movements during OCM possibly impact the later retinal development and its connection to the brain.

3.7 Studying organogenesis using *in vitro* versus *in vivo* systems

The pioneer work from the Sasai group that reported the formation of optic cups from embryonic stem cells in organoid cultures, showcased the self-organising power of cells to build the hemispherical RNE in a minimalistic system (Eiraku et al., 2011; Nakano et al., 2012). The authors also reported successful recapitulation of retinal development and generation of retinal neurons (Eiraku et al., 2011; Nakano et al., 2012). This work paved the way for numerous more studies on the generation of retinal neurons or pigment epithelium in 3D cultures (Boucherie et al., 2013; Decembrini et al., 2014; Gonzalez-Cordero et al., 2013; Nakano et al., 2012; Santos-Ferreira et al., 2016; Volkner et al., 2016; Zhong et al., 2014; Zhu et al., 2013). Such an *in vitro* approach has provided a great tool for therapeutic and pharmaceutical research. However, when it comes to understanding the mechanism of organogenesis, there are various differences between the *in vitro* and *in vivo* scenarios of optic cup formation. Unlike in the animal model systems (Kwan et al., 2012; Young and Hodas, 1964), optic cup formation in culture conditions crucially depends on cell proliferation (Eiraku et al., 2011). The basal actomyosin enrichment revealed from my work, has not been observed in the *in vitro* optic cups (Eiraku et al., 2011). Furthermore, the efficiency of invagination is lower in these 3D culture systems and does not occur reproducibly (Volkner et al., 2016). Therefore, the conclusions about the organogenesis mechanisms proposed from *in vitro* studies should be interpreted with caution. The use of different molecular and cellular strategies in the different species highlights the fact that distinct morphogenetic strategies can be used to reach a similar architecture. In simple terms, there could be various ways to solve a problem that finally give the same solution. Thus, although *in vitro* optic cup formation exemplifies a reductionist approach to understand organogenesis, it does not explain the actual *in vivo* process of organ formation. Therefore, it is important to

complement such approaches by studying organogenesis using *in vivo* systems, which has been a central theme of my work.

To summarise, my work has made an important contribution to understand how epithelial morphogenesis shapes the retinal neuroepithelium in the developing zebrafish embryos. Beyond this particular organogenesis event and biology of the eye, it gives important insights into diverse fields of morphogenesis, epithelial cell biology, collective cell migration, cell-matrix interaction and developmental control of cell behaviours.

4. Experimental outlook

My work presented here has expanded our understanding on the morphogenesis of the zebrafish retinal neuroepithelium (RNE). In this chapter, I would like to discuss some of the open questions that me and future lab members will follow upon, the experimental strategies to investigate these questions and some preliminary data.

4.1 Investigating the dynamics of the basal lamina components during RNE morphogenesis

The extracellular matrix of epithelia – the basal lamina and cell-matrix attachment play a key role in RNE morphogenesis. This was shown by the defects in RNE invagination resulting from perturbed integrin trafficking and loss of *laminin-α1* (*lama1)* (Bogdanovic et al., 2012; Bryan et al., 2016; Kwan, 2014; Martinez-Morales et al., 2009). In addition, my work presented here highlights the importance of basal lamina and cell-matrix attachment for the collective cell migration during rim involution. To this date, the localisation of different ECM components at different stages of RNE morphogenesis has been investigated using fixed sample immunohistochemistry (Kwan, 2014). However, the basal lamina is not just a static substratum for the epithelial cells, but plays an active role in epithelial morphogenesis (Jayadev and Sherwood, 2017; Morrissey and Sherwood, 2015). It is becoming clear that in many systems the basal lamina undergoes constant remodelling in structure as well as composition (Loganathan et al., 2016; Morrissey and Sherwood, 2015). However, so far, all the studies on RNE morphogenesis, including my work, lack an understanding of the dynamics of basal lamina during optic cup formation.

Visualising the dynamics of basal lamina components by live-imaging has been challenging due to lack of proper tools. Fluorescently labelled primary antibodies against matrix components have been used in chick (Aleksandrova et al., 2012), hydra (Aufschnaiter et al., 2011) and mammalian explant cultures (Harunaga et al., 2014) to visualise and track the convective movement of the matrix or the relative movement between cells and the lamina (Loganathan et al., 2016). However, this approach should be interpreted with caution because antibody binding can also abrogate the interactions of matrix component with cells or other matrix molecules. For example, anti-laminin antibodies block the function of laminin and perturb the induction of epithelial polarity (Ekblom, 1989; Klein et al., 1988). Nevertheless, new advancements in systems of *C. elegans* and *Drosophila* have generated tagged-version of basal lamina components. In *C. elegans* transgenic lines expressing fluorescently labelled laminin and collagen have been established (Hagedorn and

Sherwood, 2011; Kao et al., 2006) and have allowed live-imaging of the basal lamina. For instance, live-imaging of laminin dynamics has given important insights into the role of laminin deposition in epithelial polarity establishment (Rasmussen et al., 2012). In *Drosophila*, a protein trap screen identified a transgenic line that tagged the *collagen IV* gene (Morin et al., 2001). It has allowed visualisation of Collagen IV dynamics in *Drosophila* development and to study its role in shaping the *Drosophila* egg chamber (Haigo and Bilder, 2011) and the wing imaginal disc (Ma et al., 2017; Pastor-Pareja and Xu, 2011). However, such tools to visualise ECM dynamics have been lacking for zebrafish (Jessen, 2015). A recent study used fibronectin construct *fn1a-GFP* under a tissue specific promoter, to visualise fibronectin localisation during somitogenesis (Julich et al., 2015). However, it will be ideal to express the tagged version of matrix components under endogenous gene expression loci to avoid misexpression at the wrong place, at the wrong time or in the wrong amount. Therefore, I set out to develop tagged versions of some of the zebrafish basal lamina components.

I decided to tag ECM components laminin and fibronectin. Laminin is one of the earliest components of the basal lamina and plays a crucial rule in the organisation of other matrix components (Hohenester and Yurchenco, 2013; Mouw et al., 2014). I opted for *lama1*, which is expressed in the optic vesicle (Pickering et al., 2016) and I have shown is important for rim involution and OCM. Additionally, my data for anti-fibronectin immunostaining have shown a temporal shift in the pattern of fibronectin staining, which follows the rim cells. Therefore, as an additional ECM component, I decided to tag fibronectin *fn1a*. As cloning strategy, I opted to use bacterial artificial chromosome (BAC) recombineering to add the fluorescent tag to the proteins. BACs contain several kilobases long pieces of chromosomes and thus this approach preserves the endogenous gene regulatory regions. This is especially important for *lama1*, for which the important enhancer element lies in intron-1 (Pickering et al., 2016). Hence, cloning only the coding sequence would result in loss of important regulatory information. Thus, with the help of Aleksandra Syta and Mihail Sarov from the transgenomics facility at MPI-CBG, we generated BACs with C-terminal tagged version of *lama1* and *fn1a* with sfGFP, mKate2 and dendra tags (See section 5.2.2). Additionally, we also inserted a tol2 transposon unit in the construct to allow transgenesis in zebrafish, when injected together with the transposase RNA (See section 5.2.2).

To test, if the constructs were functional, I injected the BACs in the zebrafish embryos with transposase RNA. I tested the embryos for fluorescence. The *lama1::lama1-GFP* construct gave positive results. I fixed the embryos showing a fluorescent signal and immunostained with anti-laminin and anti-GFP antibodies. I could detect the secreted laminin-GFP in the

optic cup as well at the somite boundaries, where laminin is also located endogenously (Figure 4.1A). Furthermore, a few cells showing high expression of laminin-GFP, were also stained with laminin antibody (Figure 4.1A). Thus, the *lama1::lama1-GFP* construct most likely generates full length laminin-GFP, which is capable of being secreted from the cells. Importantly, the uninjected controls did not show GFP signal and further confirmed the specificity of the stainings (Figure 4.1B). Having established the laminin construct, I am currently growing the F0 injected fish to find germline carriers and testing the functionality of fibronectin constructs.

This strategy will allow me to visualise when and how laminin is synthesized and secreted. Additionally, investigating the fluorescence recovery after photobleaching (FRAP) would allow me to address the diffusion and turn-over dynamics of laminin in the basal lamina. This tool will further help to investigate if the rim cells move relative to the basal lamina or the basal lamina is also carried with the cells in a convective way. In summary, this construct will provide a great tool to investigate laminin dynamics in RNE morphogenesis and beyond. It will be a good tool for the entire zebrafish community to visualise and investigate the basal lamina dynamics.

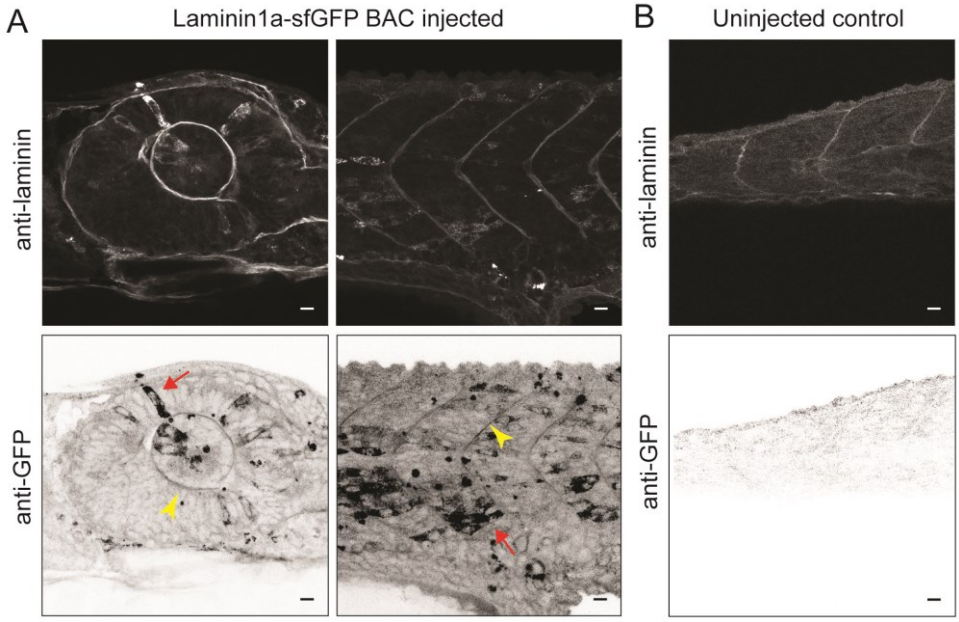

Figure 4.1: Analysis of *lama1::lama1-sfGFP* injected fish.
A) Confocal scan of the optic cup (left) and flank region (right) in *lama1::Lama1-sfGFP* injected embryo stained with anti-laminin and anti-GFP antibody. Secreted lama1-sfGFP staining (arrowhead), cell with high expression of lama1-sfGFP (arrow)
B) Confocal scan of the flank region an uninjected embryo stained with anti-laminin and anti-GFP antibody.
Scale bars = 10 µm.

4.2 Understanding the mechanisms that change the cellular behaviour of rim cells from migratory to adherent state: a transcriptomic approach.

My work showed that the rim cells change their behaviour and traverse along a mesenchymal to epithelial continuum of cellular states (see section 3.3). Upon involution, rim cells change to an adherent morphology and participate in the RNE invagination. This opens a new question: what regulates and modifies the cell behaviour from a migratory to adherent state? To answer this question, one needs to understand the differences in migratory rim cells and adherent RNE cells. Since, this migratory movement is coupled with the cell determination program, I wondered if these changes in cell behaviour are associated with transcriptional changes in the cells. Therefore, I opted for a transcriptomic analysis to identify the genes differentially expressed in the migratory versus adherent cells in the optic vesicle. Such unbiased approach would provide me information on novel candidate genes and pathways that could potentially play a role in RNE morphogenesis. Additionally, the transcriptomic analysis would provide a comprehensive list of genes expressed in the rim cells and the RNE cells, e.g. the different ECM components or the specific isoforms of any particular gene. Thus, this analysis would serve as an important resource to understand gene function in the developing eye. Such resource would also help to identify potential markers that label the rim cells specifically. Hence, to gain a genome-wide understanding of the transcriptional profile of rim and RNE cells, I opted for an RNA-seq approach.

First, I needed a strategy to isolate rim cells from the RNE cells. This was challenging since both cell populations are part of a continuous epithelium and lack any known non-overlapping markers. To this end, I made use of the observation that in control condition the GFP expression in the Tg(*vsx2::GFP*) embryos correlated with the cellular position in the optic vesicle. In the rim zone, the GFP signal was weak and in the invaginating region the GFP signal was much brighter (Figure 2.24). Therefore, I used the GFP signal from *vsx2::GFP* line as a marker to sort my cells. I chose 18–20 ss embryos for the experiment as they contained population of rim cells as well as RNE cells. I isolated optic vesicles from *vsx2::GFP* embryos and dissociated the cells mechanically. The dissociated cells were sorted by fluorescence-activated cell sorting (FACS). FACS allowed the segregation of not only the GFP negative cells, which contained prospective RPE cells and contaminant tissue if any, but also specific populations of GFP positive cells showing high and low signal. Within the GFP positive cells, I set thresholds to collect the extremities of this population and discarded the middle population to avoid a mixed group of cells (Figure 4.2B). Thus, separate ‘low GFP/rim cells’ and ‘high GFP/RNE cells’ samples were collected and used to

extract the total RNA, make a cDNA library, followed by deep sequencing and transcriptomic analysis (Figure 4.2A). The samples were collected in 4 replicates from different experiments. The sequencing was performed by the next generation sequencing facility at Biotec, TU-Dresden and the bioinformatic analysis was performed by Mathias Lesche.

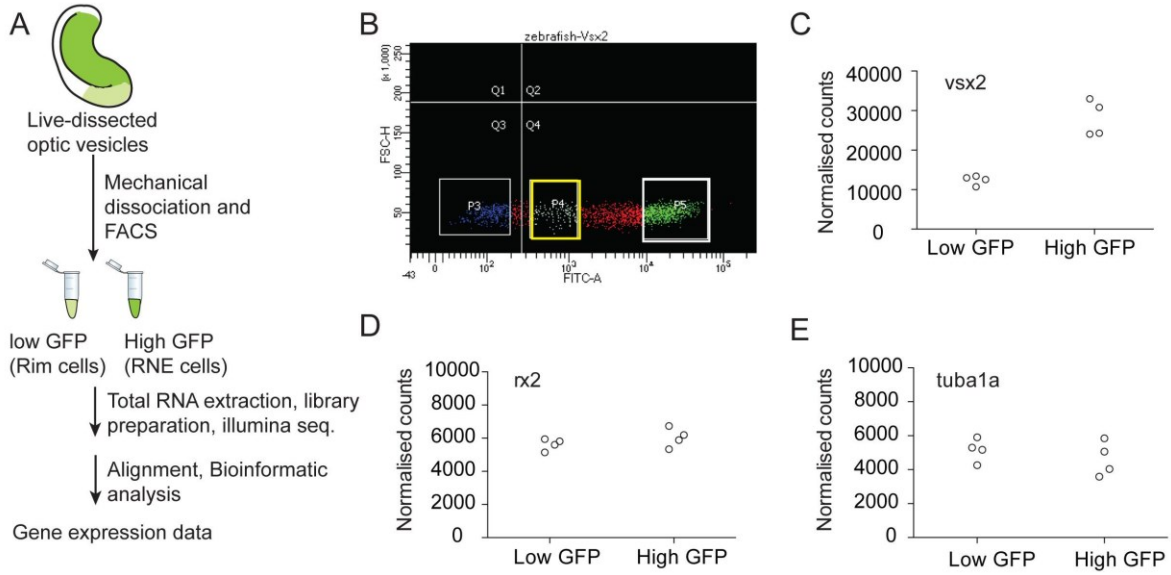

Figure 4.2: Sample preparation and initial analysis of RNA-seq data
A) Experimental pipeline for the RNA-seq experiment from sample preparation to data analysis.
B) Typical spread of cells during FACS. Q4 contains the cluster of GFP positive cells. Low GFP cells (Yellow box), High GFP cells (White box)
C,D,E) Normalised counts for *vsx2* (C), *rx2* (D) and *tuba1a* (E) in low GFP and high GFP samples. Each dot represents the value from a replicate.

Initial quality-control assessment of the data confirmed that the quality of the data was suitable for further analysis. On average, 92% of the reads mapped to unique locations in the zebrafish genome and more that 85% mapped to exonic regions (see section 5.5, Table 10,11). Furthermore, initial exploratory analysis also confirmed the fidelity of cell sorting. Indeed, the total normalised counts for *vsx2* were almost double in the high GFP sample than the low GFP sample (Figure 4.2C). As control, the eye field transcription factor *rx2* and the housekeeping gene for tubulin, *tuba1a* showed similar counts in both the samples. Thus, the initial QC check confirmed that the RNA-seq data was of good quality and faithfully represented the two populations of the cells.

Next, we performed differential gene expression analysis to identify genes enriched either in the rim cells or the RNE cells. To this end, I pruned the list of genes to only include genes showing minimum 2-fold upregulation or downregulation. To further minimise false positives, I applied a threshold to remove genes that showed less than 200 normalised counts averaged over all samples. With these criteria, 362 genes showed differentially regulated gene expression. In reference to the low GFP sample (rim cells), 79 genes were upregulated

in the high GFP sample (RNE cells) and 283 genes down regulated. To further verify the experimental strategy, I analysed the log2 fold change for the early eye transcription factors, markers for the RNE, and RPE-like genes (Figure 4.3A). As expected, the early eye transcription factors did not show any significant difference in expression (Figure 4.3A). On the other hand, the markers for retinal progenitors such as *vsx2*, *ascl1* were enriched in the high GFP (RNE) samples (Figure 4.3A). This confirmed that the high GFP sample contained the retinal progenitor cells. Interestingly, some genes known to express in the RPE were observed in the low GFP (rim cell) sample (Figure 4.3A). This raised the doubt if there was a contamination of the RPE cells. However, the key RPE transcription factors *mitfa* and *mitfb* showed very low counts. Therefore, it is possible that the rim cells still retain the bipotential nature of the optic vesicle cells and have not fully committed to the RNE fate yet. As a result, they express both RNE and RPE genes at low levels. In line with this hypothesis, the transgenic reporter lines for these RPE markers such as the *tfec* gene also show expression in the rim zone (Miesfeld et al., 2015). Furthermore, rim cells include the future retinal stem cells that give rise to RNE as well as RPE (Heermann et al., 2015; Tang et al., 2017), and hence possibly retain markers for both. To conclude, the known markers in the optic cup exhibit the expected pattern of expression in my gene expression dataset.

Next, I asked if the markers known to show patterned expression along the dorso-ventral or the naso-temporal axis in the optic cup showed any differential gene expression in these samples. Interestingly, the dorsal markers were enriched in the high GFP (RNE cell) sample, whereas ventral markers were enriched in the low GFP (rim cell) sample (Figure 4.2B). This is in line with the observation that rim involution is predominant on the ventral side of the developing optic cup (Heermann et al., 2015; Kwan et al., 2012). This raises the possibility that the regulators of dorso-ventral patterning could be linked with regulation of cell behaviour. Indeed, BMP4 overexpression that dorsalises the optic cup blocks rim migration (Heermann et al., 2015). Thus, my data reflect the known pattern of gene expression along the dorso-ventral axis and might be useful to further dissect the mechanisms that regulate rim and RNE cell behaviours. On the other hand, the markers of naso-temporal patterning did not show strong differential gene expression. This is in line with the observation that at 18 ss, many cells expressing temporal markers reside in the invaginating RNE (Picker et al., 2009). Furthermore, previous experiments that nasalised or temporalised the optic vesicle did not impact optic cup architecture (Picker et al., 2009). This suggests that naso-temporal patterning is not strongly correlated with the regulation of cell behaviour. It is in line with my results that the rim-migration-defective cells in *ezrin* morphants express the appropriate naso-temporal markers and yet have morphogenetic defects. Taken together, these data reveal that the high GFP and low GFP samples rightly correspond to the RNE and rim cells

respectively. The dorso-ventral patterning reflected in these samples could play a role in regulation of cell behaviour. In contrast, the correlation with naso-temporal patterning seems weak.

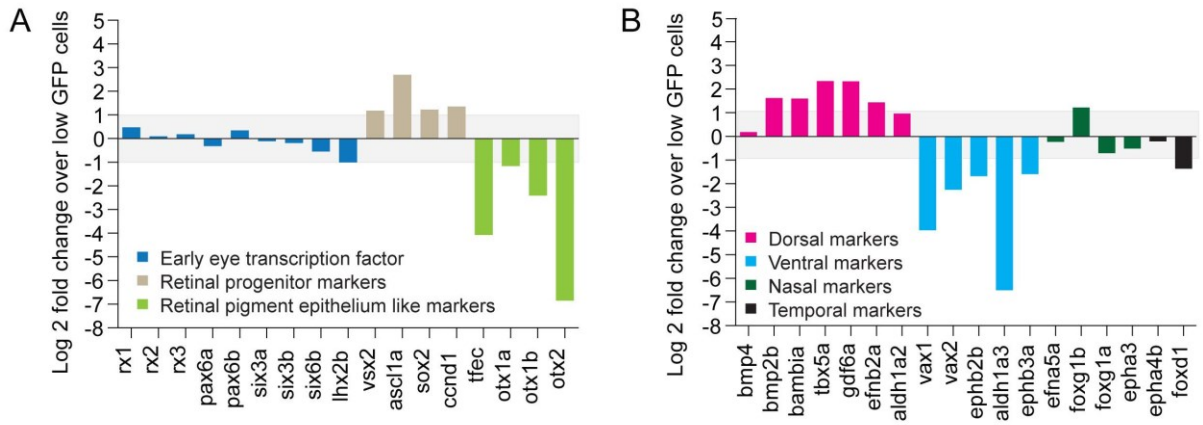

Figure 4.3: Differential gene expression analysis of known players in eye development.
A,B) Log2 fold change in expression over low GFP cells for known transcriptional factors in early eye development (A) and markers for developmental patterning in the optic cup (B).
The grey box marks the area of less than 2-fold change.

Table 4: Top GO terms (Cellular components)

GO Term	P-value	Z-score	Combined Score	Genes
focal adhesion (GO:0005925)	0.012567699	-4.752223798	4.635451768	AHNAK;FBLIM1;ACTN1;TNC;CD99L2;HSPG2;CNN2;LIMA1;PPFIBP1;RRAS;PALLD;DLC1;GNB2
stress fiber (GO:0001725)	0.004702506	-2.859744371	2.7894745	CNN2;LIMA1;FBLIM1;ACTN1
clathrin-coated pit (GO:0005905)	0.007841086	-2.812298157	2.743194138	RAMP2;FCHO2;ACKR3

I have collected a comprehensive gene expression data set that can now be used to investigate the molecular and cellular mechanisms involved in rim involution and RNE morphogenesis. Using this data set, I performed gene ontology analysis for cellular components. Interestingly, the prominent GO terms for cellular components were focal adhesion, stress fiber and clathrin coated pits (Table 4). This is in line with my cellular characterisation so far, which has highlighted the importance of these structures in rim involution and RNE invagination. This further strengthens the fidelity of the sample preparation. These data can be further harvested to identify specific candidate genes that potentially regulate the cellular behaviours. The next steps would include verifying the differential expression of these candidate genes using RNA in situ hybridisation, followed by functional tests (loss and gain-of-function studies). Such approach would open a new avenue to understand the cellular mechanisms in RNE morphogenesis.

5. Material and methods

5.1 Zebrafish methods

5.1.1 Zebrafish strains and transgenic lines

Zebrafish were maintained and bred at 26.5°C. Embryos were raised at 28°C and then transferred to 21°C at around 80% epiboly stage to slow down the development. At 8 ss embryos were transferred back and maintained henceforth at 28°C. All animal work was performed in accordance with European Union (EU) directive 2011/63/EU as well as the German Animal Welfare Act. For the details of the strains and transgenic lines see Table 5.

Table 5: List of zebrafish strains and transgenic lines

Zebrafish strains and transgenic lines	**Reference**
Wild-type strain WT-AB	RRID:ZIRC_ZL1
Wild-type strain WT-TL	RRID:ZIRC_ZL86
Tg(*actb1:GFP--utrCH*)	(Behrndt et al., 2012)
Tg(*actb2:mCherry-Hsa.UTRN*)	(Compagnon et al., 2014)
Tg(*actb1:myl12.1-EGFP*)	(Maitre et al., 2012)
Tg(*actb1:HRAS-EGFP*) vu119	(Cooper et al., 2005)
Tg(*centrin-GFP*)	(Randlett et al., 2011)
Tg(*vsx2::GFP*)	(Kimura et al., 2006)
Tg(*-8.0 Cldb::lyn-GFP*)	(Haas and Gilmour, 2006)
Tg(*HGn42A::EGFP*)	(Nagayoshi et al., 2008)
Tg(*bactin:mKate2-ras*)	This study

5.1.2 Morpholino injections

Morpholinos (Gene Tools) were injected in the yolk at the one-cell stage. The injection mix was prepared in water and the injection volume was 0.5–1.5 nl. Table 6 enlists the details about the morpholino oligos and Table 7 describes the phenotypic variation in the morphants.

Table 6: Morpholinos used in this study

Gene	Morpholino sequence	ng/embryo	Reference
laminin-α1	5'TCATCCTCATCTCCATCATCGCTCA3'	0.4	(Pollard et al., 2006)
ojoplano	5'ggactcacccaTCAGAAATTCAGCC3'	3.8	(Martinez-Morales et al., 2009)
ezrin	5'GATGTAGATGCCGATTCCTCTCGTC3'	1.6	(Link et al., 2006)
p53	5'GCGCCATTGCTTTGCAAGAATTG3'	2	(Robu et al., 2007)
lmx1b.1	5'TTGAAGGACTTACCGAGCATAACTC3'	0.84	(McMahon et al., 2009)
lmx1b.2	5'GTGTGTGTGAAACTCACCCAGCATC3'	0.84	(McMahon et al., 2009)

Table 7: Phenotypic variation for morpholino injections

***laminin-α1* Morpholino injection**	No. of embryos	Percentage
Epithelial accumulation at the ventro-temporal side	54	47.0
Protruding lens phenotype without epithelial accumulation	36	31.3
No apparent optic cup phenotype	16	13.9
Severe phenotype (developmental delay or extreme deformities)	9	7.8
Total	115	100
***opo* Morpholino injection**	No. of embryos	Percentage
Epithelial accumulation at the ventro-temporal side	43	40.95
Flat eye phenotype without epithelial accumulation	28	26.67
No apparent optic cup phenotype	22	20.95
Severe phenotype (developmental delay or extreme deformities)	12	11.43
Total	105	100
***ezrin* Morpholino injection**	No. of embryos	Percentage
Epithelial accumulation at the ventro-temporal side	39	50.0
Optic cup phenotype without epithelial accumulation	16	20.5
No apparent optic cup phenotype	7	9.0
Severe phenotype (developmental delay or extreme deformities)	16	20.5
Total	78	100

5.1.3 RNA and plasmid injections

To label the entire tissue, mRNA was injected into the cytoplasm of one-cell stage embryo. To sparsely label the cells, either plasmid DNA was injected into the cytoplasm of one-cell stage embryo or mRNA was injected in a single blastomere at 16–32-cell stage. mRNA was synthesized using the Ambion mMessage mMachine kit and injected at 50-60 pg per embryo, whereas DNA was injected at 15 pg per embryo. The injection mix was prepared in water and the injection volume was 0.5–1.5 nl.

5.1.4 Zebrafish transgenesis

1 nl of the mix of Tol2 plasmid Tol2-bactin::mKate2-ras (20 ng/µl) and Tol2 transposase mRNA (30 ng/µl) was prepared in water and injected into the cytoplasm of one-cell stage embryos. F_0 embryos with observed fluorescence signal were grown to adulthood and germline carriers were identified by outcross with wild-type fish.

1 nl of the mix of recombinant BAC DNA (100 ng/µl) and Tol2 transposase RNA (50 ng/µl) was prepared in water and injected into the cytoplasm of one-cell stage embryos. F_0 embryos were observed and selected based on the fluorescence signal. The experiments were performed with F_0 embryos.

5.1.5 Transplantations

Donor embryos (GFP positive, Tg*(actb1:HRAS-EGFP)*) were injected with *opo* or *ezrin* morpholino mixed with the *p53* morpholino. Embryos were dechorionated at high to sphere stage and some tens of cells from the donor embryos were transferred into the animal pole of the acceptor embryos (mCherry positive, Tg*(actb2:mCherry-Hsa.UTRN)*). Transplanted embryos were then transferred to E3 medium supplemented with 100 U penicillin and streptomycin (Thermo Fischer Scientific).

5.1.6 Heat-shock-driven gene expression

Embryos injected with heat-shock-driven constructs were incubated at 15 ss in a water bath at 37°C for 20 min.

5.1.7 Drug treatments

Rockout (Santa Cruz, sc-203237) and Aphidicolin (Aphi) (Sigma, A0781) stocks were dissolved in DMSO. Hydroxyurea (HU) (Sigma, 8627) stock solution was prepared in water. Final drug solutions were made in E3 medium and dechorionated embryos were incubated in it. Rockout treatment was started around 13–14 ss and was used at 100 µM with 1% DMSO (by volume) in E3. During time-lapse imaging, Rockout was used at 125 µM. For

inhibition of cell proliferation, embryos were treated with a mixture of 30 mM HU and 210 µM Aphi. HU + Aphi treatment was started at 10 ss. Equivalent amounts of DMSO or water were added as solvent control.

5.1.8 Immunostaining

Dechorionated embryos were fixed with 4% PFA in PBS overnight at 4°C, washed with PBS and then permeabilized using PBT (PBS with 0.8% Triton X-100). To improve permeability, embryos were treated with trypsin on ice for 15 min and then again washed with PBT. Embryos were blocked with 10% normal goat serum (NGS) in PBT at room temperature for 2–3 h and incubated in the primary antibody mix with 1% NGS in PBT for approximately 60 h at 4°C. After washing off the unbound primary antibody with PBT, embryos were incubated in the secondary antibody mix with 1% NGS in PBT for 60 h. The embryos were washed with PBT to remove unbound secondary antibodies and fluorophores. The samples were mounted either in agarose or in 80% glycerol.

The following antibodies and probes were used at the mentioned dilutions.
Primary antibodies:
1:50 anti-phospho-myosin (RRID:AB_330248, Cell signaling 3671), 1:500 anti-pH3 (RRID:AB_2295065, Abcam ab10543), 1:100 anti-gamma-tubulin (RRID:AB_477585, Sigma, T-6793), 1:100 anti-laminin (RRID:AB_477163, Sigma L-9393), 1:100 anti-chondroitin sulphate CS-56 (RRID:AB_298176, Abcam ab11570), 1:100 anti-fibronectin (RRID:AB_476976, Sigma F3648), 1:500 anti-tRFP (as anti-mKate2) (RRID:AB_2571743, Evrogen AB233), 1:100 anti-GFP (RRID:AB_94936, Milipore MAB3580) and 1:200 anti-PKC ζ C-20 (RRID:AB_2300359, Santa Cruz sc-216).

Secondary antibodies and fluorescent markers:
1:500 Alexa Fluor 488 anti-Rabbit (RRID:AB_141708, Invitrogen A21206), 1:500 Alexa Fluor 568 anti-Rabbit (RRID:AB_2534017, Thermo Fischer Scientific A10042), 1:500 Alexa Fluor 647 anti-Rabbit (RRID:AB_141775, Invitrogen A21245), 1:500 Alexa Fluor 488 anti-mouse (RRID:AB_141606, Invitrogen A21200), Alexa Fluor 594 anti-mouse (RRID:AB_141630, Invitrogen A21201), 1:500 Alexa Fluor 647 anti-rat (RRID:AB_141778, Invitrogen A21247), 1:50 Alexa Fluor 488 Phalloidin (RRID:AB_2315147, Molecular Probes A12379), 1:50 Rhodamine-Phalloidin (RRID:AB_2572408, Molecular probes R415), DAPI.

5.2 Molecular methods

5.2.1 Constructs and cloning strategies

The following constructs were used in this study.

pCS2+mKate2-ras (Weber et al., 2014), pCS2+Par3-GFP (Tawk et al., 2007), pCS2+GFP-UtrophinCH (Burkel et al., 2007), pCS2+DD-myl12b-GFP (Norden et al., 2009), bactin::mKate2-ras (Icha et al., 2016), hsp70::EGFP-UtrophinCH (Strzyz et al., 2015), pCS2+GFP-ras (kind gift from A. Oates), pCS2+EMTB-tdTomato (kind gift from D. Gilmour).

The following constructs were generated using the Gateway cloning system (Thermo Fisher Scientific) and the Tol2 kit (Kwan et al., 2007).

1. pCS2+Paxillin-mKate2 : Middle entry clone for zebrafish paxillin was a kind gift from Clarissa Henry (Goody and Henry, 2010). It was combined with mKate2 pENTR(R2-L3) (kind gift from Andrew Oates, Crick Institute, London, UK) and pCS2 Dest(R1-R3) backbone (Villefranc et al., 2007).

2. pCS2+Integrinbeta1b-mKate2: RNA was extracted from 24 hpf embryos using the TRI Reagent (T9424 Sigma) according to the manufacturers protocol. cDNA was synthesized using first strand cDNA synthesis kit (K1651, Fermentas/Thermo-Fischer scientific). Zebrafish Integrin b1b (NM_001034987.1) coding sequence was amplified from zebrafish cDNA to generate a middle entry clone without a stop codon at the end. The following primers were used.

5’ GGGGACAAGTTTGTACAAAAAAGCAGGCTGGatggacgtaaggctgctcc 3’

5’ GGGGACCACTTTGTACAAGAAAGCTGGGTtttgccctcatatttagggttgac 3’

It was combined with mKate2 pENTR(R2-L3) (kind gift from Andrew Oates, Crick Institute, London, UK) and pCS2 Dest(R1-R3) backbone (Villefranc et al., 2007).

3. Hsp70::EGFP-Rac1T17N :

pcDNA3-EGFP-Rac1-T17N was a gift from Gary Bokoch (Addgene plasmid # 12982) (Subauste et al., 2000). To generate a middle entry clone, EGFP-Rac-T17N sequence was amplified using the following primers:

5’ GGGGACAAGTTTGTACAAAAAAGCAGGCTGGatggtgagcaagggcgagg3’

5’ GGGGACCACTTTGTACAAGAAAGCTGGGTttacaacagcaggcattttc 3’

It was combined with the hsp70 promoter p5ENTR(L4-R1) (Kwan et al., 2007) and pTol2+pA_pDEST(R4-R2) (Villefranc et al., 2007).

4. Hsp70::mKate2-Rac1T17N :

pcDNA3-EGFP-Rac1-T17N was a gift from Gary Bokoch (Addgene plasmid # 12982) (Subauste et al., 2000). To generate a 3' entry clone, Rac-T17N fragment was amplified using the following primers:

5' GGGGACAGCTTTCTTGTACAAAGTGGCTatgcaggccatcaagtgtg 3'

5' GGGGACAACTTTGTATAATAAAGTTGCttacaacagcaggcattttctc 3'

It was combined with the hsp70 promoter p5ENTR(L4-R1) (Kwan et al., 2007), mKate2 pENTR(L1-L2) (kind gift from Andrew Oates, Crick Institute, London, UK) and pTol2+pA_pDEST(R4-R3) (Villefranc et al., 2007).

5.2.2 BAC recombineering

BAC recombineering was performed by Aleksandra Syta and Mihail Sarov from genome engineering facility at MPI-CBG.

1. BAC clones

The CHORI211 Zebrafish BAC clones with the pTARBAC2.1 backbone containing the genes of interest *lama1* (CH211-170M3) and *fn1a* (CH211-103D24) were purchased from Source BioScience. The targeted sites of each gene were confirmed by PCR (primers details in Table 8) followed by sequencing.

2. BAC recombineering

BAC recombineering was performed according to a published protocol (Fu et al., 2010). To prepare the E. coli strains carrying the BAC clones for recombineering, they were transformed with pSC101-BAD-gbaA-tet plasmid, which is used to express the λRed operon proteins after induction with L-arabinose. The pSC101-BAD-gbaA-tet plasmid contains a temperature-sensitive replicon pSC101 and a tetracycline (Tet) selection marker.

Insertion of Tol2 arms into the pTARBAC2.1 backbone

For integration of Tol2 arms into the BAC clones with pTARBAC backbone, a Tol2-amp cassette was used. The cassette contained long recombineering homology arms for the pTARBAC2.1 sequence (5' arm - 224 bp and 3' arm – 193 bp) and the amplicillin (Amp) selection marker and was a kind gift from Tatjana Sauka-Spengler (Trinh et al., 2017). The plasmid was further modified to include a R6K origin of replication by Pavel Vopalensky and was a kind gift from Nadine Vastenhouw. The cassette was amplified by PCR from the R6K-TARBAC-Tol2 plasmid.

The E. coli strains carrying the BAC clones and the pSC101-BAD-gbaA-tet plasmid were grown in LB containing Chloramphenicol and Amp at 30°C and expression of the Red proteins was induced by adding L-Arabinose to a final concentration of 0.2% and incubated at 37°C for 45 min with shaking. The cells were electroporated with the Tol2-amp cassette (500 ng), grown at 30°C and colonies were selected for the Tol2-Amp integration (for colony PCR primers details in Table 8).

Table 8 : Primers used for BAC recombineering

Primer name	Sequence
Control primers for targeted sites	
Lama1-F	TGACTGTGTCAGAGCATTTG
Lama1-R	TGGAATGTGCATGTGTTGGA
Fn1-F	TTGAGGGACAGGTTACATGT
Fn1-R	AAGAGACTGGCAGTAGACTC
Primers for Tol2-Amp integration into pTARBAC2.1	
TARBAC-Tol2-F	GCTGTCGGAATGGACGATATC
TARBAC-Tol2-R	TAGAACGGAGTAACCTCGGTG
Oligos used for tagging cassettes	
Fn1-HA-F	ttgagtgcctgagaccagacctgttagcagatgcccatagccctcatgatGAAGTGCATACCAATCAGGACCCGC
Fn1-HA-R	ctgtgggccgtgtcctctccagtattggacaaaattcaaatgcagatttaCTTGTCGTCGTCATCCTTGTAGTCG
Lama1-HA-F	tcagctctgcgttcacactcctgcacgtttcccctcactcctgccctgcgGAAGTGCATACCAATCAGGACCCGC
Lama1-HA-R	acacacaggagggctgatatctctacaggtacagctgttgtgtgtgtttaCTTGTCGTCGTCATCCTTGTAGTCG

Tagging of Lama 1 and Fn1

Both genes were C-terminally tagged with three different tags: 2xTY1-**Dendra**-FRT-rpsl-Kan-FRT-3xFLAG, 2xTY1-**GFP**-V5-preTEV-BLRP-FRT-rpsl-Kan-FRT-3xFLAG and 2xTY1-**mKate**-FRT-rpsl-Kan-FRT-3xFLAG. The constructs contained kanamycin selection marker flanked with FRT sites, which are removable through Flp/FRT site-specific recombination. Tagging cassettes containing 50 bp 5' and 3' homology arms to each gene were amplified from R6K plasmids carrying respective tags. The oligos used to obtain the cassettes are listed in Table 8

For tagging, E. coli strains carrying the BAC-Tol2-Amp clones and the pSC101-BAD-gbaA-tet were electroporated with respective tagging cassette, grown at 37°C. At this temperature, the temperature-sensitive pSC101-BAD-gbaA-tet plasmid did not replicate and was removed gradually from the culture. For the removal of Kanamycin marker, the cells were transformed with a pRedFlp-hgr plasmid with Anhydrotetracyclin inducible Flippase (Flp) expression, temperature-sensitive replicon pSC101 and hygromycin selection marker. The fresh culture

of E. coli strains carrying the tagged BAC-Tol2-Amp clones and the pRedFlp plasmid was re-grown in LB containing chloramphenicol, Amp, hygromycin and anhydrotetracyclin (200 ng/ml) at 30°C for 3 hrs. The cells were plated on LB agar plates with chloramphenicol, Amp, hygromycin and incubated ON at 30°C. To test for kanamycin sensitivity, the clones were then grown on plates with and without kanamycin. Clones that grew only on the plates without kanamycin were further confirmed by sequencing.

The following antibiotic concentrations were used: 100 µg/ml Amp, 12.5 µg/ml chloramphenicol, 100 µg/ml hygromycin, 15 µg/ml kanamycin, 4 µg/ml tetracyclin.

5.2.3 Western blot

24 hpf embryos were deyolked manually and samples were boiled in SDS-loading buffer at 98°C. For each condition, protein samples from 5 embryos were used and run on 4–12% polyacrylamide NuPAGE Bis-Tris gel (NP0321BOX; ThermoFisher Scientific) and blotted onto a PVDF membrane (Amersham Hybond P 0.45 PVDF, 10600023 GE Healthcare Life Sciences). Primary antibodies were incubated at room temperature for 1 h or overnight at 4°C and secondary antibodies were incubated at room temperature for 45 min. The staining was detected using enhanced chemiluminescent detection reagents (Amersham RPN2106, GE Healthcare Life Sciences) and a photosensitive film using the Kodak Photofilm Developer X-Omat 2000. Following antibodies dilutions were used: 1:500 anti-laminin (RRID:AB_477163, Sigma L-9393), 1:500 anti-phospho-ERM (RRID:AB_2262427, Cell Signaling 3141), 1:10000 Anti-α-Tubulin (RRID:AB_477582, Sigma T6074), 1:20000 peroxidase conjugated anti-Mouse (RRID:AB_2340061, Jackson Immuno 315-035-003), 1:20000 peroxidase conjugated anti-Rabbit (RRID:AB_2313567, Jackson Immuno 111-035-003).

5.3 Image acquisition

5.3.1 Brightfield imaging

Dechorionated embryos were anaesthetized with 0.04% MS-222 (Sigma) and mounted on a drop of 3% methylcellulose in E3 medium. Images were taken on a Leica M165C scope with an MC170 HD camera.

5.3.2 *in vivo* time-lapse imaging

Dechorionated embryos were mounted in 0.6% low melting agarose in E3 medium on glass bottom dishes for spinning disk confocal microscopy and in a glass capillary for light sheet microscopy. Embryos were anaesthetized using 0.04% MS-222 (Sigma).

An Andor spinning disk system equipped with a 40x silicon oil objective (NA=1.25) and a heating chamber was used. Z stacks of 90 µm depth were acquired with optical section of 0.7 µm every 3–5 min for about 6-7 h.
For time-lapse imaging of *HRAS-GFP*, *GFP-UtrophinCH*, *myl12.1-EGFP* transgenic embryos and paxillin-mKate2 RNA injected embryos (Movie 1, 2 and 9), a Zeiss Light sheet Z.1 microscope with a Zeiss Plan-Apochromat 20x water-dipping objective (NA=1.0) and sample chamber heated to 28°C was used.
To visualise the three-dimensional data over time, maximum intensity projections were used.

5.3.3 Confocal Scans

Imaging was performed on Zeiss LSM 710 confocal microscopes with a 40x water-immersion objective (NA=1.2).

5.4 Image analysis

Image analysis was performed using Fiji (Schindelin et al., 2012). Statistical analysis and graphical representation were performed using the Prism software package.

5.4.1 Apical and basal area analysis of invaginating RNE cells

To measure the apical and basal areas of the invaginating cells, embryos were mounted on their lateral side. The optical section below the developing lens placode was analysed for basal areas and the apical side of the same cells was analysed for apical areas. A rectangular area was marked where the apical and basal endfeet of the RNE cells were observable. The number of cells in this area was calculated using the multipoint tool in Fiji (Schindelin et al., 2012). Cells present only partially in the field were counted only on the left and the top border of the rectangle.

5.4.2 Actomyosin distribution analysis

The average intensity distribution of phalloidin and anti-phosphomyosin staining along the apicobasal axis of the RNE was measured using a custom-made Fiji compatible Python script by Benoit Lombardot and Robert Haase (source code available at (Sidhaye and Norden, 2017)). The region of interest was defined as a 10 µm x 10 µm x h cuboid, with h being the height of the apicobasal axis of the RNE (Figure 2.4B). Using this region of interest, an average intensity value was calculated for each point along the apicobasal axis. The axis length was normalized to 100. To compare different samples, the average intensities were normalized to the highest average intensity value along the axis. Such analysis was performed for five different regions each in multiple optic cups.

5.4.3 Invagination angle analysis

The invagination angle was measured manually using the angle tool in Fiji (Schindelin et al., 2012). The invagination angle was defined as the angle held by the inner lips of the optic cup at the center of the optic cup base (schematic in Figure 2.5E). The angle was measured at three different central optical sections for each optic cup and the average value was used as the angle of invagination. Such analysis was performed for multiple optic cups.

5.4.4 Rim cell speed analysis

The basal side of the rim cells was tracked manually using MTrackJ plugin in Fiji (Meijering et al., 2012). The rim cell speed was calculated as a ratio of the track length to the track duration.

5.4.5 Integrin intensity analysis

Ras-GFP and Integrin-mKate2 RNA injected embryos were used as controls or were co-injected with *opo* morpholino. These embryos were imaged at 24 hpf. Single optical sections featuring complete apico-basal length of RNE cells were chosen for analysis. A 20-pixel thick line was manually marked along the apicobasal axis of RNE. The average integrin-mKate2 intensity was calculated along the line for 0–5 µm (basal) and 25–30 µm (central) length from the base. A ratio of basal average intensity to central average intensity was calculated for each embryo. Such analysis was performed for 5 different embryos each for control and morphant embryos.

5.5 Transcriptomic profiling by RNA-seq

5.5.1 Sample preparation, cell sorting and RNA isolation for RNA-seq

10 Optic vesicles each were dissected manually from about 18 ss wild-type (control) embryos and Tg(*vsx2::GFP*) embryos. The dissected optic vesicles were kept in 100 µl PBS at room temperature. The cells were dissociated manually by pipetting several times and the volume was adjusted to 300 µl. This procedure was performed within half an hour and samples were used for FACS.

FACS was performed with the help of the Cell technologies facility at MPI-CBG. Single cell suspensions were analysed by flow cytometry using the FACS ARIA FUSION (BD Biosciences) in conjunction with the FACS Diva software (BD Biosciences). The subsequent cell sorting and counting of absolute numbers of defined subpopulations was performed by the same set-up. Figure 5.1 shows the representative profiles for control and vsx2::GFP

samples. Quadrant 4 marks the actual GFP positive cells (Figure 5.1 A,C). FACS was performed to collect two groups of cells, 'low GFP' (marked by P4 in Figure 5.1C) and 'high GFP' (marked by P5 in Figure 5.1C). The middle population of cells was discarded to avoid potentially overlapping cells. The sorted cells were collected in RNeasy Lysis Buffer RLT with 1% 2–mercaptoethanol. Total RNA was extracted using the RNeasy Plus Micro kit (Qiagen). The RNA quality was checked using bioanalyzer system (Agilent Genomics). Samples were collected in four replicates on different days. The details about the samples are included in Table 9.

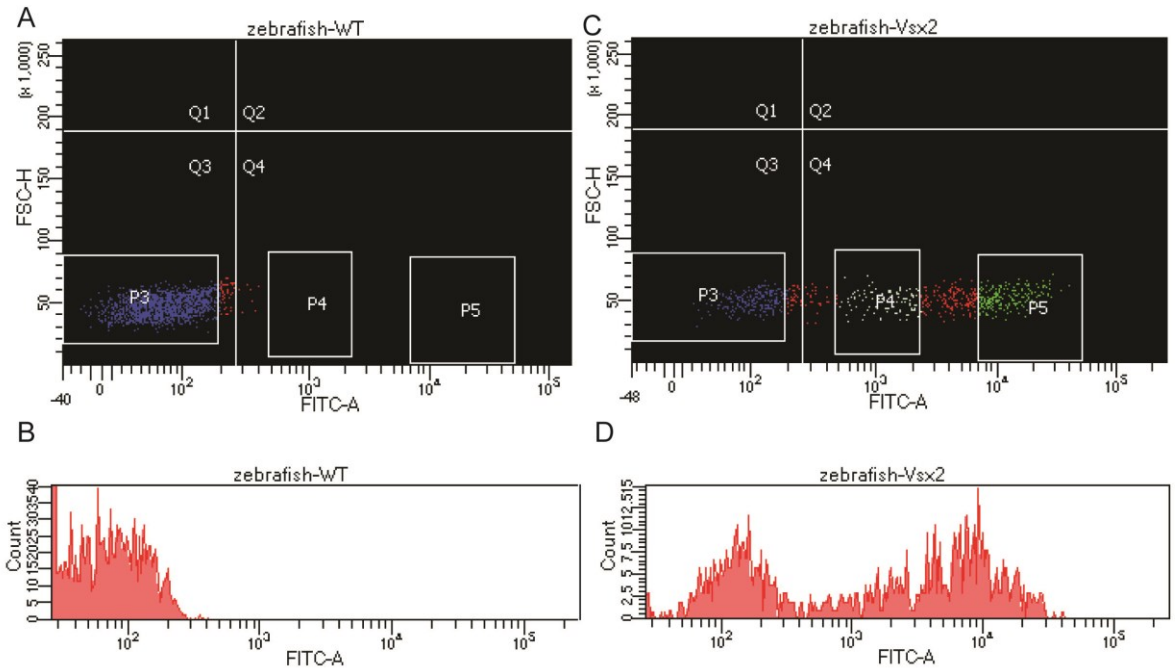

Figure 5.1: FACS profile of wild-type control and *vsx2::GFP* samples
A,C) Fluorescence levels of isolated optic vesicle cells during flow cytometry for wild-type/control (A) and *vsx2::GFP* (C) sample. Low GFP cells (P4), high GFP cells (P5). Each dot represents a single cell. FSC-H (Forward light scatter- Height).
B,D) Counts of isolated cells during flow cytometry versus fluorescence levels for wild-type/control (B) and *vsx2::GFP* (D) sample. FITC-A (signal upon excitation with 488nm laser)
Fluorescence intensity axis shown in log scale.

Table 9: Samples for transcriptomic analysis

Sample	Number of harvested cells	Total RNA conc. (pg/µl)	RNA integrity number (RIN)
Low GFP_1	294	53	8.6
Low GFP_2	104	51	7.8
Low GFP_3	236	59	7.3
Low GFP_4	418	163	5.6
High GFP_1	325	140	7.5
High GFP_2	202	130	7.8
High GFP_3	315	53	9.1
High GFP_4	563	204	5.8

Table 10: Alignment statistics of RNA-seq samples

Sample	Total reads	Aligned	Rate	rRNA	rRNA rate
Low GFP_1	24,254,471	22,401,448	0.924	273,257	0.011
Low GFP_2	28,174,805	26,635,367	0.945	244,598	0.009
Low GFP_3	54,588,841	51,417,255	0.942	540,319	0.01
Low GFP_4	60,867,299	57,120,923	0.938	619,942	0.01
High GFP_1	26,972,612	25,270,705	0.937	67,731	0.003
High GFP_2	25,458,916	23,885,004	0.938	330,096	0.013
High GFP_3	48,476,762	45,709,858	0.943	445,412	0.009
High GFP_4	57,074,348	52,927,654	0.927	656,965	0.012

Table 11: Alignment profile of RNA-seq samples

Sample	Exonic	Intronic	Intergenic	Expression efficiency	Transcripts	Genes
Low GFP_1	0.876	0.076	0.054	0.803	32183	15815
Low GFP_2	0.9	0.054	0.046	0.851	31546	15321
Low GFP_3	0.869	0.071	0.06	0.819	33157	16188
Low GFP_4	0.858	0.081	0.06	0.805	33129	16143
High GFP_1	0.893	0.058	0.049	0.836	30626	14977
High GFP_2	0.875	0.068	0.057	0.821	29842	14635
High GFP_3	0.853	0.083	0.063	0.804	33927	16655
High GFP_4	0.853	0.085	0.062	0.791	31572	15452

5.5.2 Library preparation and sequencing

Library preparation and subsequent sequencing were performed by the Deep Sequencing Group headed by Dr. Andreas Dahl (BIOTEC, TU Dresden). Samples were prepared in batches due to different delivery dates. LowGFP 1, LowGFP 2, HighGFP 1 and HighGFP 2 were prepared together. LowGFP 3, LowGFP 4, HighGFP 3 and HighGFP 4 were prepared together in the second batch.

For the RNA-seq experiment, the SMARTer Ultra Low Input RNA for Illumina Sequencing Kit - HV from Takara Bio USA (formerly known as Clontech Laboratories) was used to reverse transcribe the RNA and amplify full-length cDNA according to the user manual. After amplification of cDNA, the cDNA was sheared to a fragment length of 200 bp in the ultrasonicator Covaris LE220, followed by a library prep using NEBNext® Ultra DNA Library Prep Kit for Illumina (NEB). The resulting libraries were pooled and sequenced on an Illumina® HiSeq 2500, resulting in ca. 25 – 60 million single-end reads.

5.5.3 Alignment and Quality assessment

Alignment and analysis were performed by Mathias Lesche (Deep Sequencing Group, BIOTEC, TU Dresden). FastQC (http://www.bioinformatics.babraham.ac.uk/) and RNA-SeQC (v1.1.8) were used to perform a basic quality control on the sequenced fragments. Alignment of the fragments to zebrafish reference genome (release GRCz10) was done with GSNAP (v2017-03-17) (Wu and Nacu, 2010) and Ensembl annotation 81 (release July 2015) was used to detect fragments spanning splice sites. Table 10 and 11 show the details of the alignment.

5.5.4 Gene Expression analysis

The uniquely aligned fragments were counted with featureCounts (v1.5.2) (Liao et al., 2014) and with the Ensembl annotation 81. Non-strand specific counting was applied. The raw counts were normalized based on the library size and testing for differential gene expression between the two conditions, LowGFP and HighGFP, was performed with the DESeq2 R package (v1.15.51) (Love et al., 2014). Accepting a maximum of 10% false discovery rate (padj < 0.1) for the comparison, genes with normalized counts > 200 averaged in both conditions and a log2 fold change of < -1 or > 1 were considered regulated.

5.5.5 Gene enrichment analysis

Gene enrichment analysis and GO term analysis was performed on the list of regulated genes using open source tool Enrichr (Chen et al., 2013; Kuleshov et al., 2016). The GO term analysis was performed for GO cellular component using 2017 database.

6. Bibliography

Adler, R., and Belecky-Adams, T.L. (2002). The role of bone morphogenetic proteins in the differentiation of the ventral optic cup. Development *129*, 3161-3171.

Ahtiainen, L., Lefebvre, S., Lindfors, P.H., Renvoise, E., Shirokova, V., Vartiainen, M.K., Thesleff, I., and Mikkola, M.L. (2014). Directional cell migration, but not proliferation, drives hair placode morphogenesis. Dev Cell *28*, 588-602.

Aleksandrova, A., Czirok, A., Szabo, A., Filla, M.B., Hossain, M.J., Whelan, P.F., Lansford, R., and Rongish, B.J. (2012). Convective tissue movements play a major role in avian endocardial morphogenesis. Developmental biology *363*, 348-361.

Aman, A., and Piotrowski, T. (2008). Wnt/beta-catenin and Fgf signaling control collective cell migration by restricting chemokine receptor expression. Dev Cell *15*, 749-761.

Amano, M., Ito, M., Kimura, K., Fukata, Y., Chihara, K., Nakano, T., Matsuura, Y., and Kaibuchi, K. (1996). Phosphorylation and activation of myosin by Rho-associated kinase (Rho-kinase). J Biol Chem *271*, 20246-20249.

Araya, C., Ward, L.C., Girdler, G.C., and Miranda, M. (2016). Coordinating cell and tissue behavior during zebrafish neural tube morphogenesis. Developmental dynamics : an official publication of the American Association of Anatomists *245*, 197-208.

Aufschnaiter, R., Zamir, E.A., Little, C.D., Ozbek, S., Munder, S., David, C.N., Li, L., Sarras, M.P., Jr., and Zhang, X. (2011). In vivo imaging of basement membrane movement: ECM patterning shapes Hydra polyps. J Cell Sci *124*, 4027-4038.

Bazin-Lopez, N., Valdivia, L.E., Wilson, S.W., and Gestri, G. (2015). Watching eyes take shape. Curr Opin Genet Dev *32*, 73-79.

Behesti, H., Holt, J.K., and Sowden, J.C. (2006). The level of BMP4 signaling is critical for the regulation of distinct T-box gene expression domains and growth along the dorso-ventral axis of the optic cup. BMC Dev Biol *6*, 62.

Behrndt, M., Salbreux, G., Campinho, P., Hauschild, R., Oswald, F., Roensch, J., Grill, S.W., and Heisenberg, C.P. (2012). Forces driving epithelial spreading in zebrafish gastrulation. Science *338*, 257-260.

Bernadskaya, Y., and Christiaen, L. (2016). Transcriptional Control of Developmental Cell Behaviors. Annu Rev Cell Dev Biol *32*, 77-101.

Berrier, A.L., and Yamada, K.M. (2007). Cell-matrix adhesion. J Cell Physiol *213*, 565-573.

Bianco, A., Poukkula, M., Cliffe, A., Mathieu, J., Luque, C.M., Fulga, T.A., and Rorth, P. (2007). Two distinct modes of guidance signalling during collective migration of border cells. Nature *448*, 362-365.

Block, E.R., Matela, A.R., SundarRaj, N., Iszkula, E.R., and Klarlund, J.K. (2004). Wounding induces motility in sheets of corneal epithelial cells through loss of spatial constraints: role of heparin-binding epidermal growth factor-like growth factor signaling. J Biol Chem *279*, 24307-24312.

Bogdanovic, O., Delfino-Machin, M., Nicolas-Perez, M., Gavilan, M.P., Gago-Rodrigues, I., Fernandez-Minan, A., Lillo, C., Rios, R.M., Wittbrodt, J., and Martinez-Morales, J.R. (2012). Numb/Numbl-Opo antagonism controls retinal epithelium morphogenesis by regulating integrin endocytosis. Dev Cell *23*, 782-795.

Boucherie, C., Mukherjee, S., Henckaerts, E., Thrasher, A.J., Sowden, J.C., and Ali, R.R. (2013). Brief report: self-organizing neuroepithelium from human pluripotent stem cells facilitates derivation of photoreceptors. Stem Cells *31*, 408-414.

Bresnick, A.R. (1999). Molecular mechanisms of nonmuscle myosin-II regulation. Curr Opin Cell Biol *11*, 26-33.

Brown, K.E., Keller, P.J., Ramialison, M., Rembold, M., Stelzer, E.H., Loosli, F., and Wittbrodt, J. (2010). Nlcam modulates midline convergence during anterior neural plate morphogenesis. Developmental biology *339*, 14-25.

Bryan, C.D., Chien, C.B., and Kwan, K.M. (2016). Loss of laminin alpha 1 results in multiple structural defects and divergent effects on adhesion during vertebrate optic cup morphogenesis. Developmental biology *416*, 324-337.

Burkel, B.M., von Dassow, G., and Bement, W.M. (2007). Versatile fluorescent probes for actin filaments based on the actin-binding domain of utrophin. Cell Motil Cytoskeleton *64*, 822-832.

Burridge, K., and Wittchen, E.S. (2013). The tension mounts: stress fibers as force-generating mechanotransducers. The Journal of cell biology *200*, 9-19.

Campbell, K., and Casanova, J. (2016). A common framework for EMT and collective cell migration. Development *143*, 4291-4300.

Carpenter, A.C., Smith, A.N., Wagner, H., Cohen-Tayar, Y., Rao, S., Wallace, V., Ashery-Padan, R., and Lang, R.A. (2015). Wnt ligands from the embryonic surface ectoderm regulate 'bimetallic strip' optic cup morphogenesis in mouse. Development *142*, 972-982.

Caussinus, E., Colombelli, J., and Affolter, M. (2008). Tip-cell migration controls stalk-cell intercalation during Drosophila tracheal tube elongation. Curr Biol *18*, 1727-1734.

Cavodeassi, F., Ivanovitch, K., and Wilson, S.W. (2013). Eph/Ephrin signalling maintains eye field segregation from adjacent neural plate territories during forebrain morphogenesis. Development *140*, 4193-4202.

Cetera, M., Ramirez-San Juan, G.R., Oakes, P.W., Lewellyn, L., Fairchild, M.J., Tanentzapf, G., Gardel, M.L., and Horne-Badovinac, S. (2014). Epithelial rotation promotes the global alignment of contractile actin bundles during Drosophila egg chamber elongation. Nature communications *5*, 5511.

Charras, G., and Paluch, E. (2008). Blebs lead the way: how to migrate without lamellipodia. Nat Rev Mol Cell Biol *9*, 730-736.

Charras, G., and Sahai, E. (2014). Physical influences of the extracellular environment on cell migration. Nat Rev Mol Cell Biol *15*, 813-824.

Chauhan, B.K., Disanza, A., Choi, S.Y., Faber, S.C., Lou, M., Beggs, H.E., Scita, G., Zheng, Y., and Lang, R.A. (2009). Cdc42- and IRSp53-dependent contractile filopodia tether presumptive lens and retina to coordinate epithelial invagination. Development *136*, 3657-3667.

Chen, E.Y., Tan, C.M., Kou, Y., Duan, Q., Wang, Z., Meirelles, G.V., Clark, N.R., and Ma'ayan, A. (2013). Enrichr: interactive and collaborative HTML5 gene list enrichment analysis tool. BMC Bioinformatics *14*, 128.

Clark, B.S., Cui, S., Miesfeld, J.B., Klezovitch, O., Vasioukhin, V., and Link, B.A. (2012). Loss of Llgl1 in retinal neuroepithelia reveals links between apical domain size, Notch activity and neurogenesis. Development *139*, 1599-1610.

Collinet, C., Rauzi, M., Lenne, P.F., and Lecuit, T. (2015). Local and tissue-scale forces drive oriented junction growth during tissue extension. Nat Cell Biol *17*, 1247-1258.

Compagnon, J., Barone, V., Rajshekar, S., Kottmeier, R., Pranjic-Ferscha, K., Behrndt, M., and Heisenberg, C.P. (2014). The notochord breaks bilateral symmetry by controlling cell shapes in the zebrafish laterality organ. Dev Cell *31*, 774-783.

Cooper, M.S., Szeto, D.P., Sommers-Herivel, G., Topczewski, J., Solnica-Krezel, L., Kang, H.C., Johnson, I., and Kimelman, D. (2005). Visualizing morphogenesis in transgenic zebrafish embryos using BODIPY TR methyl ester dye as a vital counterstain for GFP. Developmental dynamics : an official publication of the American Association of Anatomists *232*, 359-368.

Cox, J., Jackson, A.P., Bond, J., and Woods, C.G. (2006). What primary microcephaly can tell us about brain growth. Trends Mol Med *12*, 358-366.

D'Amato, R.J., Loughnan, M.S., Flynn, E., and Folkman, J. (1994). Thalidomide is an inhibitor of angiogenesis. Proceedings of the National Academy of Sciences of the United States of America *91*, 4082-4085.

Dambly-Chaudiere, C., Cubedo, N., and Ghysen, A. (2007). Control of cell migration in the development of the posterior lateral line: antagonistic interactions between the chemokine receptors CXCR4 and CXCR7/RDC1. BMC Dev Biol *7*, 23.

David, N.B., Sapede, D., Saint-Etienne, L., Thisse, C., Thisse, B., Dambly-Chaudiere, C., Rosa, F.M., and Ghysen, A. (2002). Molecular basis of cell migration in the fish lateral line: role of the chemokine receptor CXCR4 and of its ligand, SDF1. Proceedings of the National Academy of Sciences of the United States of America *99*, 16297-16302.

Davidson, L.A. (2012). Epithelial machines that shape the embryo. Trends Cell Biol *22*, 82-87.

Davidson, L.A., and Keller, R.E. (1999). Neural tube closure in Xenopus laevis involves medial migration, directed protrusive activity, cell intercalation and convergent extension. Development *126*, 4547-4556.

Dawes-Hoang, R.E., Parmar, K.M., Christiansen, A.E., Phelps, C.B., Brand, A.H., and Wieschaus, E.F. (2005). folded gastrulation, cell shape change and the control of myosin localization. Development *132*, 4165-4178.

Decembrini, S., Koch, U., Radtke, F., Moulin, A., and Arsenijevic, Y. (2014). Derivation of traceable and transplantable photoreceptors from mouse embryonic stem cells. Stem cell reports *2*, 853-865.

Diaz de la Loza, M.C., Diaz-Torres, A., Zurita, F., Rosales-Nieves, A.E., Moeendarbary, E., Franze, K., Martin-Bermudo, M.D., and Gonzalez-Reyes, A. (2017). Laminin Levels Regulate Tissue Migration and Anterior-Posterior Polarity during Egg Morphogenesis in Drosophila. Cell Rep *20*, 211-223.

Dominguez-Gimenez, P., Brown, N.H., and Martin-Bermudo, M.D. (2007). Integrin-ECM interactions regulate the changes in cell shape driving the morphogenesis of the Drosophila wing epithelium. J Cell Sci *120*, 1061-1071.

Dona, E., Barry, J.D., Valentin, G., Quirin, C., Khmelinskii, A., Kunze, A., Durdu, S., Newton, L.R., Fernandez-Minan, A., Huber, W*., et al.* (2013). Directional tissue migration through a self-generated chemokine gradient. Nature *503*, 285-289.

Dorman, J.B., James, K.E., Fraser, S.E., Kiehart, D.P., and Berg, C.A. (2004). bullwinkle is required for epithelial morphogenesis during Drosophila oogenesis. Developmental biology *267*, 320-341.

Duchek, P., and Rorth, P. (2001). Guidance of cell migration by EGF receptor signaling during Drosophila oogenesis. Science *291*, 131-133.

Duchek, P., Somogyi, K., Jekely, G., Beccari, S., and Rorth, P. (2001). Guidance of cell migration by the Drosophila PDGF/VEGF receptor. Cell *107*, 17-26.

Eaton, S., Auvinen, P., Luo, L., Jan, Y.N., and Simons, K. (1995). CDC42 and Rac1 control different actin-dependent processes in the Drosophila wing disc epithelium. The Journal of cell biology *131*, 151-164.

Eiraku, M., Adachi, T., and Sasai, Y. (2012). Relaxation-expansion model for self-driven retinal morphogenesis: a hypothesis from the perspective of biosystems dynamics at the multi-cellular level. Bioessays *34*, 17-25.

Eiraku, M., Takata, N., Ishibashi, H., Kawada, M., Sakakura, E., Okuda, S., Sekiguchi, K., Adachi, T., and Sasai, Y. (2011). Self-organizing optic-cup morphogenesis in three-dimensional culture. Nature *472*, 51-56.

Ekblom, P. (1989). Developmentally regulated conversion of mesenchyme to epithelium. FASEB J *3*, 2141-2150.

Ekker, S.C., Ungar, A.R., Greenstein, P., von Kessler, D.P., Porter, J.A., Moon, R.T., and Beachy, P.A. (1995). Patterning activities of vertebrate hedgehog proteins in the developing eye and brain. Curr Biol *5*, 944-955.

England, S.J., Blanchard, G.B., Mahadevan, L., and Adams, R.J. (2006). A dynamic fate map of the forebrain shows how vertebrate eyes form and explains two causes of cyclopia. Development *133*, 4613-4617.

Ewald, A.J., Brenot, A., Duong, M., Chan, B.S., and Werb, Z. (2008). Collective epithelial migration and cell rearrangements drive mammary branching morphogenesis. Dev Cell *14*, 570-581.

Farooqui, R., and Fenteany, G. (2005). Multiple rows of cells behind an epithelial wound edge extend cryptic lamellipodia to collectively drive cell-sheet movement. J Cell Sci *118*, 51-63.

Fehon, R.G., McClatchey, A.I., and Bretscher, A. (2010). Organizing the cell cortex: the role of ERM proteins. Nat Rev Mol Cell Biol *11*, 276-287.

Felix, M.A., and Barkoulas, M. (2015). Pervasive robustness in biological systems. Nat Rev Genet *16*, 483-496.

Fernald, R.D. (2000). Evolution of eyes. Curr Opin Neurobiol *10*, 444-450.

Friedl, P., and Gilmour, D. (2009). Collective cell migration in morphogenesis, regeneration and cancer. Nat Rev Mol Cell Biol *10*, 445-457.

Friedl, P., and Wolf, K. (2010). Plasticity of cell migration: a multiscale tuning model. The Journal of cell biology *188*, 11-19.

Fristrom, D. (1988). The cellular basis of epithelial morphogenesis. A review. Tissue Cell *20*, 645-690.

Frydman, H.M., and Spradling, A.C. (2001). The receptor-like tyrosine phosphatase lar is required for epithelial planar polarity and for axis determination within drosophila ovarian follicles. Development *128*, 3209-3220.

Fu, J., Teucher, M., Anastassiadis, K., Skarnes, W., and Stewart, A.F. (2010). A recombineering pipeline to make conditional targeting constructs. Methods Enzymol *477*, 125-144.

Fuhrmann, S. (2010). Eye morphogenesis and patterning of the optic vesicle. Current topics in developmental biology *93*, 61-84.

Fuhrmann, S., Zou, C., and Levine, E.M. (2014). Retinal pigment epithelium development, plasticity, and tissue homeostasis. Exp Eye Res *123*, 141-150.

Fujimura, N., Taketo, M.M., Mori, M., Korinek, V., and Kozmik, Z. (2009). Spatial and temporal regulation of Wnt/beta-catenin signaling is essential for development of the retinal pigment epithelium. Developmental biology *334*, 31-45.

Furutani-Seiki, M., and Wittbrodt, J. (2004). Medaka and zebrafish, an evolutionary twin study. Mech Dev *121*, 629-637.

Gago-Rodrigues, I., Fernandez-Minan, A., Letelier, J., Naranjo, S., Tena, J.J., Gomez-Skarmeta, J.L., and Martinez-Morales, J.R. (2015). Analysis of opo cis-regulatory landscape uncovers Vsx2 requirement in early eye morphogenesis. Nature communications *6*, 7054.

Gato, A., Martin, C., Alonso, M.I., Martinez-Alvarez, C., and Moro, J.A. (2001). Chondroitin sulphate proteoglycan is involved in lens vesicle morphogenesis in chick embryos. Exp Eye Res *73*, 469-478.

Gerhardt, H., Golding, M., Fruttiger, M., Ruhrberg, C., Lundkvist, A., Abramsson, A., Jeltsch, M., Mitchell, C., Alitalo, K., Shima, D.*, et al.* (2003). VEGF guides angiogenic sprouting utilizing endothelial tip cell filopodia. The Journal of cell biology *161*, 1163-1177.

Ghabrial, A.S., Levi, B.P., and Krasnow, M.A. (2011). A systematic screen for tube morphogenesis and branching genes in the Drosophila tracheal system. PLoS Genet *7*, e1002087.

Gilmour, D., Rembold, M., and Leptin, M. (2017). From morphogen to morphogenesis and back. Nature *541*, 311-320.

Girdler, G.C., Araya, C., Ren, X., and Clarke, J.D. (2013). Developmental time rather than local environment regulates the schedule of epithelial polarization in the zebrafish neural rod. Neural Dev *8*, 5.

Gomez, J.M., Wang, Y., and Riechmann, V. (2012). Tao controls epithelial morphogenesis by promoting Fasciclin 2 endocytosis. The Journal of cell biology *199*, 1131-1143.

Gonzalez-Cordero, A., West, E.L., Pearson, R.A., Duran, Y., Carvalho, L.S., Chu, C.J., Naeem, A., Blackford, S.J.I., Georgiadis, A., Lakowski, J.*, et al.* (2013). Photoreceptor precursors derived from three-dimensional embryonic stem cell cultures integrate and mature within adult degenerate retina. Nat Biotechnol *31*, 741-747.

Goody, M.F., and Henry, C.A. (2010). Dynamic interactions between cells and their extracellular matrix mediate embryonic development. Mol Reprod Dev *77*, 475-488.

Grammont, M. (2007). Adherens junction remodeling by the Notch pathway in Drosophila melanogaster oogenesis. The Journal of cell biology *177*, 139-150.

Graw, J. (2010). Eye development. Current topics in developmental biology *90*, 343-386.

Greene, N.D., and Copp, A.J. (2014). Neural tube defects. Annu Rev Neurosci *37*, 221-242.

Gregory, T.R. (2008). The Evolution of Complex Organs. Evolution: Education and Outreach *1*, 358-389.

Greiling, T.M., and Clark, J.I. (2009). Early lens development in the zebrafish: a three-dimensional time-lapse analysis. Developmental dynamics : an official publication of the American Association of Anatomists *238*, 2254-2265.

Gutzman, J.H., Graeden, E.G., Lowery, L.A., Holley, H.S., and Sive, H. (2008). Formation of the zebrafish midbrain-hindbrain boundary constriction requires laminin-dependent basal constriction. Mech Dev *125*, 974-983.

Haas, P., and Gilmour, D. (2006). Chemokine signaling mediates self-organizing tissue migration in the zebrafish lateral line. Dev Cell *10*, 673-680.

Haeger, A., Wolf, K., Zegers, M.M., and Friedl, P. (2015). Collective cell migration: guidance principles and hierarchies. Trends Cell Biol *25*, 556-566.

Hagedorn, E., and Sherwood, D. (2011). Optically Highlighting Basement Membrane Components in C. elegans.

Hagglund, A.C., Berghard, A., and Carlsson, L. (2013). Canonical Wnt/beta-Catenin Signalling Is Essential for Optic Cup Formation. Plos One *8*.

Haigo, S.L., and Bilder, D. (2011). Global tissue revolutions in a morphogenetic movement controlling elongation. Science *331*, 1071-1074.

Haigo, S.L., Hildebrand, J.D., Harland, R.M., and Wallingford, J.B. (2003). Shroom induces apical constriction and is required for hingepoint formation during neural tube closure. Curr Biol *13*, 2125-2137.

Harada, T., Harada, C., and Parada, L.F. (2007). Molecular regulation of visual system development: more than meets the eye. Genes Dev *21*, 367-378.

Harris, T.J., and Tepass, U. (2010). Adherens junctions: from molecules to morphogenesis. Nat Rev Mol Cell Biol *11*, 502-514.

Harunaga, J.S., Doyle, A.D., and Yamada, K.M. (2014). Local and global dynamics of the basement membrane during branching morphogenesis require protease activity and actomyosin contractility. Developmental biology *394*, 197-205.

Hasegawa, Y., Takata, N., Okuda, S., Kawada, M., Eiraku, M., and Sasai, Y. (2016). Emergence of dorsal-ventral polarity in ESC-derived retinal tissue. Development *143*, 3895-3906.

Heasman, S.J., and Ridley, A.J. (2008). Mammalian Rho GTPases: new insights into their functions from in vivo studies. Nat Rev Mol Cell Biol *9*, 690-701.

Heermann, S., Schutz, L., Lemke, S., Krieglstein, K., and Wittbrodt, J. (2015). Eye morphogenesis driven by epithelial flow into the optic cup facilitated by modulation of bone morphogenetic protein. Elife *4*.

Hohenester, E., and Yurchenco, P.D. (2013). Laminins in basement membrane assembly. Cell Adh Migr *7*, 56-63.

Holt, C. (1980). Cell movements in *Xenopus* eye development. Nature *287*.

Horne-Badovinac, S., and Bilder, D. (2005). Mass transit: epithelial morphogenesis in the Drosophila egg chamber. Developmental dynamics : an official publication of the American Association of Anatomists *232*, 559-574.

Horne-Badovinac, S., Lin, D., Waldron, S., Schwarz, M., Mbamalu, G., Pawson, T., Jan, Y., Stainier, D.Y., and Abdelilah-Seyfried, S. (2001). Positional cloning of heart and soul reveals multiple roles for PKC lambda in zebrafish organogenesis. Curr Biol *11*, 1492-1502.

Horsford, D.J., Nguyen, M.T., Sellar, G.C., Kothary, R., Arnheiter, H., and McInnes, R.R. (2005). Chx10 repression of Mitf is required for the maintenance of mammalian neuroretinal identity. Development *132*, 177-187.

Hotulainen, P., and Lappalainen, P. (2006). Stress fibers are generated by two distinct actin assembly mechanisms in motile cells. The Journal of cell biology *173*, 383-394.

Huang, J., Rajagopal, R., Liu, Y., Dattilo, L.K., Shaham, O., Ashery-Padan, R., and Beebe, D.C. (2011). The mechanism of lens placode formation: a case of matrix-mediated morphogenesis. Developmental biology *355*, 32-42.

Hyer, J., Kuhlman, J., Afif, E., and Mikawa, T. (2003). Optic cup morphogenesis requires pre-lens ectoderm but not lens differentiation. Developmental biology *259*, 351-363.

Icha, J., Kunath, C., Rocha-Martins, M., and Norden, C. (2016). Independent modes of ganglion cell translocation ensure correct lamination of the zebrafish retina. The Journal of cell biology *215*, 259-275.

Ikegami, S., Taguchi, T., Ohashi, M., Oguro, M., Nagano, H., and Mano, Y. (1978). Aphidicolin prevents mitotic cell division by interfering with the activity of DNA polymerase-alpha. Nature *275*, 458-460.

Iskratsch, T., Wolfenson, H., and Sheetz, M.P. (2014). Appreciating force and shape-the rise of mechanotransduction in cell biology. Nat Rev Mol Cell Biol *15*, 825-833.

Ivanovitch, K., Cavodeassi, F., and Wilson, Stephen W. (2013). Precocious Acquisition of Neuroepithelial Character in the Eye Field Underlies the Onset of Eye Morphogenesis. Dev Cell.

Iwasaki, T., Murata-Hori, M., Ishitobi, S., and Hosoya, H. (2001). Diphosphorylated MRLC is required for organization of stress fibers in interphase cells and the contractile ring in dividing cells. Cell Struct Funct *26*, 677-683.

Jayadev, R., and Sherwood, D.R. (2017). Basement membranes. Curr Biol *27*, R207-R211.

Jessen, J.R. (2015). Recent advances in the study of zebrafish extracellular matrix proteins. Developmental biology *401*, 110-121.

Johnson, D., and Wilkie, A.O. (2011). Craniosynostosis. Eur J Hum Genet *19*, 369-376.

Julich, D., Cobb, G., Melo, A.M., McMillen, P., Lawton, A.K., Mochrie, S.G., Rhoades, E., and Holley, S.A. (2015). Cross-Scale Integrin Regulation Organizes ECM and Tissue Topology. Dev Cell *34*, 33-44.

Kadzik, R.S., Cohen, E.D., Morley, M.P., Stewart, K.M., Lu, M.M., and Morrisey, E.E. (2014). Wnt ligand/Frizzled 2 receptor signaling regulates tube shape and branch-point formation in the lung through control of epithelial cell shape. Proceedings of the National Academy of Sciences of the United States of America *111*, 12444-12449.

Kao, G., Huang, C.C., Hedgecock, E.M., Hall, D.H., and Wadsworth, W.G. (2006). The role of the laminin beta subunit in laminin heterotrimer assembly and basement membrane function and development in C. elegans. Developmental biology *290*, 211-219.

Kim, H.Y., Varner, V.D., and Nelson, C.M. (2013). Apical constriction initiates new bud formation during monopodial branching of the embryonic chicken lung. Development *140*, 3146-3155.

Kim, J.Y., Park, R., Lee, J.H., Shin, J., Nickas, J., Kim, S., and Cho, S.H. (2016). Yap is essential for retinal progenitor cell cycle progression and RPE cell fate acquisition in the developing mouse eye. Developmental biology *419*, 336-347.

Kimura, Y., Okamura, Y., and Higashijima, S. (2006). alx, a zebrafish homolog of Chx10, marks ipsilateral descending excitatory interneurons that participate in the regulation of spinal locomotor circuits. J Neurosci *26*, 5684-5697.

Kinoshita, N., Sasai, N., Misaki, K., and Yonemura, S. (2008). Apical accumulation of Rho in the neural plate is important for neural plate cell shape change and neural tube formation. Mol Biol Cell *19*, 2289-2299.

Klein, G., Langegger, M., Timpl, R., and Ekblom, P. (1988). Role of laminin A chain in the development of epithelial cell polarity. Cell *55*, 331-341.

Klinowska, T.C., Soriano, J.V., Edwards, G.M., Oliver, J.M., Valentijn, A.J., Montesano, R., and Streuli, C.H. (1999). Laminin and beta1 integrins are crucial for normal mammary gland development in the mouse. Developmental biology *215*, 13-32.

Kolahi, K.S., White, P.F., Shreter, D.M., Classen, A.K., Bilder, D., and Mofrad, M.R. (2009). Quantitative analysis of epithelial morphogenesis in Drosophila oogenesis: New insights based on morphometric analysis and mechanical modeling. Developmental biology *331*, 129-139.

Kondo, T., and Hayashi, S. (2013). Mitotic cell rounding accelerates epithelial invagination. Nature *494*, 125-129.

Kong, D., Wolf, F., and Grosshans, J. (2017). Forces directing germ-band extension in Drosophila embryos. Mech Dev *144*, 11-22.

Kovacs, M., Toth, J., Hetenyi, C., Malnasi-Csizmadia, A., and Sellers, J.R. (2004). Mechanism of blebbistatin inhibition of myosin II. J Biol Chem *279*, 35557-35563.

Krause, M., and Gautreau, A. (2014). Steering cell migration: lamellipodium dynamics and the regulation of directional persistence. Nature Reviews Molecular Cell Biology *15*, 577-590.

Kuleshov, M.V., Jones, M.R., Rouillard, A.D., Fernandez, N.F., Duan, Q., Wang, Z., Koplev, S., Jenkins, S.L., Jagodnik, K.M., Lachmann, A.*, et al.* (2016). Enrichr: a comprehensive gene set enrichment analysis web server 2016 update. Nucleic Acids Res *44*, W90-97.

Kwan, K.M. (2014). Coming into focus: the role of extracellular matrix in vertebrate optic cup morphogenesis. Developmental dynamics : an official publication of the American Association of Anatomists *243*, 1242-1248.

Kwan, K.M., Fujimoto, E., Grabher, C., Mangum, B.D., Hardy, M.E., Campbell, D.S., Parant, J.M., Yost, H.J., Kanki, J.P., and Chien, C.B. (2007). The Tol2kit: a multisite gateway-based construction kit for Tol2 transposon transgenesis constructs. Developmental dynamics : an official publication of the American Association of Anatomists *236*, 3088-3099.

Kwan, K.M., Otsuna, H., Kidokoro, H., Carney, K.R., Saijoh, Y., and Chien, C.B. (2012). A complex choreography of cell movements shapes the vertebrate eye. Development *139*, 359-372.

Lamb, T.D., Collin, S.P., and Pugh, E.N., Jr. (2007). Evolution of the vertebrate eye: opsins, photoreceptors, retina and eye cup. Nat Rev Neurosci *8*, 960-976.

Lang, R.A., Herman, K., Reynolds, A.B., Hildebrand, J.D., and Plageman, T.F., Jr. (2014). p120-catenin-dependent junctional recruitment of Shroom3 is required for apical constriction during lens pit morphogenesis. Development *141*, 3177-3187.

Lecuit, T., and Le Goff, L. (2007). Orchestrating size and shape during morphogenesis. Nature *450*, 189-192.

Leptin, M., and Grunewald, B. (1990). Cell shape changes during gastrulation in Drosophila. Development *110*, 73-84.

Levine, M., and Davidson, E.H. (2005). Gene regulatory networks for development. Proceedings of the National Academy of Sciences of the United States of America *102*, 4936-4942.

Lewellyn, L., Cetera, M., and Horne-Badovinac, S. (2013). Misshapen decreases integrin levels to promote epithelial motility and planar polarity in Drosophila. The Journal of cell biology *200*, 721-729.

Li, J., Chatzeli, L., Panousopoulou, E., Tucker, A.S., and Green, J.B. (2016). Epithelial stratification and placode invagination are separable functions in early morphogenesis of the molar tooth. Development *143*, 670-681.

Li, Z., Joseph, N.M., and Easter, S.S., Jr. (2000). The morphogenesis of the zebrafish eye, including a fate map of the optic vesicle. Developmental dynamics : an official publication of the American Association of Anatomists *218*, 175-188.

Liao, Y., Smyth, G.K., and Shi, W. (2014). featureCounts: an efficient general purpose program for assigning sequence reads to genomic features. Bioinformatics *30*, 923-930.

Link, V., Carvalho, L., Castanon, I., Stockinger, P., Shevchenko, A., and Heisenberg, C.P. (2006). Identification of regulators of germ layer morphogenesis using proteomics in zebrafish. J Cell Sci *119*, 2073-2083.

Liu, I.S., Chen, J.D., Ploder, L., Vidgen, D., van der Kooy, D., Kalnins, V.I., and McInnes, R.R. (1994). Developmental expression of a novel murine homeobox gene (Chx10): evidence for roles in determination of the neuroretina and inner nuclear layer. Neuron *13*, 377-393.

Loganathan, R., Rongish, B.J., Smith, C.M., Filla, M.B., Czirok, A., Bénazéraf, B., and Little, C.D. (2016). Extracellular matrix motion and early morphogenesis. Development *143*, 2056-2065.

Love, M.I., Huber, W., and Anders, S. (2014). Moderated estimation of fold change and dispersion for RNA-seq data with DESeq2. Genome Biol *15*, 550.

Lowery, L.A., and Sive, H. (2004). Strategies of vertebrate neurulation and a re-evaluation of teleost neural tube formation. Mech Dev *121*, 1189-1197.

Lupo, G., Gestri, G., O'Brien, M., Denton, R.M., Chandraratna, R.A., Ley, S.V., Harris, W.A., and Wilson, S.W. (2011). Retinoic acid receptor signaling regulates choroid fissure closure through independent mechanisms in the ventral optic cup and periocular mesenchyme. Proceedings of the National Academy of Sciences of the United States of America *108*, 8698-8703.

Ma, M., Cao, X., Dai, J., and Pastor-Pareja, J.C. (2017). Basement Membrane Manipulation in Drosophila Wing Discs Affects Dpp Retention but Not Growth Mechanoregulation. Dev Cell *42*, 97-106 e104.

Macdonald, R., Barth, K.A., Xu, Q., Holder, N., Mikkola, I., and Wilson, S.W. (1995). Midline signalling is required for Pax gene regulation and patterning of the eyes. Development *121*, 3267-3278.

Maitre, J.L., Berthoumieux, H., Krens, S.F., Salbreux, G., Julicher, F., Paluch, E., and Heisenberg, C.P. (2012). Adhesion functions in cell sorting by mechanically coupling the cortices of adhering cells. Science *338*, 253-256.

Malicki, J., and Driever, W. (1999). oko meduzy mutations affect neuronal patterning in the zebrafish retina and reveal cell-cell interactions of the retinal neuroepithelial sheet. Development *126*, 1235-1246.

Malicki, J., Jo, H., and Pujic, Z. (2003). Zebrafish N-cadherin, encoded by the glass onion locus, plays an essential role in retinal patterning. Developmental biology *259*, 95-108.

Manjon, C., Sanchez-Herrero, E., and Suzanne, M. (2007). Sharp boundaries of Dpp signalling trigger local cell death required for Drosophila leg morphogenesis. Nat Cell Biol *9*, 57-63.

Maroto, M., Bone, R.A., and Dale, J.K. (2012). Somitogenesis. Development *139*, 2453-2456.

Martin, A.C., and Goldstein, B. (2014). Apical constriction: themes and variations on a cellular mechanism driving morphogenesis. Development *141*, 1987-1998.

Martin, A.C., Kaschube, M., and Wieschaus, E.F. (2009). Pulsed contractions of an actin-myosin network drive apical constriction. Nature *457*, 495-499.

Martinez-Morales, J.R., Rembold, M., Greger, K., Simpson, J.C., Brown, K.E., Quiring, R., Pepperkok, R., Martin-Bermudo, M.D., Himmelbauer, H., and Wittbrodt, J. (2009). ojoplano-mediated basal constriction is essential for optic cup morphogenesis. Development *136*, 2165-2175.

Martinez-Morales, J.R., and Wittbrodt, J. (2009). Shaping the vertebrate eye. Curr Opin Genet Dev *19*, 511-517.

Masai, I. (2003). N-cadherin mediates retinal lamination, maintenance of forebrain compartments and patterning of retinal neurites. Development *130*, 2479-2494.

Matsumura, F. (2005). Regulation of myosin II during cytokinesis in higher eukaryotes. Trends Cell Biol *15*, 371-377.

McClure, K.D., and Schubiger, G. (2005). Developmental analysis and squamous morphogenesis of the peripodial epithelium in Drosophila imaginal discs. Development *132*, 5033-5042.

McMahon, C., Gestri, G., Wilson, S.W., and Link, B.A. (2009). Lmx1b is essential for survival of periocular mesenchymal cells and influences Fgf-mediated retinal patterning in zebrafish. Developmental biology *332*, 287-298.

Megraw, T.L., Sharkey, J.T., and Nowakowski, R.S. (2011). Cdk5rap2 exposes the centrosomal root of microcephaly syndromes. Trends Cell Biol *21*, 470-480.

Meijering, E., Dzyubachyk, O., and Smal, I. (2012). Methods for cell and particle tracking. Methods Enzymol *504*, 183-200.

Mic, F.A., Molotkov, A., Molotkova, N., and Duester, G. (2004). Raldh2 expression in optic vesicle generates a retinoic acid signal needed for invagination of retina during optic cup formation. Developmental dynamics : an official publication of the American Association of Anatomists *231*, 270-277.

Miesfeld, J.B., Gestri, G., Clark, B.S., Flinn, M.A., Poole, R.J., Bader, J.R., Besharse, J.C., Wilson, S.W., and Link, B.A. (2015). Yap and Taz regulate retinal pigment epithelial cell fate. Development.

Molotkov, A., Molotkova, N., and Duester, G. (2006). Retinoic acid guides eye morphogenetic movements via paracrine signaling but is unnecessary for retinal dorsoventral patterning. Development *133*, 1901-1910.

Monier, B., Gettings, M., Gay, G., Mangeat, T., Schott, S., Guarner, A., and Suzanne, M. (2015). Apico-basal forces exerted by apoptotic cells drive epithelium folding. Nature *518*, 245-248.

Morata, G. (2001). How Drosophila appendages develop. Nat Rev Mol Cell Biol *2*, 89-97.

Morin, X., Daneman, R., Zavortink, M., and Chia, W. (2001). A protein trap strategy to detect GFP-tagged proteins expressed from their endogenous loci in Drosophila. Proceedings of the National Academy of Sciences of the United States of America *98*, 15050-15055.

Morishita, Y., Hironaka, K.I., Lee, S.W., Jin, T., and Ohtsuka, D. (2017). Reconstructing 3D deformation dynamics for curved epithelial sheet morphogenesis from positional data of sparsely-labeled cells. Nature communications *8*, 15.

Morrissey, M.A., and Sherwood, D.R. (2015). An active role for basement membrane assembly and modification in tissue sculpting. J Cell Sci *128*, 1661-1668.

Mouw, J.K., Ou, G., and Weaver, V.M. (2014). Extracellular matrix assembly: a multiscale deconstruction. Nat Rev Mol Cell Biol *15*, 771-785.

Mui, S.H., Kim, J.W., Lemke, G., and Bertuzzi, S. (2005). Vax genes ventralize the embryonic eye. Genes Dev *19*, 1249-1259.

Nagayoshi, S., Hayashi, E., Abe, G., Osato, N., Asakawa, K., Urasaki, A., Horikawa, K., Ikeo, K., Takeda, H., and Kawakami, K. (2008). Insertional mutagenesis by the Tol2 transposon-mediated enhancer trap approach generated mutations in two developmental genes: tcf7 and synembryn-like. Development *135*, 159-169.

Nakano, T., Ando, S., Takata, N., Kawada, M., Muguruma, K., Sekiguchi, K., Saito, K., Yonemura, S., Eiraku, M., and Sasai, Y. (2012). Self-formation of optic cups and storable stratified neural retina from human ESCs. Cell stem cell *10*, 771-785.

Ng, B.F., Selvaraj, G.K., Santa-Cruz Mateos, C., Grosheva, I., Alvarez-Garcia, I., Martin-Bermudo, M.D., and Palacios, I.M. (2016). alpha-Spectrin and integrins act together to regulate actomyosin and columnarization, and to maintain a monolayered follicular epithelium. Development *143*, 1388-1399.

Nguyen, M., and Arnheiter, H. (2000). Signaling and transcriptional regulation in early mammalian eye development: a link between FGF and MITF. Development *127*, 3581-3591.

Nicolás-Pérez, M., Kuchling, F., Letelier, J., Polvillo, R., Wittbrodt, J., and Martínez-Morales, J.R. (2016). Analysis of cellular behavior and cytoskeletal dynamics reveal a constriction mechanism driving optic cup morphogenesis. eLife *5*.

Nieto, M.A. (2013). Epithelial plasticity: a common theme in embryonic and cancer cells. Science *342*, 1234850.

Nikolic, D.L., Boettiger, A.N., Bar-Sagi, D., Carbeck, J.D., and Shvartsman, S.Y. (2006). Role of boundary conditions in an experimental model of epithelial wound healing. Am J Physiol Cell Physiol *291*, C68-75.

Nishimura, T., Honda, H., and Takeichi, M. (2012). Planar cell polarity links axes of spatial dynamics in neural-tube closure. Cell *149*, 1084-1097.

Nishimura, T., and Takeichi, M. (2008). Shroom3-mediated recruitment of Rho kinases to the apical cell junctions regulates epithelial and neuroepithelial planar remodeling. Development *135*, 1493-1502.

Norden, C., Young, S., Link, B.A., and Harris, W.A. (2009). Actomyosin is the main driver of interkinetic nuclear migration in the retina. Cell *138*, 1195-1208.

Okenve-Ramos, P., and Llimargas, M. (2014). Fascin links Btl/FGFR signalling to the actin cytoskeleton during Drosophila tracheal morphogenesis. Development *141*, 929-939.

Oltean, A., Huang, J., Beebe, D.C., and Taber, L.A. (2016). Tissue growth constrained by extracellular matrix drives invagination during optic cup morphogenesis. Biomechanics and modeling in mechanobiology.

Omori, Y., and Malicki, J. (2006). oko meduzy and related crumbs genes are determinants of apical cell features in the vertebrate embryo. Curr Biol *16*, 945-957.

Osterfield, M., Berg, C.A., and Shvartsman, S.Y. (2017). Epithelial Patterning, Morphogenesis, and Evolution: Drosophila Eggshell as a Model. Dev Cell *41*, 337-348.

Osterfield, M., Du, X., Schupbach, T., Wieschaus, E., and Shvartsman, S.Y. (2013). Three-dimensional epithelial morphogenesis in the developing Drosophila egg. Dev Cell *24*, 400-410.

Osterfield, M., Schupbach, T., Wieschaus, E., and Shvartsman, S.Y. (2015). Diversity of epithelial morphogenesis during eggshell formation in drosophilids. Development *142*, 1971-1977.

Pandit, T., Jidigam, V.K., Patthey, C., and Gunhaga, L. (2015). Neural retina identity is specified by lens-derived BMP signals. Development *142*, 1850-1859.

Panousopoulou, E., and Green, J.B. (2016). Invagination of Ectodermal Placodes Is Driven by Cell Intercalation-Mediated Contraction of the Suprabasal Tissue Canopy. PLoS biology *14*, e1002405.

Pastor-Pareja, J.C., and Xu, T. (2011). Shaping cells and organs in Drosophila by opposing roles of fat body-secreted Collagen IV and perlecan. Dev Cell *21*, 245-256.

Paulus, J.D., and Halloran, M.C. (2006). Zebrafish bashful/laminin-alpha 1 mutants exhibit multiple axon guidance defects. Developmental dynamics : an official publication of the American Association of Anatomists *235*, 213-224.

Pearl, E.J., Li, J., and Green, J.B. (2017). Cellular systems for epithelial invagination. Philos Trans R Soc Lond B Biol Sci *372*.

Peters, N.C., and Berg, C.A. (2016). Dynamin-mediated endocytosis is required for tube closure, cell intercalation, and biased apical expansion during epithelial tubulogenesis in the Drosophila ovary. Developmental biology *409*, 39-54.

Peters, N.C., Thayer, N.H., Kerr, S.A., Tompa, M., and Berg, C.A. (2013). Following the 'tracks': Tramtrack69 regulates epithelial tube expansion in the Drosophila ovary through Paxillin, Dynamin, and the homeobox protein Mirror. Developmental biology *378*, 154-169.

Petrie, R.J., and Yamada, K.M. (2012). At the leading edge of three-dimensional cell migration. J Cell Sci *125*, 5917-5926.

Picker, A., and Brand, M. (2005). Fgf signals from a novel signaling center determine axial patterning of the prospective neural retina. Development *132*, 4951-4962.

Picker, A., Cavodeassi, F., Machate, A., Bernauer, S., Hans, S., Abe, G., Kawakami, K., Wilson, S.W., and Brand, M. (2009). Dynamic coupling of pattern formation and morphogenesis in the developing vertebrate retina. PLoS biology *7*, e1000214.

Pickering, J. (2012). The expression and regulation of lama1, a gene encoding Laminin alpha 1, during zebrafish development (University of Sheffield).

Pickering, J., Cunliffe, V.T., Van Eeden, F., and Borycki, A.G. (2016). Hedgehog signalling acts upstream of Laminin alpha1 transcription in the zebrafish paraxial mesoderm. Matrix Biol.

Pittack, C., Grunwald, G.B., and Reh, T.A. (1997). Fibroblast growth factors are necessary for neural retina but not pigmented epithelium differentiation in chick embryos. Development *124*, 805-816.

Plageman, T.F., Jr., Chauhan, B.K., Yang, C., Jaudon, F., Shang, X., Zheng, Y., Lou, M., Debant, A., Hildebrand, J.D., and Lang, R.A. (2011). A Trio-RhoA-Shroom3 pathway is required for apical constriction and epithelial invagination. Development *138*, 5177-5188.

Plageman, T.F., Jr., Chung, M.I., Lou, M., Smith, A.N., Hildebrand, J.D., Wallingford, J.B., and Lang, R.A. (2010). Pax6-dependent Shroom3 expression regulates apical constriction during lens placode invagination. Development *137*, 405-415.

Pollard, S.M., Parsons, M.J., Kamei, M., Kettleborough, R.N., Thomas, K.A., Pham, V.N., Bae, M.K., Scott, A., Weinstein, B.M., and Stemple, D.L. (2006). Essential and overlapping roles for laminin alpha chains in notochord and blood vessel formation. Developmental biology *289*, 64-76.

Polyakov, O., He, B., Swan, M., Shaevitz, J.W., Kaschube, M., and Wieschaus, E. (2014). Passive mechanical forces control cell-shape change during Drosophila ventral furrow formation. Biophys J *107*, 998-1010.

Porazinski, S., Wang, H., Asaoka, Y., Behrndt, M., Miyamoto, T., Morita, H., Hata, S., Sasaki, T., Krens, S.F.G., Osada, Y.*, et al.* (2015). YAP is essential for tissue tension to ensure vertebrate 3D body shape. Nature *521*, 217-221.

Poujade, M., Grasland-Mongrain, E., Hertzog, A., Jouanneau, J., Chavrier, P., Ladoux, B., Buguin, A., and Silberzan, P. (2007). Collective migration of an epithelial monolayer in response to a model wound. Proceedings of the National Academy of Sciences of the United States of America *104*, 15988-15993.

Prochazka, J., Prochazkova, M., Du, W., Spoutil, F., Tureckova, J., Hoch, R., Shimogori, T., Sedlacek, R., Rubenstein, J.L., Wittmann, T.*, et al.* (2015). Migration of Founder Epithelial Cells Drives Proper Molar Tooth Positioning and Morphogenesis. Dev Cell *35*, 713-724.

Pujic, Z., and Malicki, J. (2001). Mutation of the zebrafish glass onion locus causes early cell-nonautonomous loss of neuroepithelial integrity followed by severe neuronal patterning defects in the retina. Developmental biology *234*, 454-469.

Randlett, O., Poggi, L., Zolessi, F.R., and Harris, W.A. (2011). The oriented emergence of axons from retinal ganglion cells is directed by laminin contact in vivo. Neuron *70*, 266-280.

Rasmussen, J.P., Reddy, S.S., and Priess, J.R. (2012). Laminin is required to orient epithelial polarity in the C. elegans pharynx. Development *139*, 2050-2060.

Rembold, M., Loosli, F., Adams, R.J., and Wittbrodt, J. (2006). Individual cell migration serves as the driving force for optic vesicle evagination. Science *313*, 1130-1134.

Ribeiro, C., Ebner, A., and Affolter, M. (2002). In vivo imaging reveals different cellular functions for FGF and Dpp signaling in tracheal branching morphogenesis. Dev Cell *2*, 677-683.

Ribeiro, C., Neumann, M., and Affolter, M. (2004). Genetic control of cell intercalation during tracheal morphogenesis in Drosophila. Curr Biol *14*, 2197-2207.

Ridley, A.J., Schwartz, M.A., Burridge, K., Firtel, R.A., Ginsberg, M.H., Borisy, G., Parsons, J.T., and Horwitz, A.R. (2003). Cell migration: integrating signals from front to back. Science *302*, 1704-1709.

Robu, M.E., Larson, J.D., Nasevicius, A., Beiraghi, S., Brenner, C., Farber, S.A., and Ekker, S.C. (2007). p53 activation by knockdown technologies. PLoS Genet *3*, e78.

Rolo, A., Skoglund, P., and Keller, R. (2009). Morphogenetic movements driving neural tube closure in Xenopus require myosin IIB. Developmental biology *327*, 327-338.

Rorth, P. (2009). Collective cell migration. Annu Rev Cell Dev Biol *25*, 407-429.

Sai, X., and Ladher, R.K. (2008). FGF signaling regulates cytoskeletal remodeling during epithelial morphogenesis. Curr Biol *18*, 976-981.

Salbreux, G., Charras, G., and Paluch, E. (2012). Actin cortex mechanics and cellular morphogenesis. Trends Cell Biol *22*, 536-545.

Santos-Ferreira, T., Volkner, M., Borsch, O., Haas, J., Cimalla, P., Vasudevan, P., Carmeliet, P., Corbeil, D., Michalakis, S., Koch, E.*, et al.* (2016). Stem Cell-Derived Photoreceptor Transplants Differentially Integrate Into Mouse Models of Cone-Rod Dystrophy. Invest Ophthalmol Vis Sci *57*, 3509-3520.

Sasagawa, S., Takabatake, T., Takabatake, Y., Muramatsu, T., and Takeshima, K. (2002). Axes establishment during eye morphogenesis in Xenopus by coordinate and antagonistic actions of BMP4, Shh, and RA. Genesis *33*, 86-96.

Sauka-Spengler, T., and Bronner-Fraser, M. (2008). A gene regulatory network orchestrates neural crest formation. Nat Rev Mol Cell Biol *9*, 557-568.

Schepis, A., Sepich, D., and Nelson, W.J. (2012). alphaE-catenin regulates cell-cell adhesion and membrane blebbing during zebrafish epiboly. Development *139*, 537-546.

Schepsky, A., Bruser, K., Gunnarsson, G.J., Goodall, J., Hallsson, J.H., Goding, C.R., Steingrimsson, E., and Hecht, A. (2006). The microphthalmia-associated transcription factor Mitf interacts with beta-catenin to determine target gene expression. Molecular and Cellular Biology *26*, 8914-8927.

Schindelin, J., Arganda-Carreras, I., Frise, E., Kaynig, V., Longair, M., Pietzsch, T., Preibisch, S., Rueden, C., Saalfeld, S., Schmid, B.*, et al.* (2012). Fiji: an open-source platform for biological-image analysis. Nat Methods *9*, 676-682.

Schoenwolf, G.C., and Franks, M.V. (1984). Quantitative analyses of changes in cell shapes during bending of the avian neural plate. Developmental biology *105*, 257-272.

Schroeder, T.E. (1970). Neurulation in Xenopus laevis. An analysis and model based upon light and electron microscopy. J Embryol Exp Morphol *23*, 427-462.

Schwarz, M., Cecconi, F., Bernier, G., Andrejewski, N., Kammandel, B., Wagner, M., and Gruss, P. (2000). Spatial specification of mammalian eye territories by reciprocal transcriptional repression of Pax2 and Pax6. Development *127*, 4325-4334.

Sedykh, I., Yoon, B., Roberson, L., Moskvin, O., Dewey, C.N., and Grinblat, Y. (2017). Zebrafish zic2 controls formation of periocular neural crest and choroid fissure morphogenesis. Developmental biology.

Semina, E.V., Bosenko, D.V., Zinkevich, N.C., Soules, K.A., Hyde, D.R., Vihtelic, T.S., Willer, G.B., Gregg, R.G., and Link, B.A. (2006). Mutations in laminin alpha 1 result in complex, lens-independent ocular phenotypes in zebrafish. Developmental biology *299*, 63-77.

Sidhaye, J., and Norden, C. (2017). Concerted action of neuroepithelial basal shrinkage and active epithelial migration ensures efficient optic cup morphogenesis. Elife *6*.

Simpson, K.J., Selfors, L.M., Bui, J., Reynolds, A., Leake, D., Khvorova, A., and Brugge, J.S. (2008). Identification of genes that regulate epithelial cell migration using an siRNA screening approach. Nat Cell Biol *10*, 1027-1038.

Solnica-Krezel, L. (2005). Conserved patterns of cell movements during vertebrate gastrulation. Curr Biol *15*, R213-228.

Solnica-Krezel, L. (2006). Gastrulation in zebrafish -- all just about adhesion? Curr Opin Genet Dev *16*, 433-441.

Straight, A.F., Cheung, A., Limouze, J., Chen, I., Westwood, N.J., Sellers, J.R., and Mitchison, T.J. (2003). Dissecting temporal and spatial control of cytokinesis with a myosin II Inhibitor. Science *299*, 1743-1747.

Strzyz, P.J., Lee, H.O., Sidhaye, J., Weber, I.P., Leung, L.C., and Norden, C. (2015). Interkinetic nuclear migration is centrosome independent and ensures apical cell division to maintain tissue integrity. Dev Cell *32*, 203-219.

Strzyz, P.J., Matejcic, M., and Norden, C. (2016). Heterogeneity, Cell Biology and Tissue Mechanics of Pseudostratified Epithelia: Coordination of Cell Divisions and Growth in Tightly Packed Tissues. International review of cell and molecular biology *325*, 89-118.

Subauste, M.C., Von Herrath, M., Benard, V., Chamberlain, C.E., Chuang, T.-H., Chu, K., Bokoch, G.M., and Hahn, K.M. (2000). Rho family proteins modulate rapid apoptosis induced by cytotoxic T lymphocytes and Fas. Journal of Biological Chemistry *275*, 9725-9733.

Sun, Z., Amourda, C., Shagirov, M., Hara, Y., Saunders, T.E., and Toyama, Y. (2017). Basolateral protrusion and apical contraction cooperatively drive Drosophila germ-band extension. Nat Cell Biol *19*, 375-383.

Sunyer, R., Conte, V., Escribano, J., Elosegui-Artola, A., Labernadie, A., Valon, L., Navajas, D., Garcia-Aznar, J.M., Munoz, J.J., Roca-Cusachs, P.*, et al.* (2016). Collective cell durotaxis emerges from long-range intercellular force transmission. Science *353*, 1157-1161.

Suzuki, M., Morita, H., and Ueno, N. (2012). Molecular mechanisms of cell shape changes that contribute to vertebrate neural tube closure. Dev Growth Differ *54*, 266-276.

Svoboda, K.K., and O'Shea, K.S. (1987). An analysis of cell shape and the neuroepithelial basal lamina during optic vesicle formation in the mouse embryo. Development *100*, 185-200.

Tang, N., and Marshall, W.F. (2012). Centrosome positioning in vertebrate development. J Cell Sci *125*, 4951-4961.

Tang, N., Marshall, W.F., McMahon, M., Metzger, R.J., and Martin, G.R. (2011). Control of mitotic spindle angle by the RAS-regulated ERK1/2 pathway determines lung tube shape. Science *333*, 342-345.

Tang, X., Gao, J., Jia, X., Zhao, W., Zhang, Y., Pan, W., and He, J. (2017). Bipotent progenitors as embryonic origin of retinal stem cells. The Journal of cell biology *216*, 1833-1847.

Tawk, M., Araya, C., Lyons, D.A., Reugels, A.M., Girdler, G.C., Bayley, P.R., Hyde, D.R., Tada, M., and Clarke, J.D. (2007). A mirror-symmetric cell division that orchestrates neuroepithelial morphogenesis. Nature *446*, 797-800.

Tojkander, S., Gateva, G., and Lappalainen, P. (2012). Actin stress fibers--assembly, dynamics and biological roles. J Cell Sci *125*, 1855-1864.

Trinh, L.A., Chong-Morrison, V., Gavriouchkina, D., Hochgreb-Hagele, T., Senanayake, U., Fraser, S.E., and Sauka-Spengler, T. (2017). Biotagging of Specific Cell Populations in Zebrafish Reveals Gene Regulatory Logic Encoded in the Nuclear Transcriptome. Cell Rep *19*, 425-440.

Veien, E.S., Rosenthal, J.S., Kruse-Bend, R.C., Chien, C.B., and Dorsky, R.I. (2008). Canonical Wnt signaling is required for the maintenance of dorsal retinal identity. Development *135*, 4101-4111.

Vicente-Manzanares, M., Ma, X., Adelstein, R.S., and Horwitz, A.R. (2009). Non-muscle myosin II takes centre stage in cell adhesion and migration. Nat Rev Mol Cell Biol *10*, 778-790.

Viktorinova, I., Konig, T., Schlichting, K., and Dahmann, C. (2009). The cadherin Fat2 is required for planar cell polarity in the Drosophila ovary. Development *136*, 4123-4132.

Villefranc, J.A., Amigo, J., and Lawson, N.D. (2007). Gateway compatible vectors for analysis of gene function in the zebrafish. Developmental dynamics : an official publication of the American Association of Anatomists *236*, 3077-3087.

Vitorino, P., and Meyer, T. (2008). Modular control of endothelial sheet migration. Genes Dev *22*, 3268-3281.

Volkner, M., Zschatzsch, M., Rostovskaya, M., Overall, R.W., Busskamp, V., Anastassiadis, K., and Karl, M.O. (2016). Retinal Organoids from Pluripotent Stem Cells Efficiently Recapitulate Retinogenesis. Stem cell reports *6*, 525-538.

Wang, Y., and Riechmann, V. (2007). The role of the actomyosin cytoskeleton in coordination of tissue growth during Drosophila oogenesis. Curr Biol *17*, 1349-1355.

Weber, I.P., Ramos, A.P., Strzyz, P.J., Leung, L.C., Young, S., and Norden, C. (2014). Mitotic position and morphology of committed precursor cells in the zebrafish retina adapt to architectural changes upon tissue maturation. Cell Rep *7*, 386-397.

Wei, X., Cheng, Y., Luo, Y., Shi, X., Nelson, S., and Hyde, D.R. (2004). The zebrafish Pard3 ortholog is required for separation of the eye fields and retinal lamination. Developmental biology *269*, 286-301.

Wei, X., and Malicki, J. (2002). nagie oko, encoding a MAGUK-family protein, is essential for cellular patterning of the retina. Nat Genet *31*, 150-157.

Westenskow, P., Piccolo, S., and Fuhrmann, S. (2009). beta-catenin controls differentiation of the retinal pigment epithelium in the mouse optic cup by regulating Mitf and Otx2 expression. Development *136*, 2505-2510.

Widmann, T.J., and Dahmann, C. (2009a). Dpp signaling promotes the cuboidal-to-columnar shape transition of Drosophila wing disc epithelia by regulating Rho1. J Cell Sci *122*, 1362-1373.

Widmann, T.J., and Dahmann, C. (2009b). Wingless signaling and the control of cell shape in Drosophila wing imaginal discs. Developmental biology *334*, 161-173.

William A. Harris, V.H. (1991). Neuronal determination without cell division in xenopus embryos. Neuron *6*, p499-515.

Williamson, K.A., and FitzPatrick, D.R. (2014). The genetic architecture of microphthalmia, anophthalmia and coloboma. Eur J Med Genet *57*, 369-380.

Wu, T.D., and Nacu, S. (2010). Fast and SNP-tolerant detection of complex variants and splicing in short reads. Bioinformatics *26*, 873-881.

Yamaguchi, M., Imai, F., Tonou-Fujimori, N., and Masai, I. (2010). Mutations in N-cadherin and a Stardust homolog, Nagie oko, affect cell-cycle exit in zebrafish retina. Mech Dev *127*, 247-264.

Yarrow, J.C., Totsukawa, G., Charras, G.T., and Mitchison, T.J. (2005). Screening for cell migration inhibitors via automated microscopy reveals a Rho-kinase inhibitor. Chem Biol *12*, 385-395.

Yasumoto, K., Takeda, K., Saito, H., Watanabe, K., Takahashi, K., and Shibahara, S. (2002). Microphthalmia-associated transcription factor interacts with LEF-1, a mediator of Wnt signaling. Embo J *21*, 2703-2714.

Ybot-Gonzalez, P., Savery, D., Gerrelli, D., Signore, M., Mitchell, C.E., Faux, C.H., Greene, N.D., and Copp, A.J. (2007). Convergent extension, planar-cell-polarity signalling and initiation of mouse neural tube closure. Development *134*, 789-799.

Young, C.W., and Hodas, S. (1964). Hydroxyurea: Inhibitory Effect on DNA Metabolism. Science *146*, 1172-1174.

Young, P.E., Pesacreta, T.C., and Kiehart, D.P. (1991). Dynamic changes in the distribution of cytoplasmic myosin during Drosophila embryogenesis. Development *111*, 1-14.

Yurchenco, P.D. (2011). Basement membranes: cell scaffoldings and signaling platforms. Cold Spring Harb Perspect Biol *3*.

Zhao, L., Saitsu, H., Sun, X., Shiota, K., and Ishibashi, M. (2010). Sonic hedgehog is involved in formation of the ventral optic cup by limiting Bmp4 expression to the dorsal domain. Mech Dev *127*, 62-72.

Zhong, X., Gutierrez, C., Xue, T., Hampton, C., Vergara, M.N., Cao, L.H., Peters, A., Park, T.S., Zambidis, E.T., Meyer, J.S.*, et al.* (2014). Generation of three-dimensional retinal tissue with functional photoreceptors from human iPSCs. Nature communications *5*, 4047.

Zhou, C.J., Molotkov, A., Song, L.Y., Li, Y.H., Pleasure, D.E., Pleasure, S.J., and Wang, Y.Z. (2008). Ocular Coloboma and Dorsoventral Neuroretinal Patterning Defects in Lrp6 Mutant Eyes. Developmental Dynamics *237*, 3681-3689.

Zhu, Y., Carido, M., Meinhardt, A., Kurth, T., Karl, M.O., Ader, M., and Tanaka, E.M. (2013). Three-dimensional neuroepithelial culture from human embryonic stem cells and its use for quantitative conversion to retinal pigment epithelium. PLoS One *8*, e54552.

Zou, C., and Levine, E.M. (2012). Vsx2 controls eye organogenesis and retinal progenitor identity via homeodomain and non-homeodomain residues required for high affinity DNA binding. PLoS Genet *8*, e1002924.

Movie Legends

Movie 1: RNE morphogenesis in the zebrafish embryo
Time-lapse imaging of cellular dynamics during RNE morphogenesis using Tg(*actb1:HRAS-EGFP*). Invagination (arrowheads) and rim involution (arrows). Imaging started around 15 ss. Time in h:min. Scale bar = 10 µm. Related to Figure 2.1A.

Movie 2: Actomyosin dynamics during RNE morphogenesis
Part 1: Time-lapse imaging of actin dynamics during RNE morphogenesis using Tg(*actb1:GFP--utrCH*). Part 2: Time-lapse imaging of myosin dynamics during RNE morphogenesis using Tg(*actb1:myl12.1-EGFP*).
GFP enrichment at the basal side of the RNE (arrowheads). Rim zone lacking basal GFP enrichment (arrows). Imaging started around 15 ss. Time in h:min and Scale bars = 10 µm. Related to Figure 2.3 A,B.

Movie 3: RNE morphogenesis in Rockout treated embryos.
Time-lapse imaging of RNE morphogenesis in Tg(*actb1:GFP--utrCH*) embryos treated with DMSO (left) and 125 µm Rockout (right). Treatment started at 13–14 ss, 2 h before imaging. Imaging started around 18 ss. Time in h:min, Scale bar = 10 µm. Related to Figure 2.6A.

Movie 4: Membrane and actin dynamics during rim involution
Part 1: Time-lapse imaging of membrane dynamics during rim involution. Mosaic expression of Par3-GFP (magenta) and mKate2-ras (green). Membrane protrusions (arrows). Part 2: Time-lapse imaging of actin dynamics during rim involution. Mosaic expression of GFP-UtrophinCH (green) and mKate2-ras (magenta). Apical utrophin localization at the adherens junctions (arrows).
Imaging started at 17–18 ss. Time in h:min. Scale bar = 10 µm. Related to Figure 2.8D,E.

Movie 5: Actin dynamics during rim involution
Time-lapse imaging of actin dynamics during rim involution. Mosaic expression of GFP-UtrophinCH (green) and mKate2-ras (magenta). Utrophin localization in the membrane protrusions (arrows). Basal utrophin enrichment (arrowheads). Imaging started at 17–18 ss. Time in h:min and scale bar = 10 µm. Related to Figure 2.9A.

Movie 6: Rim cell dynamics in Rockout treated embryos
Time-lapse imaging of actin dynamics in rim cells of Rockout treated embryos. Mosaic expression of GFP-UtrophinCH (green) and mKate2-ras (magenta). Rockout treatment

started at 13–14 ss, 2 h before imaging. Imaging started at 17–18 ss. Time in h:min. Scale bar = 10 µm. Related to Figure 2.9F.

Movie 7: Myosin dynamics during rim involution

Time-lapse imaging of myosin dynamics during rim involution. Mosaic expression of DD-myl12b-GFP (green) and mKate2-ras (magenta). Dynamic basal spots (arrows). Stable basal enrichment (arrowheads). Imaging started at 17–18 ss. Time in h:min. Scale bar = 10 µm. Related to Figure 2.9B.

Movie 8: Dynamics of cell-matrix adhesion components during rim involution

Part 1. Time-lapse imaging of integrin dynamics during rim involution. Mosaic expression of Integrinb1b-mKate2 (magenta) and GFP-ras (green). Part 2. Time-lapse imaging of paxillin dynamics during rim involution. Mosaic expression of paxillin-mKate2.

Short-lived foci (arrows). Stable basal enrichment indicative of stable focal adhesions (arrowheads). Imaging started at 17–18 ss. Time in h:min, Scale bar = 10 µm. Related to Figure 2.11A,B.

Movie 9: Paxillin dynamics during RNE morphogenesis

Time-lapse imaging of paxillin dynamics during RNE morphogenesis in paxillin-mKate2 RNA injected embryos. Imaging started around 15 ss. Time in h:min and scale bars = 10 µm. Related to Figure 2.11C

Movie 10: RNE morphogenesis in *laminin* and *opo* morphant

Part 1. Time-lapse imaging of mosaic expression of mKate2-ras in *laminin* morphant. Part 2. Time-lapse imaging of mosaic expression of mKate2-ras in *opo* morphant.

Lines mark the outline of developing optic vesicle and later RNE. Rim cells with perturbed rim involution (arrows). Imaging started 16–17 ss. Time in h:min. Scale bar = 10 µm. Related to Figure 2.16D,E.

Movie 11: Paxillin dynamics during rim involution in *laminin* morphant

Time-lapse imaging of paxillin dynamics during rim involution in *laminin* morphant with mosaic expression of GFP-ras (left) and paxillin-mKate2 (middle). Stable paxillin localisation (red arrowhead). Basal blebbing in the rim cells (blue arrowhead). Time in h:min. Scale bar = 10 µm. Related to Figure 2.18A.

Movie Legends

Movie 12: Paxillin dynamics during rim involution in *opo* morphant

Time-lapse imaging of paxillin dynamics during rim involution in *opo* morphant with mosaic expression of GFP-ras (left) and paxillin-mKate2 (middle). Paxillin foci (red arrowhead). Basal blebbing in the rim cells (blue arrowhead). Time in h:min. Scale bar = 10 μm. Related to Figure 2.18C.

Movie 13: GFP-ras expressing *opo* morphant clone in mCherry-UtrCH expressing control background

Time-lapse imaging of RNE morphogenesis in Tg(*actb1:mCherry-UtrCH*) acceptor embryo transplanted with GFP-ras positive *opo* morphant cells. *Opo* morphants cells (green), acceptor cells (*magenta*). Basal blebbing in the rim cells (arrowheads). Time in h:min. Scale bar = 10 μm.

Movie 14: RNE morphogenesis in *ezrin* morphant

Time-lapse imaging of mosaic expression of mKate2-ras in *ezrin* morphant. Lines mark the outline of developing optic vesicle and later RNE. Rim cells with perturbed rim involution (arrows). Imaging started 16–17 ss. Time in h:min. Scale bar = 10 μm. Related to Figure 2.21C.

Movie 15: *vsx2::GFP* expression during RNE morphogenesis.

Part 1. Time-lapse imaging of control RNE morphogenesis in Tg(*vsx2::GFP, bactin::mKate2-ras*). Part 2. Time-lapse imaging of RNE morphogenesis in Tg(*vsx2::GFP, bactin::mKate2-ras*) in *ezrin* morphant.

Appearance of bright GFP signal indicative of RNE fate determination (arrow). Imaging started 16–17 ss. Time in h:min. Scale bar = 10 μm. Related to Figure 2.24A.

List of Abbreviations

Amp	Ampicillin
Aphi	Aphidicolin
BAC	Bacterial artificial chromosome
bp	basepairs
DMSO	Dimethyl sulfoxide
DNA	Deoxyribonucleic acid
ECM	Extracellular matrix
EGFP	Enhanced green fluorescent protein
EMT	Epithelial-to-mesenchyme transition
FACS	Fluorescence-activated cell sorting
Flp	Flippase
GFP	Green fluorescent protein
GO	Gene ontology
hpf	Hours post fertilisation
HU	Hydroxyurea
LB	Lysogeny broth/Luria broth
Lama1	laminin-α1
MRLC	Myosin regulatory light chain
NGS	Normal goat serum
OCM	Optic cup morphogenesis
PBS	Phosphate buffer saline
PFA	Paraformaldehyde
POM	Periocular mesenchyme
RNA	Ribonucleic acid
RNE	Retinal neuroepithelium
ROCK	Rho kinase
RPE	Retinal pigment epithelium
SDS	Sodium dodecyl sulfate
sfGFP	Superfolder green fluorescent protein
ss	Somite stage
Tet	Tetracyclin

List of figures

List of tables

Acknowledgements

I would like to sincerely thank everyone who has been part of my PhD journey.

First of all, I thank Caren for giving me the opportunity to pursue my doctoral research in the Norden lab. I am thankful for her guidance, support and motivation throughout the PhD tenure. I am also thankful to my TAC members Marino Zerial, Suzanne Eaton, Jan Brugués and Guillaume Salbreux for their support and inputs. Being part of the Dresden international PhD program (DIPP) has been an enriching experience and I would like to thank the PhD office and the program coordinators for their support and for organising such a well-structured PhD program. I would also like to thank the Dresden international graduate school for Biomedicine and Bioengineering (DIGS-BB) for the DIGS-BB fellowship and the financial support during my PhD. I am also thankful to the reviewers of thesis for their valuable time.

Next, I would like to thank Niklas Iffländer, a visiting student in the Norden lab, who helped me with the proliferation inhibition experiments. I would like to thank Caren for the help with transplantation experiments. Importantly, I am thankful to the technicians in the Norden lab, Sylvia Kaufmann, Claudia Fröb and Heike Hollak for their experimental support and for the general lab organisation. This research wouldn't have been easy without their support. I would also like to thank all the past and present members of the Norden lab for the conducive environment. I would especially like to thank Jaroslav Icha and Iskra Yanakieva for the scientific discussions and support at many steps during my PhD. I am grateful to all the groups that shared their plasmid constructs mentioned in this work. Additionally, I would like to thank Eli Knust for sharing her insights on developmental biology and for her support and motivation.

This work wouldn't have been possible without the help from the facilities at MPI-CBG. I am grateful to the fish facility (Evelyn Lehmann, Jürgen Müller, Joachim Hellmig and Jens Hückman) for their support with the fish husbandry. The light microscopy facility was immensely helpful for this work. Special thanks to Jan Peychl, Britta Schroth-Diez, Bert Nitzsche, Davide Accardi and Sebastian Bundschuh for the help and support with the microscopes. I would like to thank Ina Nüsslein, Christina Eugster Oegema and Julia Jarrells from cell technologies group for the help with the FACS. I am grateful to Andreas Dahl and his next generation sequencing group for the support with the transcriptome project. Special thanks to Mathias Lesche for the bioinformatics analysis of the RNA-seq data. I also thank SFB-655 for the financial support for the RNA-seq experiments. Mihail Sarov and the

transgenomics facility helped with the BAC recombineering. I am thankful to them and specially to Aleksandra Syta, who was the technician involved. I would also like to thank all other facilities including the media kitchen, the admin staff, computer and IT support, sequencing facility, the homebase secretaries and importantly the international office (specially Carolyn) for all their support. I would like to thank everyone at MPI-CBG for the great atmosphere and the enriching experience.

I would like to thank Caren Norden, Jaroslav Icha, Máté Pálfy, Daniel Matějů, Elli Nüske, and Stephan Daetwyler for critical comments on different parts of the thesis. I am also thankful to the PhD office for the support with the doctoral proceedings.

Last but not least I would like to thank my family (Sulabha Sidhaye, Satchit Sidhaye, Deepti Sidhaye and Gandhali Bapat) and friends who have been a constant support during my PhD time. I am thankful to Mahendra Sonawane and TIFR, Mumbai for the initial training in zebrafish biology and for the foundations of my scientific training. Living in Dresden for my doctoral research was my first experience to live outside India, away from home in a place culturally, geographically and in many ways different. Therefore, I specially thank the people, whom I met in Dresden and who made my experience here enjoyable. The list is long but I would like to specially mention Akanksha Jain, Gopi Shah, Krishnendu Khan, Gauravi Deshpande, Stephan Daetwyler, Elli Nüske, Anna Bajur, Albert Thommen, Shai Joseph and Carine Stapel. I am grateful to them for all the cherishable memories I shared with them. Finally, I am grateful to my two closest friends and peers, with whom I shared this PhD journey. I have my heartfelt thanks to Daniel Matějů for being a great friend, critic and a source of motivation. Similarly, I thank Máté Pálfy from the bottom of my heart for the friendship and for the scientific and non-scientific discussions. My PhD journey wouldn't have been easy and enjoyable without these companions.

It is indeed rare to meet such a bunch of amazing people at once, who support and motivate you to do your work. This has been truly an amazing and transformative experience for me. I am grateful to each one of them.

Anlage 1

Technische Universität Dresden Medizinische Fakultät Carl Gustav Carus Promotionsordnung vom 24. Juli 2011

Erklärungen zur Eröffnung des Promotionsverfahrens

1. Hiermit versichere ich, dass ich die vorliegende Arbeit ohne unzulässige Hilfe Dritter und ohne Benutzung anderer als der angegebenen Hilfsmittel angefertigt habe; die aus fremden Quellen direkt oder indirekt übernommenen Gedanken sind als solche kenntlich gemacht.

2. Bei der Auswahl und Auswertung des Materials sowie bei der Herstellung des Manuskripts habe ich Unterstützungsleistungen von folgenden Personen erhalten:
Mathias Lesche (Bioinformatic analysis), Andreas Dahl, Next generation sequencing group at Biotec, TUD (Deep sequencing).
Alekandra Syta, Mihail Sarov, Transgenomics facility at MPI-CBG, (BAC recombineering).

3. Weitere Personen waren an der geistigen Herstellung der vorliegenden Arbeit nicht beteiligt. Insbesondere habe ich nicht die Hilfe eines kommerziellen Promotionsberaters in Anspruch genommen. Dritte haben von mir weder unmittelbar noch mittelbar geldwerte Leistungen für Arbeiten erhalten, die im Zusammenhang mit dem Inhalt der vorgelegten Dissertation stehen.

4. Die Arbeit wurde bisher weder im Inland noch im Ausland in gleicher oder ähnlicher Form einer anderen Prüfungsbehörde vorgelegt.

5. Die Inhalte dieser Dissertation wurden in folgender Form veröffentlicht:
Sidhaye, J., & Norden, C. (2017). ***Concerted action of neuroepithelial basal shrinkage and active epithelial migration ensures efficient optic cup morphogenesis.*** **eLife, 6, e22689.**

6. Ich bestätige, dass es keine zurückliegenden erfolglosen Promotionsverfahren gab.

7. Ich bestätige, dass ich die Promotionsordnung der Medizinischen Fakultät der Technischen Universität Dresden anerkenne.

8. Ich habe die Zitierrichtlinien für Dissertationen an der Medizinischen Fakultät der Technischen Universität Dresden zur Kenntnis genommen und befolgt.

Dresden

Jaydeep Sidhaye

Anlage 2

Hiermit bestätige ich die Einhaltung der folgenden aktuellen gesetzlichen Vorgaben im Rahmen meiner Dissertation

das zustimmende Votum der Ethikkommission bei Klinischen Studien, epidemiologischen Untersuchungen mit Personenbezug oder Sachverhalten, die das Medizinproduktegesetz betreffen
Aktenzeichen der zuständigen Ethikkommission: **nicht zutreffend**

die Einhaltung der Bestimmungen des Tierschutzgesetzes *Aktenzeichen der Genehmigungsbehörde zum Vorhaben/zur Mitwirkung:* **DD24-5131/354/11**

die Einhaltung des Gentechnikgesetzes
Projektnummer: **54-8451/103**

die Einhaltung von Datenschutzbestimmungen der Medizinischen Fakultät und des Universitätsklinikums Carl Gustav Carus.

Dresden,

Jaydeep Sidhaye